

# **Anthropogenic Sources and Environmental Implications of Local Groundwater Warming**

**Dissertation**

**zur Erlangung des  
Doktorgrades der Naturwissenschaften (Dr. rer. nat.)**

der

Naturwissenschaftlichen Fakultät III  
Agrar- und Ernährungswissenschaften,  
Geowissenschaften und Informatik

der Martin-Luther-Universität Halle-Wittenberg

vorgelegt von

Herrn Noethen, Maximilian

Tag der Verteidigung:

03.12.2024



Gutachter:  
Prof. Dr. Peter Bayer  
Prof. Dr. Thomas Vienken





# Abstract

Warming of the subsurface occurs at all scales and intensities, from local micro-effects in the vicinity of power cables to regional macro-effects due to surface sealing in urban areas and even global warming of the shallow subsurface in response to climate change. The consequences of subsurface warming for groundwater quality and ecology are largely unknown. Previous studies indicate that rising temperatures could lead to a decline in faunal biodiversity and an increase in microbial abundance. Conversely, local thermal anomalies are targets for the efficient placement of shallow geothermal energy systems. The identification of hotspots in groundwater temperatures enables the reuse of waste heat and thus promotes the transition to sustainable heating energy.

The overall aim of this dissertation is to analyze the role of anthropogenic sources in subsurface warming by researching their thermal impact and environmental implications at different scales. Current research gaps that need to be addressed include a classification of relevant heat source types, methods that allow an assessment of the thermal impact of anthropogenic structures at different scales, tools for reducing the data scarcity of groundwater temperature data, and fundamental research of the environmental impact of local subsurface warming.

This work presents a holistic classification of anthropogenic sources that cause subsurface warming, characterizing all relevant heat source types in detail. Thus, a comprehensive review of the current state of research is provided, including potential environmental implications and approaches aiming to utilize waste heat in the subsurface.

In a next step, underground car parks, a heat source type significantly contributing to urban subsurface warming, are examined in a field study across cities in Austria, Germany, and Switzerland. A modeling approach using geospatial datasets projects the thermal impact of underground car parks on the city of Berlin, Germany. There, the annual heat energy emitted by 5,040 structures amounts to around 0.65 PJ. The findings reveal that underground car parks possess daily, weekly, and seasonal temperature patterns reacting to surface air and traffic frequency.

To tackle groundwater temperature data scarcity, we utilize satellite data of land surface temperatures and other variables to estimate groundwater temperatures for the German federal state of Saxony-Anhalt. The results, which were validated by repeated measurements from 436 wells, have the highest resolution (500 m) and accuracy (Root Mean Squared Error = 0.74 K) compared with other studies on groundwater temperature estimates. Besides, they show a strong dependence on anthropogenic land use.

The fourth and final focus of this thesis is to assess the environmental impact of a local temperature anomaly on shallow groundwater. Thereby, a heat plume caused by a water park with a basement is analyzed and results in an intensity of up to 9 K. However, no significant deterioration in groundwater quality or ecological status can be measured. This indicates that this type of eutrophic and anoxic aquifer is resistant to moderate heat stress.

## Kurzfassung

Die Erwärmung des Untergrunds tritt auf allen Skalen und in unterschiedlicher Intensität auf, von lokalen Mikroeffekten in der Nähe von Stromkabeln bis hin zu regionalen Makroeffekten aufgrund von Oberflächenversiegelung in Städten und sogar als globale Erwärmung des Untergrunds als Reaktion auf den Klimawandel. Die Folgen der Erwärmung des Untergrunds für die Grundwasserqualität und die Ökologie sind weitgehend unbekannt. Frühere Studien deuten darauf hin, dass steigende Temperaturen zu einem Rückgang der Artenvielfalt der Fauna und einer Zunahme der mikrobiellen Abundanz führen könnten. Andererseits bieten lokale Wärmeanomalien Vorzüge für die Anwendung oberflächennaher Geothermiesysteme. Die Identifizierung von Grundwassertemperatur-Hotspots ermöglicht dabei das Recycling von Abwärme und kann so die Wärmewende unterstützen.

Hauptziel dieser Dissertation ist, die Rolle anthropogener Quellen bei der Erwärmung des Untergrunds zu analysieren, indem ihre thermischen Auswirkungen und die Folgen für die Umwelt auf verschiedenen Skalen untersucht werden. Zu den aktuellen Forschungslücken gehören eine Klassifizierung der relevanten Wärmequellentypen, Methoden, die eine Bewertung der thermischen Auswirkungen von Bauwerken auf verschiedenen Skalen ermöglichen, Werkzeuge, welche den Datenmangel von Grundwassertemperaturdaten verringern, und grundlegende Kenntnisse über die Umweltauswirkungen durch lokale Erwärmung des Untergrunds.

In dieser Arbeit wird eine ganzheitliche Klassifizierung anthropogener Wärmequellen vorgestellt, indem alle relevanten Quelltypen detailliert charakterisiert werden. Somit wird ein umfassender Überblick über den aktuellen Stand der Forschung gegeben.

In einem weiteren Kapitel werden Tiefgaragen, die wesentlich zur Erwärmung des städtischen Untergrunds beitragen, innerhalb einer Feldstudie in Städten in Österreich, Deutschland und der Schweiz untersucht. Ein Modellierungsansatz unter Verwendung von Geodatenätzen projiziert dabei thermische Auswirkungen von Tiefgaragen auf die Stadt Berlin. Die jährliche Wärmeenergie, die dort von 5.040 Bauwerken abgegeben wird, beläuft sich auf etwa 0,65 PJ. Die Ergebnisse zeigen außerdem, dass Tiefgaragen tägliche, wöchentliche und saisonale Temperaturmuster aufweisen, die auf die Oberflächenluft und die Verkehrszeiten reagieren.

Um dem Mangel an Grundwassertemperaturdaten entgegenzuwirken, werden in einem weiteren Schwerpunkt Satellitendaten der Landoberflächentemperatur und anderer Parameter verwendet, um Grundwassertemperaturen für das Bundesland Sachsen-Anhalt vorherzusagen. Die Ergebnisse, die durch wiederholte Messungen an 436 Brunnen validiert wurden, weisen die höchste Auflösung (500 m) und Genauigkeit (Wurzel des mittleren quadratischen Fehlers = 0,74 K) unter aktuellen Studien. Sie zeigen zudem eine starke Abhängigkeit von der anthropogenen Landnutzung.

Der vierte und letzte Schwerpunkt dieser Arbeit ist die Bewertung der Umweltauswirkungen von lokalen Temperaturanomalien auf oberflächennahes Grundwasser. Obwohl die in der Fallstudie durch ein Schwimmbad mit Keller verursachte Wärmefahne eine Intensität von bis zu 9 K aufweist, kann keine signifikante Verschlechterung der Grundwasserqualität oder des ökologischen Zustands nachgewiesen werden. Dies deutet darauf hin, dass diese Art von eutrophem und anoxischem Aquifer gegen moderaten Hitzestress resistent ist.

## Publications

This thesis synthesizes the following four contributions (cumulative thesis):

▷ Chapter 2 has been published as:

**Noethen, M.**, Hemmerle, H., & Bayer, P. (2022). Sources, intensities, and implications of subsurface warming in times of climate change. *Critical Reviews in Environmental Science and Technology*, 53(5), 700–722, DOI:

<https://doi.org/10.1080/10643389.2022.2083899>.

*Author contributions.* Methodology: M.N.; Writing – original draft: M.N., P.B.; Writing – review & editing: M.N., H.H., P.B.; Visualization: M.N., H.H.; Funding acquisition: P.B.; Project administration & supervision: P.B.

▷ Chapter 3 has been published as:

**Noethen, M.**, Hemmerle, H., Menberg, K., Epting, J., Benz, S. A., Blum, P., & Bayer, P. (2023). Thermal impact of underground car parks on urban groundwater. *Science of the Total Environment*, 903, 166572, DOI:

<https://doi.org/10.1016/j.scitotenv.2023.166572>.

*Author contributions.* Methodology: M.N.; Writing – original draft: M.N.; Writing – review & editing: M.N., H.H., K.M., J.E., S.B., Ph.B., Pe.B.; Visualization: M.N.; Funding acquisition: Pe.B.; Project administration & supervision: Pe.B.

▷ Chapter 4 has been published as:

**Noethen, M.**, Hemmerle, H., Meyer, L., & Bayer, P. (2024). Prognose der oberflächennahen Grundwassertemperatur in Sachsen-Anhalt. *Grundwasser – Zeitschrift der Fachsektion Hydrogeologie*, DOI:

<https://doi.org/10.1007/s00767-024-00570-z>.

*Author contributions.* Methodology: M.N., H.H.; Writing – original draft: M.N.; Writing – review & editing: M.N., H.H., L.M., P.B.; Project administration & supervision: P.B.

▷ Chapter 5 has been published as:

**Noethen, M.**, Becher, J., Menberg, K., Blum, P., Schüppler, S., Metzler, E., Rasch, G., Griebler, C., & Bayer, P. (2024). Environmental impact of an anthropogenic groundwater temperature hotspot. *Science of the Total Environment*, 955, 177153, DOI:

<https://doi.org/10.1016/j.scitotenv.2024.177153>.

*Author contributions.* Methodology: M.N., J.B., C.G.; Writing – original draft: M.N.; Writing – review & editing: M.N., J.B., M.K., Ph.B., S.S., E.M., Pe.B., G.R., C.G.; Supervision: Pe.B.

## Acknowledgments

I would like to express my deepest gratitude to everyone who has supported and guided me throughout my PhD journey. Without your encouragement, advice, and contributions, this work would not have been possible.

My greatest thanks go to my supervisor, Prof. Peter Bayer, for his constructive feedback and continuous support, but especially for his constant encouragement throughout the process. His expertise and motivation have been invaluable and I am very grateful for the opportunity to conduct research in Halle and write my thesis.

A special thanks goes to my colleagues for their collaboration and contributions. It has always been a pleasure to be part of the Applied Geology group at the University of Halle. Colleagues became friends and I am grateful for the good times we spent in Halle and the memories we created.

I would like to thank the co-authors of my research projects outside Halle who have supported and advised me in many ways, especially Philipp Blum, Kathrin Menberg, Susanne Benz and Jannis Epting. I would also like to thank the various members of the authorities in Saxony-Anhalt and throughout Germany who provided me with substantial support and valuable data during my research.

I am also thankful to the Bachelor's and Master's students as well as the student assistants, I was able to work with, for their dedication in the field and desk work and their commitment to the projects.

On a personal note, I am eternally grateful to my parents for their unconditional support, no matter where I go or what I do. My deepest thanks go to my wife Anne for her unwavering belief in me and for boosting my motivation by sharing the same dreams.

Finally, I would like to thank the Deutsche Bundesstiftung Umwelt (DBU) for providing financial support through a PhD scholarship that made this research possible.

# Contents

Abstract .....	X
Kurzfassung.....	ii
Publications.....	iii
Acknowledgments.....	iii
Contents .....	v
List of figures .....	viii
List of tables .....	x
<b>1 Introduction .....</b>	<b>1</b>
1.1 Anthropogenic impact on subsurface temperatures and potential implications.....	1
1.1.1 Natural thermal conditions of the shallow subsurface.....	1
1.1.2 Anthropogenic influence on the thermal regime of the subsurface.....	2
1.1.3 Implications of subsurface warming.....	3
1.1.4 Legal situation.....	5
1.2 Scope and objectives of this thesis .....	5
<b>2 Sources, intensities, and implications of subsurface warming in times of climate change .....</b>	<b>8</b>
Graphical abstract .....	8
2.1 Abstract.....	9
2.2 Introduction.....	9
2.3 Classification of anthropogenic heat sources.....	10
2.4 Determination of the thermal impact .....	12
2.5 Sources of subsurface warming .....	14
2.5.1 Large-scale effects .....	14
2.5.2 Small-scale structures .....	17
2.5.3 Chemical heat generation .....	21
2.5.4 Geothermal systems .....	23
2.6 Implications.....	24
2.6.1 Environmental impact.....	24
2.6.2 Utilization of subsurface waste heat.....	25
2.7 Conclusions .....	26
<b>3 Thermal impact of underground car parks on urban groundwater .....</b>	<b>29</b>
Graphical abstract .....	29
3.1 Abstract.....	30
3.2 Introduction.....	30
3.3 Materials and methods .....	32
3.3.1 Underground car park temperatures.....	32
3.3.2 Impact of underground car parks on subsurface warming of Berlin.....	34
3.4 Results and discussion.....	36
3.4.1 Underground car park temperatures.....	36
3.4.2 Impact of underground car parks on subsurface warming of Berlin.....	42
3.5 Conclusions .....	47
<b>4 Estimation of shallow groundwater temperatures in Saxony-Anhalt, Germany .....</b>	<b>49</b>

4.1	Abstract .....	50
4.2	Introduction .....	50
4.3	Materials and methods .....	51
4.3.1	Study area .....	51
4.3.2	Measurement and remote sensing data .....	52
4.3.3	Current state of research .....	53
4.3.4	Calculation and evaluation of the groundwater temperature .....	54
4.4	Results and discussion .....	55
4.4.1	Spatial distribution of groundwater temperature .....	55
4.4.2	Comparison between measured and estimated groundwater temperature .....	58
4.4.3	Influence of land use on groundwater temperature .....	59
4.5	Conclusions .....	61
<b>5</b>	<b>Environmental impact of a groundwater temperature hotspot .....</b>	<b>62</b>
	Graphical abstract .....	62
5.1	Abstract .....	63
5.2	Introduction .....	63
5.3	Materials and methods .....	65
5.3.1	Study site .....	65
5.3.2	Temperature monitoring and sample collection .....	66
5.3.3	Sample analysis .....	67
5.3.4	Classification of the ecological state .....	68
5.4	Results and discussion .....	69
5.4.1	Thermal impact on groundwater .....	69
5.4.2	Environmental impact of groundwater heating .....	71
5.5	Conclusions .....	77
<b>6</b>	<b>Synthesis .....</b>	<b>79</b>
6.1	Conclusions: Findings in the field of subsurface warming .....	79
6.2	Outlook .....	81
6.2.1	Relevance of local heat sources .....	81
6.2.2	Utilization of waste heat .....	81
6.2.3	Environmental response to subsurface warming .....	82
6.2.4	Legislation and recommendations for mitigation strategies .....	83
	<b>Appendices .....</b>	<b>84</b>
	Appendix A .....	84
	Appendix A-1: Temperature analysis datasets .....	84
	Appendix A-2: List of input parameters .....	85
	Appendix A-3: Air temperature comparison .....	86
	Appendix A-4: Maps of input data for the spatial analysis .....	87
	Appendix A-5: Temperature correlation plots for all sites .....	88
	Appendix A-6: Spatial Analysis results .....	89
	Appendix A-7: Uncertainties of spatial analysis results .....	90
	Appendix A-8: Parameter sensitivity .....	90
	Appendix B: Original version of chapter 4 in German language .....	91
	Appendix B-1: Zusammenfassung .....	91
	Appendix B-2: Einleitung .....	91
	Appendix B-3: Materialien und Methoden .....	93
	Appendix B-4: Ergebnisse und Diskussion .....	97

Appendix B-5: Fazit.....	104
Appendix C .....	105
Appendix C-1: Comparison of regression methods .....	105
Appendix C-2: Assignment of CLC classes .....	106
Appendix C-3: Estimation outliers .....	106
Appendix C-4: Results and errors per CLC group .....	106
Appendix C-5: Measurement frequency and repetitions.....	107
Appendix D .....	108
Appendix D-1: Complete sets of temperature depth profiles.....	108
Appendix D-2: Results of measured parameters per location.....	109
<b>References</b> .....	<b>I</b>
<b>Curriculum vitae</b> .....	<b>XVI</b>
<b>Declaration / Erklärung</b> .....	<b>XVIII</b>

# List of figures

Figure 1.1. Schematic temperature profile above and below ground (modified after Stauffer et al., 2013). The temperature variation in the shallow subsurface induced by seasonal air temperature fluctuations is indicated by the dashed lines. .... 1

Figure 1.2. Impressions of field studies from top to bottom: an observation well in an agricultural landscape; temperature measurement technique using an electric contact gauge; measurement of groundwater temperatures close to an underground car park; measurement of groundwater temperatures in the city center of Halle (Saale), Germany. .... 2

Figure 1.3. Illustration of the thermal impact of different heat sources (top) as a “hot footprint” and possible implications on the shallow subsurface (bottom). .... 4

Figure 2.1. Graphical overview of anthropogenic heat sources. SGES: Shallow Geothermal Energy Systems, STES: Seasonal Thermal Energy Storage. .... 11

Figure 2.2. Cases of unintended anthropogenic groundwater heating. This overview provides examples of anthropogenic structures heating groundwater. Note that the comparability of these examples is limited due to different local conditions, measurement techniques, and distances to the heat source. .... 13

Figure 2.3. Literature examples of the Anthropogenic Heat Flux (AHF) for different heat sources. Note that different methods were used to calculate the AHF and some studies give the average AHF of a heat source, while others give the AHF of single structures. The “heating” values describe a heat flux into the subsurface and the “cooling” values vice versa. .... 14

Figure 2.4. Summary of studies showing temperature change in the subsurface per decade. The historical data for the northern hemisphere (NH) air temperature is taken from Osborn et al. (2021). Note that the study from Northumberland, UK, includes data from 1907 to 2011. .... 15

Figure 2.5. (a) Time series of the groundwater temperature (urban GW) in a well 10 m next to an underground car park (UCP) and the indoor temperature at the lowest level. Additionally, the groundwater temperature of an undisturbed well outside of Cologne is plotted to show the rural background in the regarded time span. (b) Map of Berlin Wilmersdorf, Germany, showing the groundwater temperature at 15 m depth in 2016 as well as the location of subway tunnels. A strong thermal anomaly was detected in the close vicinity of a subway tunnel. Data from Henning (2016). Note that this map only shows the relevant section of the study area. Basemap: OpenStreetMap. (c) Scatter plot of groundwater temperature and pH in Bitterfeld, Germany. Wells downstream of a landfill and a waste-to-energy plant show elevated temperatures, while the groundwater downstream of the landfill is also acidic. Mean values of 16 wells between 2017 and 2021 were provided by local authorities (LHW, 2023). .... 18

Figure 3.1. Map of the study sites. Cities with studied UCP sites are indicated by dots. Berlin is represented by the city area. .... 32

Figure 3.2. Workflow chart of the calculation of heat fluxes from the measured UCPs (left) as well as the heat fluxes and heat flows for UCPs in Berlin and the anthropogenic heat flux of UCPs ( $AHF_{UCP}$ ) per district (right). Detailed versions of the maps on the right can be seen in Figure A2.  $\Delta T$ : temperature difference, U-value: thermal transmittance. .... 34

Figure 3.3. Temperature-depth-profiles of a public (Zürich #1) and a private UCP (Zürich #2), measured in observation wells inside the UCP. At the top, the UCP temperature range per level is shown with a bar, while the average groundwater temperature at 20 m bgs is indicated with a dashed line. .... 37

Figure 3.4. Time series of groundwater temperature ( $T_{GW}$ ), UCP temperature ( $T_{UCP}$ ), and surface air temperature ( $T_{Air}$ ) for six UCPs as well as temporally resolved heat fluxes through the slab into the groundwater. .... 38

Figure 3.5. UCP temperature ( $T_{UCP}$ ) and surface air temperature ( $T_{Air}$ ) correlation for six selected sites. The colors indicate the level of the UCP at which the measurement was taken. The bottom diagram contains the data for all 31 sites and the average of the results of each individual regression for the respective levels. All plots have a dashed identity line as reference. The number of measurements is marked with an n. .... 40



Figure 3.6. Weekly averaged time series of the UCP temperature ( $T_{UCP}$ ) and daily mean values for public (red) and private (green) UCPs. Thick lines represent a rolling mean (6 h) of all publicly and privately studied sites.....	41
Figure 3.7. Violin plots of the temperature difference ( $\Delta T$ ) between UCP and surface air at each level. The dots represent mean values of the individual UCPs. The number of UCPs is marked with an n. ....	41
Figure 3.8. (a) Map of Berlin showing the mean heat flux through slabs ( $q_{slab}$ ) into the groundwater per city quarter. The dashed line shows the approximate boundary of the glacial valley. (b) Map of the total heat flow ( $Q$ ) from UCPs into the groundwater per city quarter. The black polygons represent the UCPs. Districts are labeled and delimited with black lines. Hatched areas have insufficient data. Background map source: OpenStreetMap.....	43
Figure 3.9. Monthly heat flux through slab and wall and average annual heat flux from each UCP in Berlin ( $n = 5040$ ). ....	45
Figure 4.1. Maps of Saxony-Anhalt with the datasets used: (a) raster data of the Land Surface Temperature (LST); (b) raster data of Evapotranspiration (ET); (c) raster data of Snow Days (SD); (d) raster data of Building Density (BD); (e) raster data of CORINE Land Cover (CLC); (f) point data of selected monitoring wells (GWM). ....	53
Figure 4.2. Regressor contributions for the calculation of the estimated groundwater temperature per monitoring well, shown as box plots. The dashed line shows the contribution of the y-axis intercept. The mean values are marked with diamonds. ET = Evapotranspiration, SD = Snow days, BD = Building density. ....	55
Figure 4.3. Estimated groundwater temperatures (eGWT) in Saxony-Anhalt with the measured groundwater temperatures (GWT) as points. ....	56
Figure 4.4. Average measurement depth and groundwater temperature (GWT) of all monitoring wells, shown as a scatter plot with boxplot of GWT distribution at the top. The colour of the pixels indicates the number of monitoring wells (GWM).....	57
Figure 4.5. Scatter plots showing the correlation of (a) estimated (eGWT) and measured groundwater temperature (GWT); (b) Land Surface Temperature (LST) and GWT. The color of the pixels indicates the number of wells (GWM). The errors are indicated by the Root Mean Square Error (RMSE) and the Mean Error (ME). The Spearman correlation coefficient is indicated by $r$ and the coefficient of determination by $r^2$ . ....	58
Figure 4.6. Difference between estimated (eGWT) and measured groundwater temperature (GWT) as boxplot per land use group. The number of measured wells in the respective land use group is indicated by n. The mean values are marked with diamonds. ....	60
Figure 5.1. (a) Location of Hockenheim in Germany. (b) Location of the Aquadrom in Hockenheim and the position of the three reference wells in the Reilingen forest. The water protection zone II is indicated by the blue area. (c) The Aquadrom Hockenheim with all observation wells which were used in this study. The temperature labels represent the arithmetic mean over the course of a year in 5 m depth. Colors indicate reference wells (green), thermally unaffected wells (blue), and thermally affected wells (red). Basemap: OpenStreetMap.....	66
Figure 5.2. (a) Time series of monitored groundwater and air temperatures. Groundwater temperatures were recorded in 5 m depth below surface level except at P9, where the logger was installed at a depth of 15 m. All time series were smoothed with a 24 h rolling mean. (b) Temperature depth profiles of all wells, taken in November 2022. The color groups indicate the position relative to the heat source: reference wells (green), thermally unaffected wells (blue), and thermally affected wells (red). Temperature depth profiles of all campaigns are depicted in Figure D1.....	70
Figure 5.3. Selected chemical parameters of groundwater samples taken in the wells at the Aquadrom Hockenheim (thermally unaffected/affected wells) and in the Reilingen forest (reference wells). Mean values are indicated by stars. sulphate concentration threshold defined by the German drinking water regulations is shown with a dashed line. Other threshold values are outside the data ranges and are given in Table D1. ....	73

Figure 5.4. Biotic parameters of groundwater samples taken in the wells at the Aquadrom Hockenheim (thermally unaffected/affected wells) and in the Reilingen forest (reference wells). Mean values are indicated by stars. ATP = adenosine triphosphate. ....75

Figure 5.5. D-A-C index of all samples, computed following a guided approach and correlated to the groundwater temperature (GWT). The dashed line shows the critical value of the chi-squared distribution at a 99% confidence level with three degrees of freedom. ....76

## List of tables

Table 5.1. Parameters included in the Groundwater Ecosystem Status Index (GESI) and results, determined according to Eq. 2. Mean values for each well are displayed. The Groundwater-Fauna-Index (GFI) was calculated according to Eq. 1. DOC = dissolved organic carbon; ATP = adenosine triphosphate; BA = bacterial abundance, FA = faunal abundance. ....77

# 1 Introduction

## 1.1 Anthropogenic impact on subsurface temperatures and potential implications

### 1.1.1 Natural thermal conditions of the shallow subsurface

Under natural conditions, subsurface temperatures are controlled by both the terrestrial heat flow and atmospheric temperatures. A heat flux of 50–110 mW/m<sup>2</sup> is constantly emitted from the Earth's interior (Limberger et al., 2018; Lucazeau, 2019; Pollack et al., 1993), while the thermal condition at the Earth's surface varies with climate and season. This coupling with the atmosphere leads to unstable temperature conditions in the shallow subsurface, resulting in diurnal and seasonal patterns (Allen, 2009).

In consequence, atmospheric temperature fluctuations are transmitted into the subsurface in a damped form. Conductive and advective heat transport influence these conditions. These processes vary locally with soil material and groundwater flow. The zone of seasonal atmospheric influence typically reaches down to 15 m below ground, beyond which thermal conditions are typically stable. Generally, temperatures of the undisturbed shallow subsurface (<100 m) correspond approximately to the annual average air temperature. With depth, temperatures increase by around 1 K per 30 m due to the constant heat flow from the Earth's interior (Stauffer et al., 2013; Stober & Bucher, 2012). A schematic temperature profile is depicted in Figure 1.1.

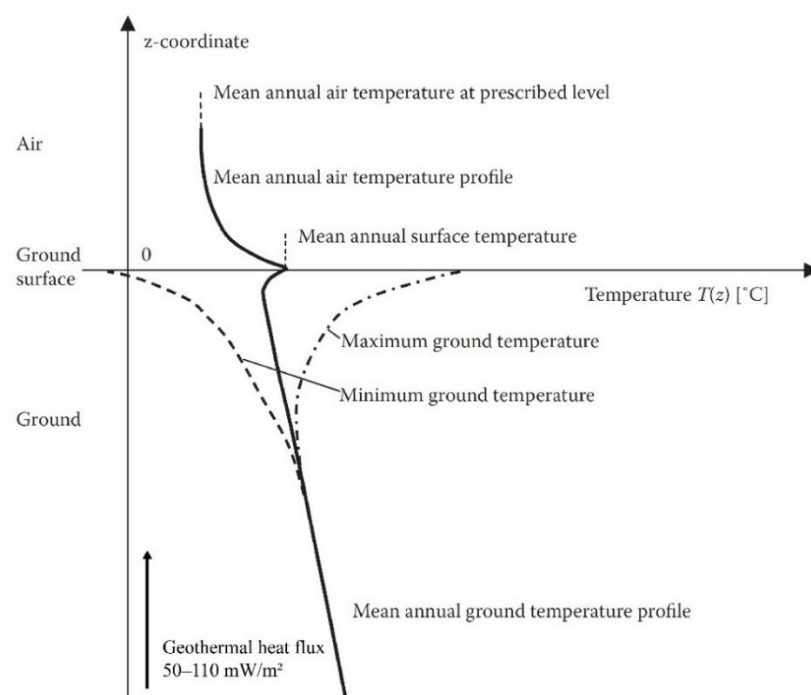


Figure 1.1. Schematic temperature profile above and below ground (modified after Stauffer et al., 2013). The temperature variation in the shallow subsurface induced by seasonal air temperature fluctuations is indicated by the dashed lines.

### 1.1.2 Anthropogenic influence on the thermal regime of the subsurface

Anthropogenic activities have been affecting the thermal conditions in the subsurface for centuries (Hemmerle et al., 2022; Visser et al., 2020). Agglomerations of heated buildings cause locally and regionally increased heat fluxes into the subsurface. The thermal signal of old European cities can be traced to depths of more than 100 m (Visser et al., 2020).

Today, a multitude of different anthropogenic heat sources additionally warms the subsurface. Among these, global climate change – driven by human-induced greenhouse gas emissions – has the most significant impact (Benz et al., 2024). Due to the coupling of atmospheric and soil temperatures, the warming of the Earth's atmosphere leads to a correspondingly intense warming of the shallow subsurface (Bates et al., 2008; Figura et al., 2011; Hemmerle & Bayer, 2020). The anthropogenic change in the surface thermal boundary condition can be measured as signals propagating downward. Additionally to this global phenomenon, anthropogenic structures, such as heated basements, tunnels, and swimming pools, heat the subsurface locally (Benz et al., 2015b; Menberg et al., 2013b).

Groundwater temperatures (GWT) can vary significantly depending on land use (see examples of land use in Figure 1.2). For example, in forests and agricultural areas, GWTs are minimally affected by human activities. In contrast, in densely urbanized areas, GWTs can be elevated by 2–5 K (Menberg et al., 2013a; Tissen et al., 2019). This increase results from the cumulative effect of numerous surface and subsurface heat sources and is commonly referred to as *Subsurface Urban Heat Island* (SUHI) (Ferguson & Woodbury, 2007; Hemmerle et al., 2022; Taniguchi & Uemura, 2005).

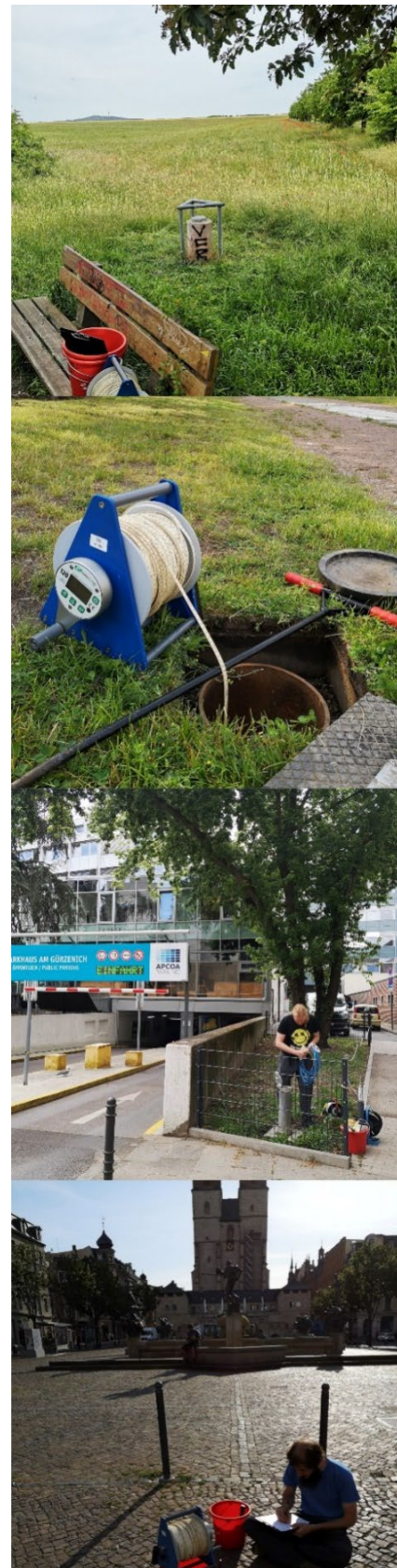


Figure 1.2. Impressions of field studies from top to bottom: an observation well in an agricultural landscape; temperature measurement technique using an electric contact gauge; measurement of groundwater temperatures close to an underground car park; measurement of groundwater temperatures in the city center of Halle (Saale), Germany.

However, in such highly developed landscapes, local anomalies can still be detected, e.g., negative outliers measured in urban green areas or positive outliers induced by buried district heating pipes leaking hot water.

Such anomalies are often caused by local anthropogenic heat sources. They can be classified according to their characteristics. For example, a distinction can be made between active and passive, intentional and unintentional influences: Geothermal applications actively and intentionally generate thermal changes in the subsurface and groundwater (Vienken et al., 2019).

For this reason, the effects of geothermal energy production on groundwater as a protected resource have been the focus of critical considerations (e.g., Beyer et al., 2016; Griebler et al., 2016; Hartog et al., 2013). Research questions about a potential threat to groundwater quality and the ecological balance were the subject of past research (Blum et al., 2021b; Brielmann et al., 2009; Griebler, 2015). There, results show that shallow geothermal energy applications can induce GWT changes leading to a degradation of groundwater quality and important ecosystem functions. With this background, Hahn et al. (2018) proposed the inclusion of the term “heat” as a type of pollution in national and European water directives for groundwater protection.

### *1.1.3 Implications of subsurface warming*

To consider whether heat is a contaminant, its impacts on the environment must first be researched. Local anthropogenic sources of subsurface warming and potential implications are illustrated in Figure 1.3. To date, initial research has been conducted aiming to understand the hydrochemical and ecological reactions of increased GWT. However, efforts by both authorities and science have not yet been able to clarify which specific GWT conditions and changes are justifiable as reference or guideline values (Blum et al., 2021b; Griebler et al., 2016).

Adapted to constant thermal conditions, both the shallow subsurface and groundwater form habitats for a variety of organisms. As the degree of thermal alteration is not known in most cases, any consequences for groundwater ecosystems are even more unclear. However, initial studies indicated that the highly adapted ecosystems in groundwater can be sensitive to thermal changes (Burns et al., 2017; Spengler, 2017). For groundwater fauna, a consistent negative correlation has been noted between GWT and the overall biodiversity in aquifers (Brielmann et al., 2009; Spengler & Hahn, 2018), as well as between GWT and the activity levels of individual crustacean species (Brielmann et al., 2011). Conversely, higher GWT yields improved conditions for bacteria (Brielmann et al., 2009; Liene et al., 2017), including *Legionella* in drinking water pipes, which grow in the temperature range of 25–50 °C (Agudelo-Vera et al., 2017; Bartram et al., 2007).

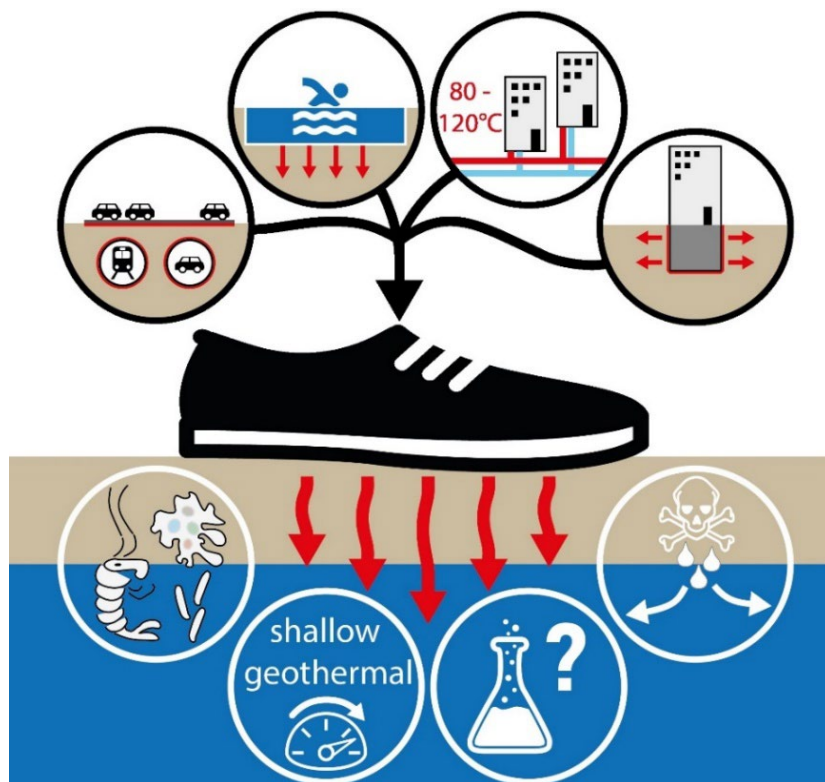


Figure 1.3. Illustration of the thermal impact of different heat sources (top) as a "hot footprint" and possible implications on the shallow subsurface (bottom).

Changes in GWT further influence geochemical and hydrochemical processes as well as the behavior of pollutants. Potential effects include increased dissolution, transport, and degradation of contaminants (Beyer et al., 2016). In areas affected by underground heat storage, where GWT can exceed 30 °C, water quality is expected to deteriorate due to the mobilization of substances such as organic carbon and heavy metals. Moreover, a reduction of dissolved oxygen can lead to anoxic conditions and initiate new redox processes (Griebler et al., 2016). Even a modest increase of just 1 K can reduce oxygen saturation by up to 4% and lower the pH by 0.02. Also, manganese, which is critical for drinking water production, is increasingly released and weathering processes are intensified (Riedel, 2019).

In contrast, additional heat in the subsurface can be recovered for heating applications, simultaneously cooling the subsurface to a natural level (Attard et al., 2020; Epting et al., 2020b). In this respect, the technically usable geothermal potential in urban areas can be increased by 40% compared to rural areas. At the same time, in anthropogenically heated environments, geothermal cooling applications are then less efficient (Di Donna et al., 2021). As a result, increasing attention is being paid to the recovery of waste heat in cities (Bayer et al., 2019). However, with the rising number of shallow geothermal energy system installations in urban areas, a demand for management of this resource becomes apparent to prevent interference between geothermal systems (Attard et al., 2020; Epting, 2017).



#### 1.1.4 Legal situation

In addition to the intentional thermal changes in the subsurface, the unintentional influences are often neglected. Thereby, the diversity of anthropogenic influences and causes complicate adaptations of regulation in practice, that would ideally be embedded in a binding legal framework.

The use of underground heating and cooling, and the thermal development of the subsurface in densely populated areas are potentially in conflict with the area-wide groundwater protection in many countries (Blum et al., 2021b). Despite intensive research into technical, economic, and ecological aspects, there is still a lack of clear (and science-based) regulations on the extent to which the thermal regime in the subsurface may be influenced (Vienken et al., 2016).

Hähnlein et al. (2010) reviewed the legal status of shallow geothermal energy use in 60 countries worldwide. They found that most countries lack regulations for absolute GWT thresholds. In countries with a legal framework, the permitted maximum induced temperature change ranges between  $\pm 3$  and  $\pm 11$  K relative to the initial GWT.

The thermal status of groundwater should be protected from avoidable anthropogenic influences (Griebler, 2015). Thermal changes in soil and groundwater are regulated in Germany concerning geothermal use – although not by legally binding limit values, but based on recommendations and guidelines of the federal states (Griebler, 2015; Hähnlein et al., 2011). For example, a discharge temperature between 5 and 20 °C is recommended for the operation of geothermal systems in the German state of Baden-Württemberg (Bauer et al., 2009). For unintended GWT changes, e.g., through tunnels, basements, or district heating networks, there are no legal frameworks worldwide (Blum et al., 2021b), although they can cause even higher GWT changes than would be permissible for geothermal applications (e.g., Menberg et al., 2013a; Yeşiller & Hanson, 2003).

Hence, the specifications of GWT limit values in the different countries are inconsistent and often not science-based. At the same time, such simple specifications in practice ignore the complexity of the real conditions (Hähnlein et al., 2011). By not considering the unintended thermal impacts, there is an imbalance between regulatory practice and the thermal conditions of the subsurface.

## 1.2 Scope and objectives of this thesis

To date, several open research questions remain in the field of subsurface warming: How much heat do different anthropogenic heat sources emit? How significant are these sources for the warming of the subsurface? Which implications do local temperature anomalies have on groundwater? What are meaningful threshold values for thermal pollution of groundwater?

In this thesis, the thermal effects of anthropogenic heat sources are to be investigated holistically. For this, known source types must first be classified and

categorized according to their characteristics. Detailed investigations, which include hydrogeological and thermal boundary conditions, are necessary to make statements on the relevance of individual heat source and recommendations on how to deal with thermal alteration of the subsurface.

To address research gaps, this thesis will focus particularly on heat sources that have not specifically studied in previous research, such as underground car parks and swimming pools. Thermal changes caused by geothermal technologies (e.g., borehole heat exchangers or groundwater heat pumps), which have already been studied in detail (e.g., Mielke et al., 2014; Vienken et al., 2019; Yasukawa et al., 2009), will be considered as references but not analyzed in depth. Focus is laid on the shallow groundwater, while the unsaturated zone is considered as a medium for heat transport. Hence, all implications of thermal alteration refer to shallow groundwater, but not the unsaturated zone. Further, this thesis prioritizes the local effects of heat sources. Since the overall impact of the heat source types is to be studied as well, transferring the local scale results to the regional scale becomes necessary.

The overall aim of this thesis is to analyze the anthropogenic sources for local subsurface warming in respect to their thermal impact and environmental implications at different scales. Thus, the following objectives are addressed in this thesis:

- i. The first objective is to identify and classify sources of subsurface warming according to their characteristics. A categorization enables joint consideration and adapted measures to counteract subsurface warming. In addition, a comprehensive overview of previous research on the sources of subsurface warming and the resulting implications is to be provided. This objective is tackled in **Chapter 2**, where, for the first time, a classification of anthropogenic heat sources is developed.
- ii. The second objective is to investigate the thermal impact of the heat source type *underground car parks*. This is realized in **Chapter 3** by examining existing as well as collecting new data at different sites across Central Europe. Thereby, the intensity and spatial development of thermal anomalies in the subsurface of this source type is investigated. Upscaling the thermal impact based on extensive spatial data sets enables assessing the contribution of underground car parks to city-wide subsurface warming.
- iii. The third objective, tackled in **Chapter 4**, is to further develop an approach to estimate shallow GWT with the help of remote sensing data. It aims to close the gap between the demand of highly resolved data of GWT distribution in planning, and the scarcity of information on subsurface properties. This estimation approach is to be applied on the state of Saxony-Anhalt, Germany.
- iv. The fourth objective aims on researching the implications of local thermal anomalies for the environment. For this, a case study at a water park is conducted in **Chapter 5**. New insights are gained by researching the



---

environmental impacts of a thermal plume on the groundwater environment at this site, with a particular focus on hydrochemical and ecological changes.

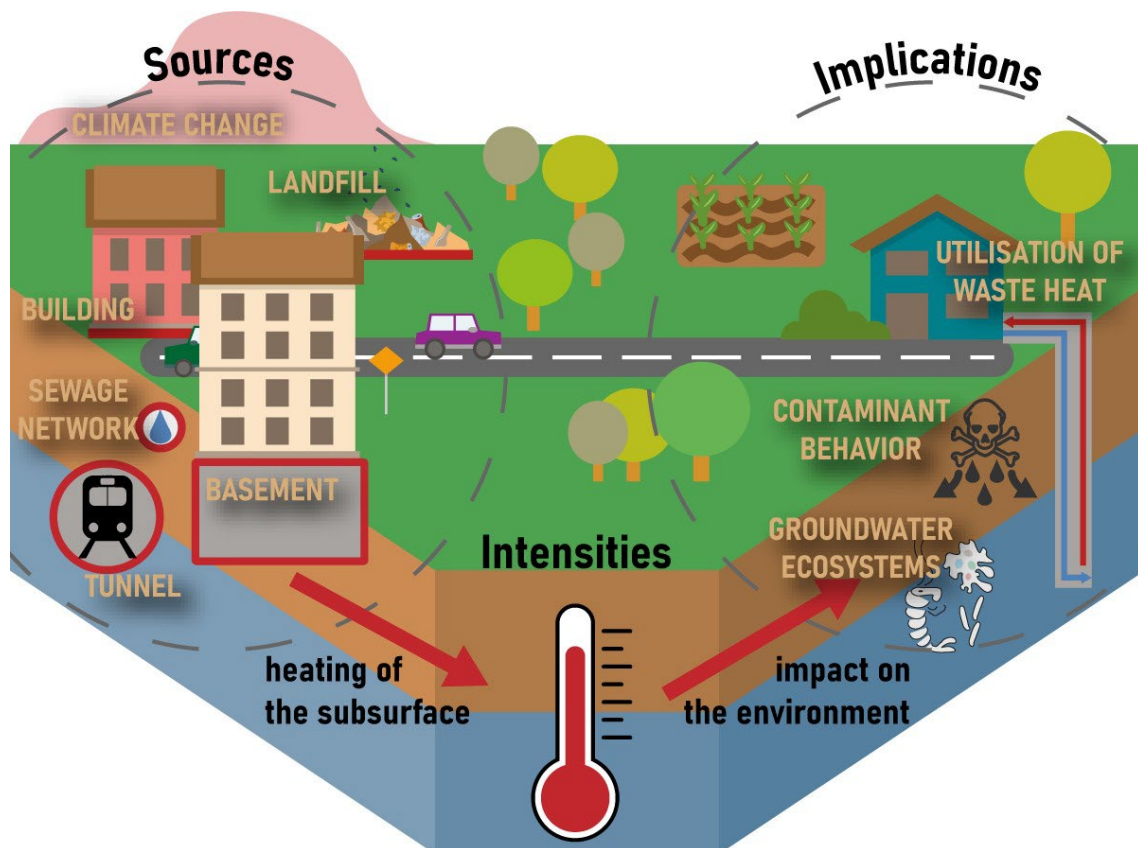
Based on the scientific studies in Chapters 2 to 5, Chapter 6 provides a summary of their findings and addresses the research questions outlined in the introduction, discussing the various advancements in the field of subsurface warming. Ultimately, the remaining and subsequent research questions to be tackled in the future are considered.

## 2 Sources, intensities, and implications of subsurface warming in times of climate change

This chapter is reproduced from:

Noethen, M., Hemmerle, H., & Bayer, P. (2022). Sources, intensities, and implications of subsurface warming in times of climate change. *Critical Reviews in Environmental Science and Technology*, 53(5), 700-722, DOI: <https://doi.org/10.1080/10643389.2022.2083899>.

### Graphical abstract



## 2.1 Abstract

Anthropogenic warming of the atmosphere is one if not the most pressing challenge we face in the 21st century. While our state of knowledge on human drivers of atmospheric warming is advancing rapidly, little so can be said if we turn our view toward the Earth's interior. Intensifying land use and atmospheric climate change condition the changing thermal state of the subsurface at different scales and intensities. Temperature is proven to be a driving factor for the quality of our largest freshwater resource: groundwater. But there is only insufficient knowledge on which sources of heat exist underground, how they relate in their intensity of subsurface warming, and which consequences this warming implies on associated environments, ecosystems, and resources. In this review, we propose a differentiated classification based on (1) the geometry of the heat source, (2) the scale at which the subsurface is heated, (3) the process that generates the heat, and (4) the intention of heat release. Furthermore, we discuss the intensities of subsurface warming, the density of induced heat fluxes, as well as their abundance, and draw implications for depending processes and ecosystems in the subsurface and the potential of recycling this waste heat with geothermal installations.

## 2.2 Introduction

Enhanced greenhouse gas emissions yield an imbalance in Earth's energy budget. Due to their great impact on climate change, priority is set on their effect on atmospheric global warming. Only around 5% of the excess heat is taken up by land (von Schuckmann et al., 2020) which manifests in trailing in-situ underground warming when compared to temperature trends in the atmosphere (Arias et al., 2021). Without surface warming, the thermal regime in shallow ground would be equilibrated and only respond to the seasonal oscillation in surface temperature in the top few meters (Taylor & Stefan, 2009). Meanwhile, the effects of global warming manifest down to depths of up to 100 m (Harris & Chapman, 1997; Lachenbruch & Marshall, 1986). Subsurface warming in response to atmospheric climate change is superimposed by human encroachment that changes the energy balance at the land surface. Especially in densely populated areas the thermal impact of direct anthropogenic land use is often more pronounced than the warming in response to climate change (Eggleston & McCoy, 2015). This has been measured worldwide in boreholes and groundwater wells, revealing a highly heterogeneous picture of man-made spatial and temporal temperature variations that chiefly represent interferences of multiple coexisting heat sources (Benz et al., 2017a). Local heat accumulation in the ground can be magnitudes higher than in the atmosphere but is transferred at much lower rates. As a consequence, recent anthropogenic warming imprints as a persistent signature in the subsurface (Pollack et al., 1998). Beneath many cities, the agglomeration of a multitude of anthropogenic heat sources evolved

so-called subsurface urban heat islands, with higher intensity and temperature stability than the far better-known surface and atmospheric urban heat islands (Ferguson & Woodbury, 2007; Menberg et al., 2013a; Oke, 1973; among others).

Knowledge of ground temperature and heat transport processes of individual heat sources is necessary to quantify energy flows in urbanized areas and for understanding the functioning of the ground as a heat sink and source (Bayer et al., 2019). Characterizing environmental impacts of subsurface warming, such as changes in microbial community compositions, possible deterioration of groundwater quality or contaminant behavior, is a pressing topic in environmental research. For example, heated ground cannot buffer hot summer days well and enhances heat waves in cities (Founda & Santamouris, 2017; Li & Bou-Zeid, 2013). Moreover, due to the high heat density of ground and groundwater, shallow geothermal energy is gaining attention as a renewable source for integrated heat and cold supply systems (Benz et al., 2015b; Kammen & Sunter, 2016). We can consider heated ground not only as a resource but also as natural laboratories of the conditions to be expected in the future. Unchanged global warming will continue to increase the previously long-term stable temperature of the shallow ground by several degrees during the next decades (Arias et al., 2021; Figura et al., 2015; Gunawardhana & Kazama, 2011). Permanent direct anthropogenic heat release, as it has been occurring especially in urbanized areas for at least a century, has generated modified environments that project the conditions in non-urban areas in the next century.

The objective of this study is to characterize the diversity of different anthropogenic sources that yield local ground heating, which is fundamental for understanding their interaction in areas that are heavily altered. We discuss different classification schemes and review source types, the degree, and consequences of anthropogenic ground heating. Special focus is set on thermal alteration of shallow groundwater due to its vital role as the largest resource of freshwater on Earth, as a widely unexploited energy resource, and as an important environmental variable in subterranean and groundwater dependent ecosystems.

## 2.3 Classification of anthropogenic heat sources

Anthropogenic heat sources are defined by changing the natural thermal conditions in the subsurface. To our knowledge, there exists no classification of such sources, yet. This is surprising considering the many common features, causes and effects, as well as their global appearance. We propose a classification based on the following four main characteristics:

1. The scale and size of the thermally affected zone of the heat source. The scale can be attributed to be either of global, regional, or local dimension. The local extent comprises thermal diameters of the size of centimeters (e.g., power cables) to a couple of hundred meters (e.g., infiltration). Regional scale

phenomena appear over the extent of several kilometers and are typically very large alterations of the thermal natural state induced by mining, extensive shallow geothermal applications, or altered microclimatic conditions, as often found in cities. We consider climate change as the only global heat source under which the shallow subsurface is heated by recent ground surface and atmospheric temperature rise.

2. The geometry of the heat source: We define the geometry as seen from the aerial perspective into polygonal, linear, and punctual. The geometry is particularly important for implementation of heat sources in numerical and analytical models. While most heat sources have a polygonal shape (e.g., buildings), there also exist multiple linear geometries which are typically associated to networks of pipes. Punctual geometries are found around boreholes of, for example, geothermal systems, when the projected shape is considered.
3. The process that generates or emits the heat: The processes defined in this study are long-term responses to atmospheric climate, heat release from actively heated structures (e.g., basements) and passively heated structures (e.g., trains in subway tunnels), influx of a heated fluid (leak), or (bio)chemical in-situ heat generation. Some sources are associated with different processes.
4. Further, we distinct by the intention of the heat release: Thermal alteration of the subsurface is usually only intended by application of geothermal facilities. For all other sources, the thermal change is unintended.

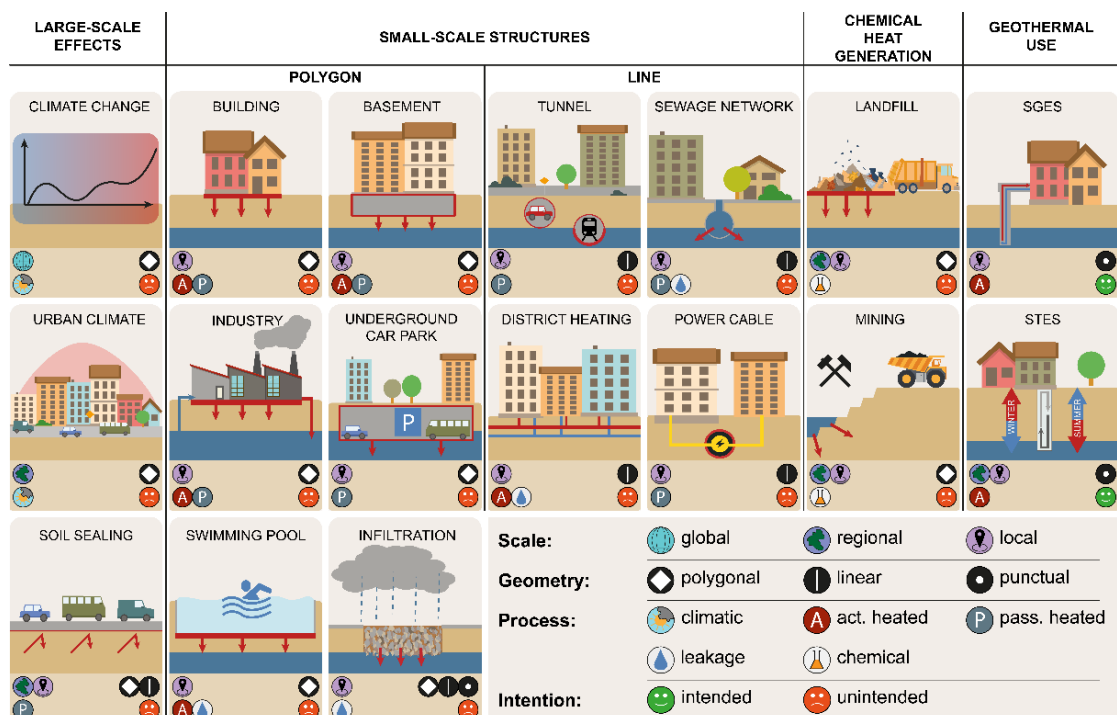


Figure 2.1. Graphical overview of anthropogenic heat sources. SGES: Shallow Geothermal Energy Systems, STES: Seasonal Thermal Energy Storage.

To introduce a comprehensible classification of primary heat sources, we decided to order them by their characteristics into large-scale effects, small-scale structures, chemical heat generation, and geothermal use as seen in Figure 2.1. To stay as concise as possible, we did not include the dimensions depth and time. We introduce the geometry as seen in map view perspective for easier implementation and to reduce the level of complexity in the description. Information on 3D geometries and the depth of thermal interaction with the environment is discussed individually for each heat source. The temporal resolution of the thermal interaction can be seasonally dependent both on the heat source itself as well as on ambient ground temperature in the seasonally affected zone. Seasonal variations of the heat source are especially relevant for shallow geothermal units, where seasonal heating or cooling is applied. However, most heat sources emit heat throughout the year. With the chosen classification, allocation in classes is not unequivocal. For example, the geometry of infiltration structures can be polygonal, linear, and even punctual.

## 2.4 Determination of the thermal impact

Investigating the thermal impact of a heat source requires in-situ measurement of soil or groundwater temperature. Observations from wells should be in close vicinity of only one heat source to avoid the influence and thermal overlapping of other sources. In practice, observation wells are typically scarce, and heat sources are rarely found as separate isolated structures, and thus interpretation of anomalous temperatures and their sources is often not straightforward. Examples of altered groundwater temperatures by different heat sources are given in Figure 2.2. Despite varying local conditions, measurement techniques and distances to the heat source, many of the polygonal and linear structures are in a comparable range of low subsurface temperature (12–30 °C). Geochemical heat sources, on the other hand, induce higher temperatures of 12–90 °C.

To evaluate the intensity of subsurface warming, the definition of a natural state (or background temperature), which is usually determined by the annually averaged conditions in unaffected rural surroundings (Epting & Huggenberger, 2013), is needed. Although the rural surrounding is not uniformly defined, values are often taken from agricultural or forest areas. This, however, already ignores potential anthropogenic impacts on temperature as caused by modifications of natural vegetation and groundwater level. Alternatively, the undisturbed shallow groundwater temperature can be approximated by the mean air temperature of a region, evapotranspiration, and snow cover period (Benz et al., 2017a).

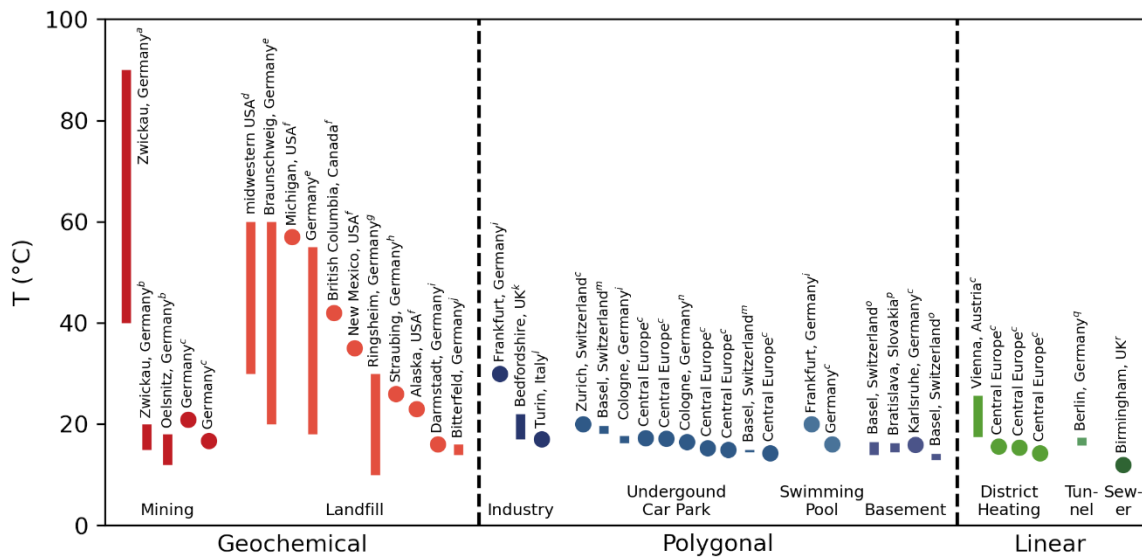


Figure 2.2. Cases of unintended anthropogenic groundwater heating. This overview provides examples of anthropogenic structures heating groundwater. Note that the comparability of these examples is limited due to different local conditions, measurement techniques, and distances to the heat source. <sup>a</sup> Willscher et al. (2010); <sup>b</sup> Felix et al. (2009); <sup>c</sup> Tissen et al. (2019); <sup>d</sup> Yeşiller and Hanson (2003); <sup>e</sup> Dernbach (1982); <sup>f</sup> Yeşiller et al. (2005); <sup>g</sup> Wiemer (1982); <sup>h</sup> Tidden and Scharer (2017); <sup>i</sup> Menberg et al. (2013b); <sup>j</sup> This study; <sup>k</sup> Westaway et al. (2015); <sup>l</sup> Bucci et al. (2017); <sup>m</sup> Becker and Epting (2021); <sup>n</sup> Zhu (2013); <sup>o</sup> Epting et al. (2017b); <sup>p</sup> Krcmar et al. (2020); <sup>q</sup> Henning (2016); <sup>r</sup> Ford and Tellam (1994).

When natural thermal conditions are known, the anthropogenic thermal impact can be quantified as anthropogenic heat intensity (AHI), which is determined by subtracting the median natural background temperatures from individual temperatures (Tissen et al., 2019). Further, the calculation of the anthropogenic heat flux (AHF) is possible. Different approaches have been applied that most often use analytical solutions and less frequently apply numerical models. Typically, they are based on Fourier's law of heat conduction to quantify vertical heat flux, considering parameters such as groundwater flow, ground thermal conductivity, and heat source type-specific insulation or leakage. Calculated AHFs for several heat sources and cities are compared in Figure 2.3. The large ranges of the AHFs result from high uncertainties in subsurface parametrization and methodological deviations. Most studies found strictly positive heat fluxes, indicating a warming of the subsurface. Only few studies reveal cases of reversed vertical heat fluxes, meaning a net cooling of the subsurface. Thermal coupling of soil and atmospheric temperatures causes an interplay of seasonal ground heat accumulation and loss. Heat sources with seasonally varying temperatures, such as tunnels or underground car parks, have the same effect. However, detailed investigations on the effect of anthropogenic structures on the seasonal temperature oscillation in the subsurface are scarce.

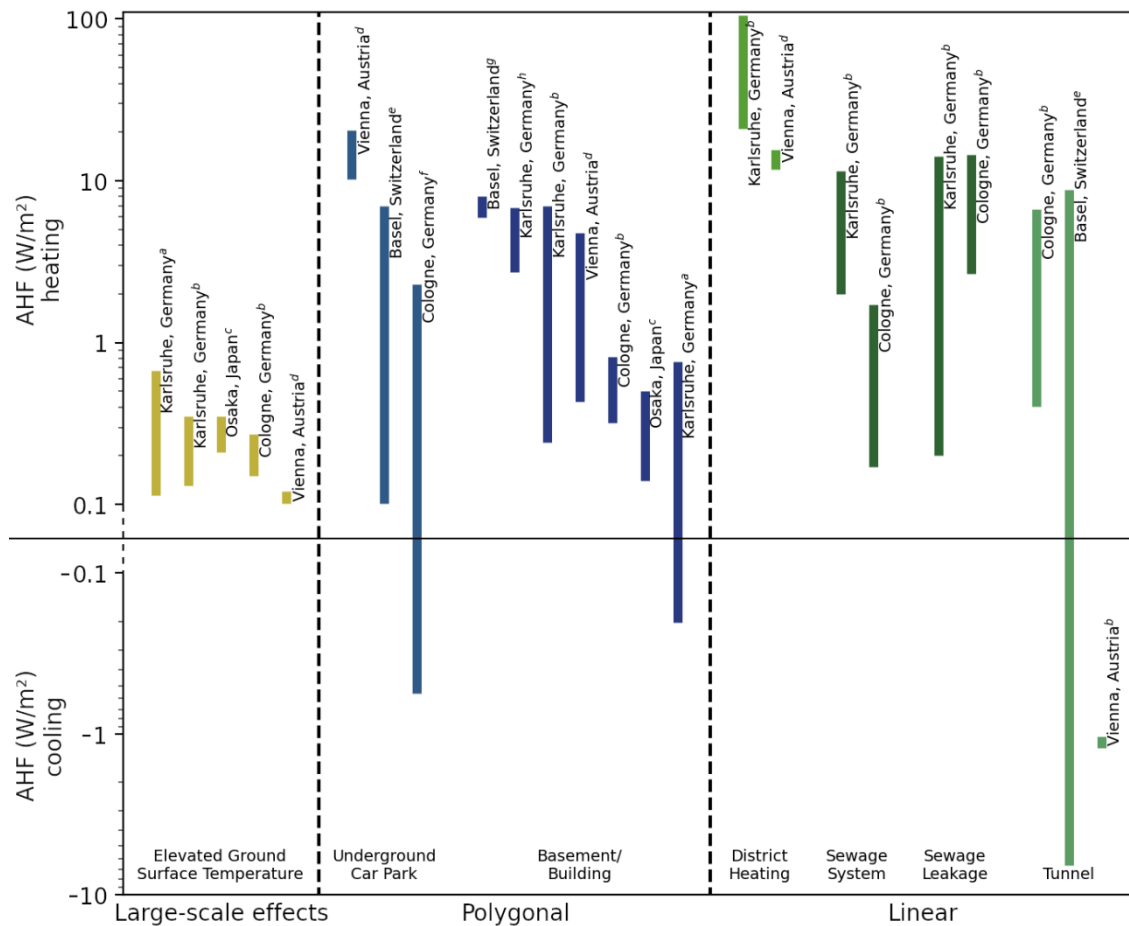


Figure 2.3. Literature examples of the Anthropogenic Heat Flux (AHF) for different heat sources. Note that different methods were used to calculate the AHF and some studies give the average AHF of a heat source, while others give the AHF of single structures. The “heating” values describe a heat flux into the subsurface and the “cooling” values vice versa. <sup>a</sup> Menberg et al. (2013a); <sup>b</sup> Benz et al. (2015b); <sup>c</sup> Benz et al. (2018b); <sup>d</sup> Tissen et al. (2021); <sup>e</sup> Becker and Epting (2021); <sup>f</sup> This study; <sup>g</sup> Mueller et al. (2018); <sup>h</sup> Lofi et al. (1977).

## 2.5 Sources of subsurface warming

### 2.5.1 Large-scale effects

The most acknowledged and largest source of subsurface warming is **climate change** (Arias et al., 2021). The thermal signal of atmospheric and land surface warming slowly propagates downward and changes the thermal conditions of the underground (Bense et al., 2020). It can be detected by analysis and inversion of borehole temperature profiles (Harris & Chapman, 1997; Pollack et al., 1998). Similarly, time series analysis of long-term temperature records logged at fixed depths reveals warming (Menberg et al., 2014). When time series of different depths are compared, time shifting of the thermal signal and attenuation with depth can be observed (Čermák et al., 2014; Hemmerle & Bayer, 2020).



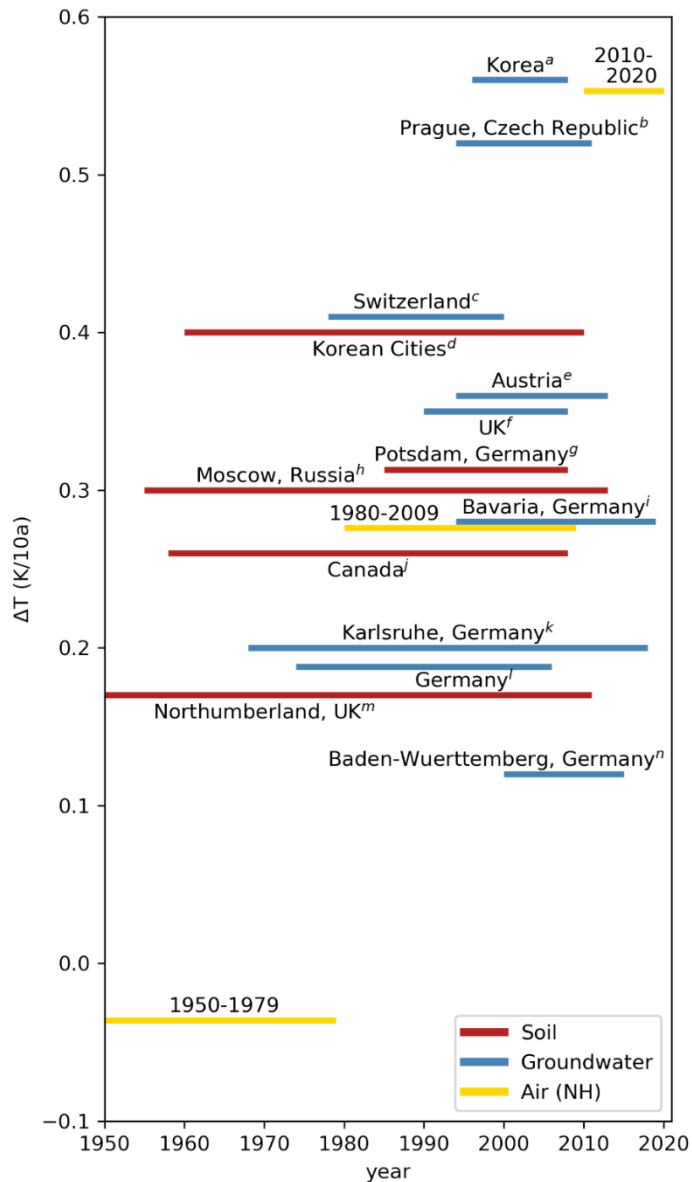


Figure 2.4. Summary of studies showing temperature change in the subsurface per decade. The historical data for the northern hemisphere (NH) air temperature is taken from Osborn et al. (2021). Note that the study from Northumberland, UK, includes data from 1907 to 2011. <sup>a</sup> Park et al. (2011); <sup>b</sup> Čermák et al. (2014); <sup>c</sup> Figura et al. (2011); <sup>d</sup> Cheon et al. (2014); <sup>e</sup> Benz et al. (2018b); <sup>f</sup> Bloomfield et al. (2013); <sup>g</sup> Henning and Limberg (2012); <sup>h</sup> Korneva and Lokoshchenko (2015); <sup>i</sup> Hemmerle and Bayer (2020); <sup>j</sup> Qian et al. (2011); <sup>k</sup> Blum et al. (2021b); <sup>l</sup> Menberg et al. (2014); <sup>m</sup> Luo and Asproudi (2015); <sup>n</sup> Riedel (2019).

A number of studies in the northern hemisphere recently focused on the thermal impact of climate change on groundwater in comparison to soil and atmosphere. Those that state a temperature lapse rate are summarized in Figure 2.4. The depicted comparison with the mean air temperature change does not account for regional variability of climate change. Aside from this, measurement depths are not consistent and potential local sources of subsurface warming are not further detailed. Still, clear trends are revealed. Studies conducted in cities report higher temperature increase, which is attributed to super-positioning of local heat sources and anthropogenic effects such as land use change and urban climate (Eggleston & McCoy, 2015). Climate change effects are often difficult to isolate and are ideally identified in areas with

minimal other anthropogenic influences. Also, single well measurements are barely representative. Instead, to mitigate the influence of local hydrogeological conditions such as groundwater depth, flow, and distance, elaborate probing in a significant number of wells at high spatial and temporal resolution is favourable (Benz et al., 2018b).

The studies summarized in Figure 2.4 show the evident link between air and subsurface temperature warming in the recent past. This trend is believed to continue according to the rise of air temperature (Blum et al., 2021b). Figura et al. (2015) predicted an increase in groundwater temperature in Swiss aquifers of 1.1–3.8 K by the end of the century, extrapolating a linear regression model for data between 1980 and 2009, while Gunawardhana and Kazama (2012) projected an aquifer warming of 1.0–4.3 K for the Sendai Plain in Japan in this period of time, depending on the applied climate scenario.

At the regional scale, the role of **urban climate** was described by Oke (1973) as an urban heat island (UHI) for air temperature. This regional rise in air temperature induces an increase in groundwater temperature beneath cities due to the coupling of air and soil temperatures (Henning & Limberg, 2012). Additional to this direct effect, there are numerous anthropogenic heat sources accumulated in cities that lead to a subsurface UHI. This regional phenomenon of elevated groundwater temperature in urban environments was extensively described in the past decades (Bucci et al., 2017; Taniguchi & Uemura, 2005) — accompanied by the emerging questions of utilizing and managing this resource (Attard et al., 2020; Mueller et al., 2018). However, most studies lack a detailed analysis on individual heat sources that cause local anomalies and agglomerate into subsurface UHIs.

A main driver of large-scale urban subsurface heat accumulation is **soil sealing** (Benz et al., 2018a). The heating effect of anthropogenic surfaces depends on several factors like material, albedo, emissivity, roughness, and the angle to the sun (Henning & Limberg, 2012; Scalenghe & Marsan, 2009), and hence differs strongly. Although material properties have been studied (Popiel & Wojtkowiak, 2013), as well as the soil sealing effect on the urban climate (Murata & Kawai, 2018), the large-scale impact on underground temperature is difficult to distinguish from other heat sources and has not been sufficiently investigated to date. However, several studies include elevated ground surface temperatures in the estimation of subsurface temperatures (Benz et al., 2015b; Hemmerle et al., 2019; Menberg et al., 2013b; Tissen et al., 2021)

Asphalt has been highlighted in the past as the material storing most solar energy (O'Malley et al., 2015), inducing the highest soil temperatures beneath it (Čermák et al., 2017). In comparison to a grass surface, asphalt can become almost 20 K hotter (LeBleu et al., 2019). In addition, surface sealing prevents air exchange between soil and atmosphere and mitigates latent heat fluxes by evapotranspiration and hereby further increases heat accumulation in the subsurface (Scalenghe & Marsan, 2009).

As shown in Figure 2.3, several studies have calculated the AHF of elevated ground surface temperatures. The ground surface temperature is not considered as a heat source itself but is influenced by soil sealing and urban climate. Hence, the ground surface temperature gives indirect information about anthropogenically elevated heat fluxes into the subsurface. The cited studies report values between 0.1 and 0.7 W/m<sup>2</sup>. In comparison to many other heat sources, these heat fluxes are at the lower end. However, the regional thermal impact of elevated ground surface temperatures is high due to its large spatial extent.

### 2.5.2 *Small-scale structures*

The anthropogenic heat sources that can be traced back to structures above or below the surface can generally be divided by the geometry in polygonal and linear structures. This characterization is especially useful for implementation of heat sources in models. Many of these heat sources share similar characteristics and are often summarized, for example, as “underground structures” (Attard et al., 2016b). Nevertheless, a closer look reveals features that are unique to each type and condition the specific heat transfer.

#### Polygonal structures

The most common anthropogenic surface structures are **buildings** without basements. They transmit heat via the ground slab to the subsurface. Although the influence of a single structure is often hardly observable, the large number of heated buildings makes them an important source of subsurface heating. Previous work in this context focused mainly on heat loss or “ground heat transfer” reduction in the field of civil engineering (Rees et al., 2000). Field tests and simulations have shown that the highest heat loss occurs at the slab edges (Thomas & Rees, 1998). Further studies have shown a strong influence of soil moisture and groundwater flow rate on the heat transfer (Janssen et al., 2004). Heat losses are highest for uninsulated buildings during the heating season (Adjali et al., 2000). Seasonal heating can be identified in temperature signals below buildings, which are rarely measured and difficult to access (Thomas & Rees, 1998).

**Industrial buildings**, such as factories or power plants, deserve special attention as they can have a large extent, strong local effects, and high indoor temperatures (Brinks et al., 2014). Also, reinjection of industrial cooling water directly into aquifers or cooling lakes can generate an additional heat input (Menberg et al., 2013a). Elevated groundwater temperatures caused by heat release from industrial buildings have been observed in particular in Europe (see Figure 2.2) (Bucci et al., 2017; Menberg et al., 2013a; Westaway et al., 2015).

Similar to buildings, heat loss from **basements** is of special interest in the field of civil engineering (Medved & Černe, 2002). Additional to the slab, here, heat is also transferred through the basement walls. Generally, the smaller the distance to the groundwater table and the higher the groundwater flow rate, the higher the heat

losses are (Bidarmaghz et al., 2019; Epting et al., 2017b). The heat flux drastically increases when the basement reaches into the saturated zone (Attard et al., 2016a; Epting et al., 2013). The thermal plume induced by basements was reported for a heated shopping center (Krcmar et al., 2020) and in different modeling studies (Attard et al., 2016a; Ferguson & Woodbury, 2004). Epting et al. (2017b) observed heat plumes reaching 16.5 °C in Basel, Switzerland, downstream of basements, and applied groundwater heat transport models to determine the influence of aquifer properties and building settings.

AHF's have been calculated in previous studies typically for both buildings and basements together, and heat losses through basement walls are not resolved in large-scale studies. The findings vary between  $-0.2$  and  $16 \text{ W/m}^2$ . Only Menberg et al. (2013b) show partly negative values, caused by spatial variability in groundwater temperature.

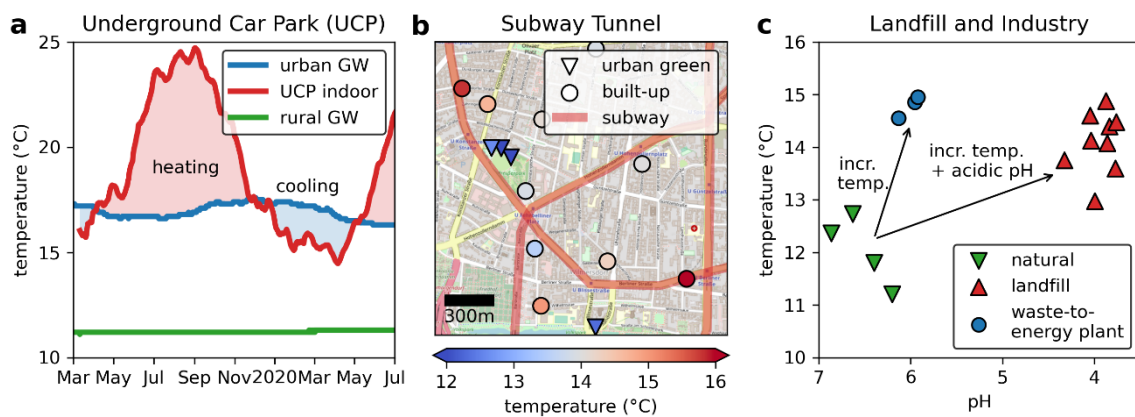


Figure 2.5. (a) Time series of the groundwater temperature (urban GW) in a well 10 m next to an underground car park (UCP) and the indoor temperature at the lowest level. Additionally, the groundwater temperature of an undisturbed well outside of Cologne is plotted to show the rural background in the regarded time span. (b) Map of Berlin Wilmersdorf, Germany, showing the groundwater temperature at 15 m depth in 2016 as well as the location of subway tunnels. A strong thermal anomaly was detected in the close vicinity of a subway tunnel. Data from Henning (2016). Note that this map only shows the relevant section of the study area. Basemap: OpenStreetMap. (c) Scatter plot of groundwater temperature and pH in Bitterfeld, Germany. Wells downstream of a landfill and a waste-to-energy plant show elevated temperatures, while the groundwater downstream of the landfill is also acidic. Mean values of 16 wells between 2017 and 2021 were provided by local authorities (LHW, 2023).

**Underground car parks (UCP)** have the same characteristics as basements, but they are typically larger and buried deeper in the subsurface. Therefore, the local thermal anomaly in the subsurface is generally higher as reported for several cities (Figure 2.2). Studies regarding UCPs have been dedicated to the role of the groundwater flow regime (Attard et al., 2016b) and the integration in urban underground management (Sartirana et al., 2020). For instance, Becker and Epting (2021) scrutinized the thermal impact of five UCPs in Basel, Switzerland, and found that the released heat strongly depends on UCP indoor temperatures and contact area with groundwater. The groundwater temperature measured downstream was increased by up to 2.7 K.

As a further example, we chose a 10 m deep UCP in the city center of Cologne, Germany (Figure 2.5a). The groundwater temperature is monitored at a well located in a distance of 10 m next to the UCP by a permanently installed datalogger. Additionally, we monitored the indoor temperature of the lowest floor at around 8 m depth. The groundwater table is deeper than the UCP at around 14 m, but the well shows an elevated groundwater temperature throughout the year. As background temperature of undisturbed conditions at the same depth, we refer to a well in the rural surroundings of Cologne, which has a temperature of around 11 °C. Therefore, the AHI of this well reaches 5–6.5 K in the studied period. During the summer months, the indoor temperature of the UCP is highest, mostly caused by high traffic of heated vehicles (Becker & Epting, 2021) and ventilation. The yearly peak in groundwater temperature at 17 m depth (17.7 °C) is shifted several months due to the depth distance of 4 m between UCP basis and groundwater. Although the influence of other heat sources can be expected, the elevated indoor temperature in the summer months indicates a strong heat flux rate into the surrounding soil and hence a local hotspot in subsurface temperature. Interestingly, from May to November, the indoor temperature is even below the groundwater temperature, thus inducing a reversed heat flow into the UCP. To put this in numbers, we calculated the AHF into the aquifer by Fourier's law, assuming a thermal conductivity of 1 W/(m·K) for the soil. The results show seasonally varying values between -0.6 and 2.3 W/m<sup>2</sup>. Other case studies, as shown in Figure 2.3, report higher AHF values, but no seasonally negative heat flux.

As containers of heated water, **swimming pools** have many similarities to structures for thermal energy storage like water-based closed seasonal thermal energy storage systems (Bott et al., 2019). However, their thermal impact depends even more on season, water temperature, and possible boiler rooms in the basement (Li et al., 2020). When it comes to heat losses of swimming pools, leakage has to be considered as well (Chapuis, 2010). Only few studies have observed elevated subsurface temperature in connection to swimming pools (Figure 2.2).

In times of increased groundwater scarcity, artificial recharge of groundwater by **infiltration** gains importance. Infiltration, which can be achieved in many different ways such as by basins (polygonal), trenches (linear), or injection wells (punctual), is generally summarized as managed aquifer recharge and has been applied for decades (Dillon et al., 2019). The infiltration of stormwater can have an impact on groundwater quality (Fischer et al., 2003) and temperature (Foulquier et al., 2009). Comparable to shallow karst systems, stormwater infiltration accelerates the recharge of groundwater and therefore increases the seasonal effect on groundwater temperature, whereas the long-term heating of groundwater is considered moderate (Foulquier et al., 2009). The greatest impact is to be expected in urban areas, where stormwater runoff is heated by artificial surfaces (LeBleu et al., 2019). Also, aquifer storage and recovery of stormwater yields an impact on groundwater quality,

including the temperature (Page et al., 2017). However, the thermal impact of artificial groundwater recharge is commonly neglected.

### Linear structures

**Tunnels** are one of the widest, deepest, and most abundant linear heat sources in the subsurface. Barla and Di Donna (2018) classified tunnels according to their thermal conditions, which can be either cold all year round (approx. 15 °C) in street tunnels and less frequently used railway tunnels, or hot (up to 30 °C in summer) in subway and deep mountain tunnels. Extreme temperatures of 35–40 °C, mainly heated by braking trains and passengers (Mortada et al., 2015), are observed in subway tunnels in several cities worldwide (Mortada, 2019). As with many other heat sources, groundwater flow strongly enhances heat exchange with the ground (Barla & Di Donna, 2018; Di Donna et al., 2021). Since these structures obstruct the natural flow of groundwater, the flow is often led through culvert pipes that further increase heat exchange (Epting et al., 2020a). Tunnels warming the ambient ground are a well-known phenomenon (Bidarmaghz et al., 2020), but are difficult to study as their main application in dense urban areas leads to an overlap with other heat sources. When considering the AHF of tunnels (Figure 2.3), car tunnels can both gain and lose heat seasonally depending on the atmospheric air temperature with the highest variations of indoor temperatures close to the exits (Becker & Epting, 2021). Case studies of car tunnels in Basel (Becker & Epting, 2021) and Vienna (Tissen et al., 2021) show net negative heat fluxes. This implies that car tunnels can cool down the subsurface, especially in urban space where the underground temperature is already elevated by anthropogenic use. Contrary to car tunnels, a case study of the subway tunnel system in Cologne (Benz et al., 2015b) reports positive heat fluxes all year round, implying that subway tunnels are warm enough during all seasons to release heat into the subsurface.

Henning (2016) investigated the subsurface temperature in the vicinity of subway tunnels in Berlin, Germany, to evaluate the magnitude of the induced temperature change. Additional to historical data from 1989 to 2014, groundwater temperature was measured in 23 observation wells, of which 14 are shown in the section, in the district Wilmersdorf in 2016 (Figure 2.5b). Only two wells show the thermal influence of the subway tunnel unequivocally. These two wells have the highest groundwater temperatures (17.4 and 15.8 °C) and the shortest distance (10 m, 30 m). The case study further illustrates the variety and superpositioning of heat sources in a city. The thermal anomaly caused by the tunnels is local and attenuated in the adjacent Preußenpark. Here, lower temperatures (11.4–12.6 °C), which are typically under urban green areas, were found.

**Sewers** have been identified as major heat source in the subsurface of cities (Menberg et al., 2013b; Tissen et al., 2021). Additionally to the conductive heat transport, leakage of wastewater yields a noticeable heat input (Benz et al., 2015b; Ford & Tellam, 1994). Leakages of sewer pipes are challenging to detect and quantify and are strongly varying regionally (Peche, 2019). While the temperature of

wastewater depends on several factors (Kretschmer et al., 2016), for Central European cities it is generally around 12–22 °C (Benz et al., 2015b; Cipolla & Maglionico, 2014; Schmid, 2008; Tissen et al., 2021). The AHF of sewage systems has been calculated by Benz et al. (2015b) for the cities of Karlsruhe and Cologne (Figure 2.3). In both cities, the average AHF from leakages is higher than the conductive heat loss of the conduits in the network. District heating pipes are also buried shallow in the ground.

Apart from a similar depth and linear shape, **district heating** pipes carry hot water of typically 60–120 °C and are usually well insulated. For economic reasons, heat losses are monitored and kept as low as possible, with typical values of 11–14% in Germany (Helbig & Weidlich, 2018). However, these numbers do not indicate whether heat loss is evenly distributed or local. Local hot spots can be caused by leakage and have been proven to be detectable by airborne thermography (Zhou et al., 2018). The effect of district heating networks on subsurface temperature can be considerable (Figure 2.2), and can for instance, result in snow melt at the ground surface (Arola & Korkka-Niemi, 2014). In Vienna, Tissen et al. (2019) detected groundwater temperatures of up to 25 °C (equalling an AHI of 13 K) in an observation well in 3.5 m distance to a district heating pipe. Relatively high AHFs of 11.8–104.7 W/m<sup>2</sup> are reported for Vienna and Karlsruhe (Figure 2.3). Such AHFs of district heating pipes can be calculated if heat loss values are accessible from public authorities. In order to reduce the consumption of fossil fuels, modern low exergy district heating systems (LowEx) utilize the different energy level needs and integrate renewable energy sources as well as waste heat from industry (Hepbasli, 2012). Because of the use of decentralized heat pumps, the supply temperatures can be kept below 45 °C (Schmidt et al., 2017). LowEx district heating systems generally have lower heat losses compared to district heating networks and therefore, the impact on subsurface temperature is reduced as well (Dolna & Mikielwicz, 2020).

Another linear heat source type is underground **power cables**. Conducting electricity warms the power cables up to 60 °C (Stegner, 2016). Numerical studies show the heat dissipation in the surrounding soil (Ochoń et al., 2015) depending on the bedding material (Stegner et al., 2017), whereas research about the overall impact on subsurface temperature is still lacking. Power cables are typically buried at shallow depth of a few meters (Stegner, 2016) to not interfere with groundwater; however, soil moisture and percolating water can significantly enhance the heat transfer (Kroener et al., 2014). In the course of ongoing energy transition and an accompanied rise in the electricity demand in many countries, there will be a broader use of high voltage power cables in the future and therefore, a growing impact on subsurface temperatures.

### 2.5.3 Chemical heat generation

Some anthropogenic sources lead to (bio)chemical reactions that generate heat in or at the (sub)surface. Often found in the proximity of cities, municipal solid waste

**landfills** are typical sources of in-situ underground heating. The generation of heat by biochemical decomposition processes is well studied (Yeşiller et al., 2005) and includes sequential aerobic and anaerobic phases over a period of several decades (Grillo, 2014). Yeşiller and Hanson (2003) monitored the temperature development in a landfill in the midwestern USA and found a warming rate of 2.6–4.0 °C/a depending on the waste age, while the rate of temperature increase is higher for newly deposited waste. Typically, a temperature of 30–60 °C is reached within landfills (Figure 2.2) (Coccia et al., 2013; Yeşiller & Hanson, 2003), even though 90 °C or higher can occur (Grillo, 2014). The lateral extent of the thermal anomaly of landfills can be substantial. For example, Mahmood et al. (2016) have observed a thermally affected zone of averagely 800 m radius using a remote sensing approach. Similar processes of biochemical decomposition can be observed at the aerobic fringe of contamination plumes (Tuxen et al., 2006). Warren and Bekins (2018) studied the heat generation at a crude oil-contaminated site with an AHI of up to 4.2 K in surrounding soil, where half of the heat is attributed to biodegradation while the other half originates from the oil pipeline itself, which is estimated to be 24 °C warm. The contamination is a source of chemical in-situ heat generation of polygonal geometry, whereas the pipeline acts as a passively heated, linear heat source.

As an example of a thermal anomaly caused by chemical heat generation, we present a landfill in Bitterfeld, Germany. This landfill is located in a coal mining area and is hosted in a former open pit mine that was filled with a mixture of overburden and industrial waste. The base of the landfill reaches into the groundwater saturated zone and causes a contamination of the groundwater downstream. Additional to the landfill as a heat source, a waste-to-energy plant was constructed in close vicinity. These two heat sources induce roughly the same temperature in the subsurface with an AHI of around 3 K, but also have a distinct chemical signature. The groundwater downstream the landfill has a higher acidity (pH below 4.5) compared to the ones downstream the waste-water plant, that show no or only a minor change in pH toward the upstream groundwater with pH values above 6 (Figure 2.5c). This exemplifies that the thermal anomaly of landfills can be correlated to exothermal processes, as illustrated in Figure 2.1. The waste-to-power plant represents an industrial building source with active heat generation.

Geochemical processes induced by **mining** can also generate heat. Especially coal mining has considerable effects on the in-situ thermal conditions. The effects are not restricted to the subsurface, but are also observed at heaps, where tailings and overburden are deposited above ground (Willscher et al., 2010). Aerobic conditions lead to the oxidation of sulfur by microbiological and particularly geochemical processes. By these, a temperature of up to 90 °C is induced in the center of heaps (Felix et al., 2009; Willscher et al., 2010). Furthermore, extreme subsurface temperatures of several hundred degrees can be reached by coal seam fires in open pit coal mines (He et al., 2020).



#### 2.5.4 Geothermal systems

The thermal impact of geothermal systems on groundwater is well studied, as their efficiency and sustainability depend on the initial as well as altered thermal conditions (Rivera et al., 2015). Since geothermal systems rely on heat exchange, the interference within the natural thermal regime is classified as both active and intended. While supplying heat for buildings is the standard application of geothermal heat pumps, the demand of geothermal energy for cooling applications is increasing (Ampofo et al., 2006) in response to global climate change (Epting et al., 2017a). There is a growing focus on solutions with sustainability and longevity, both to store and to extract thermal energy depending on the seasonal demand (García-Gil et al., 2020b). Therefore, geothermal systems can show high variability in the thermal impact throughout the year. Overall, the continuously rising number of geothermal systems and energy geostructures has an increasing impact, especially in densely populated areas (Epting et al., 2017a; Epting et al., 2013; Menberg et al., 2013a).

The most popular application of shallow geothermal energy systems (**SGES**) are ground source heat pumps. A heat carrier fluid is pumped in a closed-loop through heat exchanger tubes installed in vertical (borehole heat exchanger) or horizontal (ground heat exchanger) direction. In contrast, open-loop systems, are dependent on productive aquifers because of the direct utilization of groundwater as heat carrier fluid and are called groundwater heat pumps for this reason (Bayer et al., 2019). Such systems usually are operated with an extraction well and injection well. The thermal impact of SGES is determined by several factors like the number and depth of the boreholes, the induced temperature reduction or rise (heating or cooling), the groundwater pumping rate and the local geological and hydrogeological conditions. By knowing operating conditions and effective subsurface parameters, the induced thermal impact can be estimated. Some works monitored the thermal impact of closed-loop systems (Vienken et al., 2019) or open-loop systems (García-Gil et al., 2020b). Unlike other heat-emitting anthropogenic structures, geothermal systems underlie regulations and laws regarding the induced change of the thermal conditions. Hähnlein et al. (2010) compiled the legal status of shallow geothermal energy use in 60 countries worldwide and found that most countries have no regulations for absolute temperature thresholds, while these countries, which have a legal framework, permit a maximum induced temperature change between  $\pm 3$  and  $\pm 11$  K relative to the initial groundwater temperature.

Ground-based seasonal thermal energy storages (**STES**) are operated as closed systems like boreholes, pits, tanks, caverns, or as open systems directly in the aquifer (ATES) (Bott et al., 2019). Even if lateral heat loss is mitigated by insulation for the closed STES systems, local warming of the ambient subsurface can often be observed. The thermal impact of STES systems varies strongly and is dependent on a number of factors like the type, dimensions, temperature difference to the surrounding environment, possible insulation, and the local geological and hydrogeological

conditions. 99% of all ATES systems worldwide are operated at low storage temperatures below 25 °C, while well depths strongly vary between 20 and 1,200 m (Fleuchaus et al., 2018). Numerical simulation of low-temperature borehole TES shows a temperature rise of 2 K in 100 m distance after 30 years of operation (Mielke et al., 2014). For pit and tank TES, the heat losses are dependent on the geometry, dimension, and insulation of the storage facility. Here, operating temperatures can be as high as 80 °C (Bott et al., 2019). The thermal impact of pit and tank TES systems are rarely monitored, however, Bauer et al. (2008) observed more than 40 °C at 4.3 m below a storage after 10 years of operation, and Bodmann and Fisch (2004) report 30 °C at 4 m depth next to a storage. Bai et al. (2020) validated numerical models of predicted heat dissipation in the ground by an experimental study. The results show a good accordance between experimental and numerical study and furthermore, a storage efficiency of 62%, with a 70% fraction of the heat losses to the surrounding soil.

## 2.6 Implications

### 2.6.1 Environmental impact

It is known that thermal alteration of the subsurface poses numerous environmental threats on ecosystems hosted in the soil water, the unsaturated, and the saturated zone, as well as on groundwater dependent ecosystems (Briemann et al., 2009; Griebler et al., 2016). Temperature also is known to control bacterial activity and contaminant behavior and can hereby affect the quality and usability for the freshwater supply of groundwater, world's largest drinking water resource (Bonte et al., 2011). Environmental research is mainly focused on the impact of geothermal systems, while only few studies have considered the impact of unintended heat sources so far. However, findings from the field of geothermal energy are generally applicable to other heat sources, as long as the thermal change is comparably low, for example, for ATES, and the heat transferring process is similar, for example, conduction and advection.

Healthy **groundwater ecosystems** are generally the driving factor of groundwater quality. Their microbiological communities are adapted to constant conditions, where a change in temperature will cause shifts in community composition and microbial diversity (Briemann et al., 2009; Griebler et al., 2016; Retter et al., 2021). Another issue of groundwater quality is the abundance of prokaryotic cells, which may increase along with a rise in temperature (Lienen et al., 2017). However, Briemann et al. (2009) underlined that while a temperature increase stimulates metabolism, bacteria require energy to grow, which is limited in clean and oligotrophic groundwater systems. Also, Hartog et al. (2013) did not observe any correlation between bacteria quantities and temperature at a monitored ATES site (11–35 °C), while García-Gil et al. (2018a) even revealed a decrease in waterborne pathogenic bacteria in relation to shallow

groundwater heat pump systems, possibly due to a heat shock inflicted by the heat pumps. With groundwater fauna, a negative relationship was regularly observed between water temperature and biodiversity (Briemann et al., 2009; Spengler & Hahn, 2018) as well as the activity of individual species of crustaceans (Briemann et al., 2011).

Increasing subsurface temperature especially in the urban environment leads to higher temperatures in **drinking water distribution systems** (DWDS) (Müller et al., 2014). Although most countries have no legal standards for drinking water temperature, some countries recommend temperature limits of 20 or 25 °C at the tap to avoid extensive bacteria growth (Agudelo-Vera et al., 2020). In particular, Legionella infection poses a threat to drinking water safety, when the temperature exceeds into the growth range of 25–50 °C (Bartram et al., 2007). Therefore, it is important to monitor shallow ground temperatures in proximity of DWDS and mitigate the anthropogenic thermal impact if necessary. Besides soil sealing, linear heat sources, such as district heating networks, yield an increased impact on DWDS temperature because of the often close and parallel implementation in the shallow ground (van den Bos, 2020). In the future, the threshold of 25 °C is expected to be exceeded more often due to global warming in combination with local thermal anomalies (Agudelo-Vera et al., 2017).

The identified environmental impacts of groundwater temperature change include effects on **contaminant behaviour**. Possible effects are enhanced dissolution, transport, and degradation of contaminants (Beyer et al., 2016). Furthermore, increased concentrations of arsenic (Bonte et al., 2013) as well as pharmaceuticals and personal care products (García-Gil et al., 2018b) have been detected in connection with elevated groundwater temperatures.

Despite the known effects of thermal alteration, a moderate rise of groundwater temperature (5–10 K) is considered as a minor impact on groundwater quality (Griebler et al., 2016). However, in the future, this rate will be able to be exceeded more easily when the superposition of different heat sources, as well as climate change, amplify hotspots in subsurface temperature. In urban environments, such local hotspots can become patches more often, eventually forming a pronounced subsurface UHI and thereby, affecting groundwater quality at a regional scale. Koch et al. (2021) investigated the groundwater ecosystem status in the urban area of Karlsruhe (Germany) and found that only 35% of the wells meet the criteria for very good and good ecological conditions.

### *2.6.2 Utilization of subsurface waste heat*

Another important implication of anthropogenic heat in the subsurface is an elevated geothermal potential for heating (Epting et al., 2020b). Rivera et al. (2017) found that the technically usable potential in urban areas can be 40% higher than in rural areas. On the other hand, geothermal applications for cooling loose efficiency in

an anthropogenically heated environment (Di Donna et al., 2021). Therefore, the recovery of waste heat in cities is widely discussed (Bayer et al., 2019). With continuously increasing numbers of SGES in cities, there will be an emerging need for management of this resource by municipal authorities (Epting et al., 2017a) to avoid interferences of the geothermal systems (Attard et al., 2020).

Beside common geothermal systems there also are direct utilisations of the waste heat of earth-contact structures. These are known as energy geostructures (Brandl, 2006). Such applications not only allow to combine existing structures with geothermal systems but can also take advantage of anthropogenically generated waste heat. Typically, energy geostructures are equipped with heat exchanger pipes, which lead to a heat pump. The hereby extracted heat can, for example, supply buildings. These closed-loop systems allow for an easier integration in structures. Energy piles, the most common of these technologies, are thermoactive foundations to stabilize and heat (or cool) buildings simultaneously (Sani et al., 2019) and are proven applicable (Zito et al., 2021). Energy tunnels have the heat exchange pipes installed in tunnel linings, while the energy is mostly utilized for local facilities such as schools (Adam & Markiewicz, 2009; Barla & Di Donna, 2018). The research focus is mainly on subway tunnels due to their high energy potential in the urban environment (Epting et al., 2020a). Energy walls are thermoactive retaining walls of buildings, including diaphragm and sheet pile walls (Rammal et al., 2020). The thermoactive energy slabs are similar to energy walls but have only one side with earth contact and thus, are less effective (Lee et al., 2021). Energy anchors are thermoactive piles, driven into soil or rock to stabilize structures, for example, tunnels or retaining walls (Adam & Markiewicz, 2009; Brandl, 2006). Recovery of sewage heat is possible with energy sewer pipes (Cipolla & Maglionico, 2014). They can either be equipped with heat exchange pipes at the base of the sewage pipe (Adam & Markiewicz, 2009) or an external heat exchanger is installed (Schmid, 2008). However, high variations in sewage temperature are a challenge for this technology (Kretschmer et al., 2016). For landfill waste heat recovery, conventional shallow geothermal systems are applied (Coccia et al., 2013; Tidden & Scharrer, 2017). Although closed-loop systems are the most common application, there also is the possibility to extract the heat with open-loop systems (Grillo, 2014). This, however, might cause problems if the groundwater is contaminated. The geothermal potential in landfills is typically high, but longevity limitations result from the decomposition period. A further overview of energy geostructures and in-situ examples is given by Loveridge et al. (2020).

## 2.7 Conclusions

This review paper highlights the importance of single anthropogenic heat sources to subsurface warming. Currently, there is no consistent classification of anthropogenic heat sources that covers the variability and diversity of characteristics

described in this study. Such a classification is the basis for defining guidelines and a legal framework for heat sources of the same characteristics. Different kinds of thermal impacts will require different legal thresholds. Actively heated sources could be governed by a maximum induced temperature difference in the surrounding subsurface and sources that passively emit heat could require a statutory insulation. Further, it is helpful for designing and quantifying thermal boundary conditions in model parametrisation. The environmental impacts caused by increasing subsurface temperature are hardly researched so far despite their crucial importance to groundwater ecosystems and resources. In this work, we provide a holistic overview of the known anthropogenic sources of subsurface warming and their characteristics. In this regard, we propose four main characteristics to classify anthropogenic heat sources.

The first characteristic, the scale, orders heat sources by the extent of the thermally affected zone. Heat sources are classified into local, regional, and even global (climate change). Secondly, the geometry allows us to classify the heat sources by their shape, which is especially handy when heat sources are to be implemented in models as boundary conditions. We defined three geometries based on the aerial perspective: polygonal, linear, and punctual. The third classification applies to the process of heat generation. Process types can be climatic for above local scale heat sources that warm the underground from the surface, direct active (e.g., swimming pools) or passive heating (e.g., basements) of the subsurface, leakage of a fluid with elevated temperature, or heat that is generated in-situ by a chemical process. The fourth characteristic, the intention, particularly shows that besides intended geothermal applications, all anthropogenic sources heat the subsurface unintended.

However, none of the introduced approaches is unambiguous in all cases — hence, we proposed a classification by outstanding characteristics. The subsequent review of anthropogenic heat sources follows this classification in order to give a consistent and easily accessible structure. The analysis of the relevant literature on the one hand shows the magnitude of the thermal impact of the different heat sources, but on the other hand also reveals a significant research gap regarding the thermal impact of individual heat sources, as well as the implications of the elevated ground(-water) temperature. Ultimately, the discovered knowledge gaps revealed several topics that need to be addressed by future works:

1. To date, studies investigating anthropogenic subsurface warming are performed almost exclusively at district or city scale and integrate local heat sources only as agglomerations or undifferentiated bulk effects. The thermal impact of singular heat sources, however, is typically not considered specifically due to sparse density of measurement points. Filling this gap gives insight into the emitted heat at individual locations but also allows to calculate overall contributions to subsurface warming in general. In fact, some potential heat

sources remain to be proven as contributors to subsurface heating like soil heating (agriculture and sport), thermally activated traffic areas, or electrical substations.

2. In this study, we introduced a classification by the process of heat generation. This is only a fraction of the mechanisms and factors that play a role in the underground emission of heat. Therefore, process understanding is another key component to disentangle anthropogenic subsurface warming. Detailed case studies are needed to ascertain the quantitative and qualitative relevance of single parameters like depth to groundwater or insulation.
3. Little is known about the impact thermal change has on subsurface ecosystems. Groundwater, as one of our most valuable resources, is well worth protecting from any possible threat – including thermal alteration. Open questions include temperature thresholds for groundwater ecosystems, changes of hydrogeochemical conditions as well as the establishment of thermal protection zones. Other environmental implications like the influence on DWDS or contaminant behaviour remain to be studied more thoroughly.
4. The huge geothermal potential created by waste heat has already been topic of research in the past years. Still, there is a need for research regarding the application of geothermal systems in connection with heat sources, as well as the regulation in densely populated areas in order to maximize the recovery of emitted waste heat. Smart solutions like energy geostructures need to go hand in hand with shallow subsurface management by local authorities for an efficient and sustainable operation of geothermal installations.

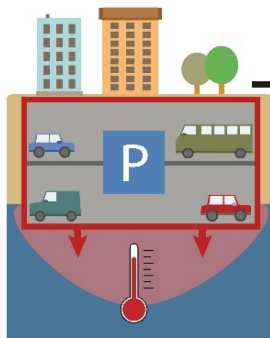
### 3 Thermal impact of underground car parks on urban groundwater

This chapter is reproduced from:

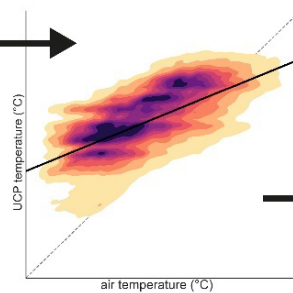
Noethen, M., Hemmerle, H., Menberg, K., Epting, J., Benz, S. A., Blum, P., & Bayer, P. (2023). Thermal impact of underground car parks on urban groundwater. *Science of the Total Environment*, 903, 166572, DOI: <https://doi.org/10.1016/j.scitotenv.2023.166572>.

#### Graphical abstract

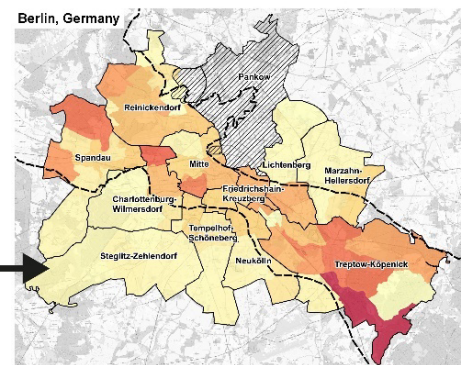
Temperature time series of 31 underground car parks



Regression model to predict underground car park temperature based on surface air temperature



Upscaling the thermal impact to city-scale



### 3.1 Abstract

Built-up areas are known to heavily impact the thermal regime of the shallow subsurface. In many cities, the answer to densification is to increase the height and depth of buildings, which leads to a steady growth in the number of underground car parks. These underground car parks are heated by waste heat from car engines and are typically several degrees warmer than the surrounding subsurface, which makes them a heat source for ambient subsurface and groundwater. Thus, the objective of this study is to investigate the thermal impact of 31 underground car parks in six cities and to upscale the thermal impact that underground car parks have on the subsurface in Berlin, Germany. Underground car parks have daily, weekly, and seasonal temperature patterns that respond to air circulation and traffic frequency, resulting in net heat fluxes of 0.3 to 15.5 W/m<sup>2</sup> at the measured sites. For the studied underground car parks in Berlin, the emitted annual thermal energy is about 0.65 PJ. Recycling this waste heat with geothermal heat pumps would provide a sustainable alternative for green energy and counteract the urban heat island by cooling of the shallow subsurface.

### 3.2 Introduction

Groundwater is highly important not only as our largest available freshwater resource but also because it provides an extensive habitat for subsurface ecosystems that are valuable to our society (Boulton et al., 2008; Griebler & Avramov, 2015; Hancock et al., 2005). Due to their purification function, a deterioration of groundwater ecosystems could lead to a decrease in groundwater quality (Bonte et al., 2011; Brielmann et al., 2009). For sustainable cities, it is therefore necessary to protect these vulnerable ecosystems. In addition to various other anthropogenic influences such as salt pollution and organic chemicals (Becher et al., 2022), temperature increase is assumed to pose a threat to groundwater fauna (Griebler et al., 2016). Thus, changing groundwater temperatures in cities lead to a decline in the biodiversity of fauna and can affect groundwater quality (Blum et al., 2021b; Koch et al., 2021; Spengler & Hahn, 2018). Furthermore, a temperature increase in the shallow subsurface can lead to increased temperatures in drinking water distribution systems (Agudelo-Vera et al., 2017; Gunkel et al., 2022). Especially in urban areas, they are often installed close to underground infrastructure and therefore directly affected (van den Bos, 2020). Exceeding recommended temperature limits of 20 to 25 °C can result in bacterial growth in drinking water (Agudelo-Vera et al., 2020).

Temperatures in the urban environment are altered by various anthropogenic sources. So-called urban heat islands indicate increased air temperatures in cities (Oke, 1973). The same observation has been made for the subsurface. Due to a number of different heat sources, such as basements, tunnels, and surface sealing (Attard et al., 2016a; Noethen et al., 2022; Tissen et al., 2021), groundwater temperatures



beneath cities are permanently elevated, which is typically referred to as subsurface urban heat island (Ferguson & Woodbury, 2004; Hemmerle et al., 2022; Menberg et al., 2013a; among others). In general, temperatures scale with building density and in urban centers, increased groundwater temperatures of up to 7 K can be observed (Böttcher & Zosseder, 2022; Menberg et al., 2013a). In historical cities, such anomalies can be traced to depths of >60 m below the surface, proving that regional subsurface warming went along with urban expansion in the past (Visser et al., 2020). Intensities and drivers of urban subsurface warming have been intensively studied (Benz et al., 2018a; Menberg et al., 2013b) as has the exploration of accumulated waste heat as a geothermal resource (Benz et al., 2022; Menberg et al., 2015; Tissen et al., 2021). Nevertheless, there is a lack of knowledge about the characteristics of heat sources and their impact in the context of an urban environment. Especially in the densest agglomerations, it is difficult to distinguish between individual heat sources as their effects overlap and add up to regional scale thermal anomalies.

Within European inner-city settings, these heat sources typically include a large number of underground car parks (UCP). They have been observed in association with hot spots in groundwater temperatures (Becker & Epting, 2021; Zhu et al., 2015). However, UCPs are often generalized as basements (e.g., Benz et al., 2015b; Menberg et al., 2013b), underground structures (Attard et al., 2016a), or subsurface buildings (Epting et al., 2017b). This ignores that UCPs, in comparison to regular basements, extend over several levels and, although typically not insulated, are passively heated by traffic (Becker & Epting, 2021). For these reasons, UCPs can be more effective heat sources than basements (Noethen et al., 2022). Becker and Epting (2021) directly addressed UCPs as heat sources and found that public UCPs have higher temperatures than private ones due to higher traffic volumes. Rotta Loria et al. (2022) found a positive linear relationship between air and UCP temperatures.

UCP air tends to be warmer than surface air in winter and cooler in summer. Although it is proven that UCPs can create local hot spots, their overall contribution to urban subsurface warming has not been sufficiently investigated yet. To overcome this gap the first objective of this study is to evaluate the thermal state of 31 UCPs in Central Europe with respect to (i) ambient air temperature, (ii) the usage type and traffic load of the UCP, and (iii) the thermal impact they have on groundwater. The second objective is to use the information gained from the reference underground car parks to upscale the thermal impact at the city-scale for Berlin. We perform a spatial and temporal analysis to assess heat fluxes of 5040 UCPs in Berlin and present the contribution of UCPs to urban subsurface warming.

### 3.3 Materials and methods

#### 3.3.1 Underground car park temperatures

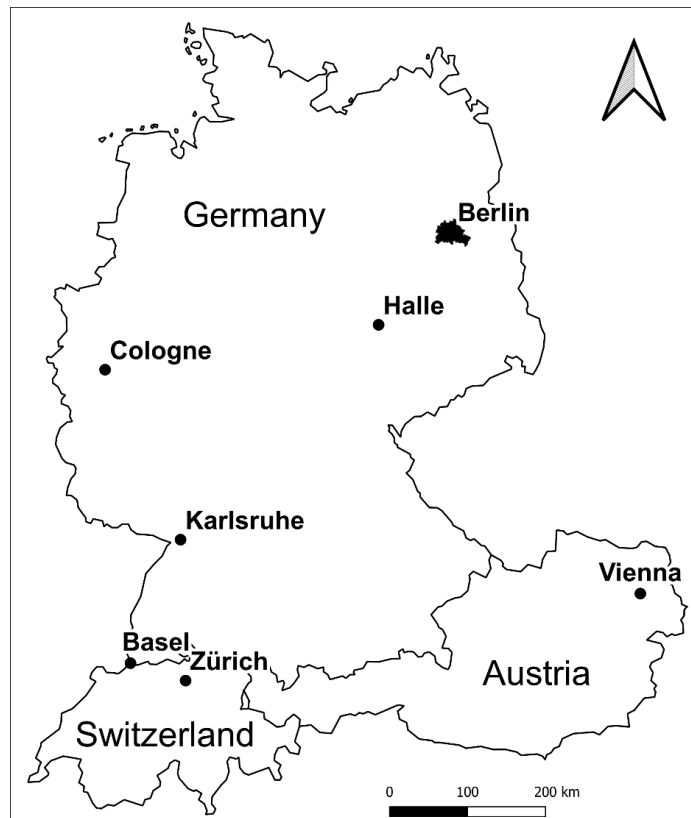
##### Monitoring sites and data

The monitored UCPs are located in major cities in Germany, Austria, and Switzerland. We investigate ten UCPs in Cologne (Cologne #1 to #10), one in Halle and one in Karlsruhe, twelve in Vienna (Vienna #1 to #12), five in Basel (Basel #1 to #5), and two in Zürich (Zürich #1 and #2) (Figure 3.1). The exact location of the UCPs is not disclosed for data protection reasons.

The data used for the temperature analysis include time series of air temperature in the UCPs ( $T_{UCP}$ ), air temperature outside the UCP ( $T_{Air}$ ), and groundwater temperature ( $T_{GW}$ ), where available. For six sites with nearby groundwater observation wells, temperature-depth-profiles, measured between 2013 and 2022, were also available. We also recorded information on the depth of the UCP and the type of use (private/public). Information and sources of all datasets are given in Table A1. The measurement of  $T_{UCP}$  was carried out in several field campaigns, over several years (2014–2022) and with varying equipment and personnel. Hence, there are variations in the placement of the device and in the accuracy and resolution of the data. However, all the devices used have a minimum accuracy of  $\pm 0.5$  K and a minimum resolution of 0.1 K.

$T_{Air}$  data were obtained from the nearest available weather station for each UCP. Due to the differences in microclimatic conditions between weather station and UCP,  $T_{Air}$  could deviate from the true value. For example, in some cities such as Cologne or Karlsruhe, the weather station is positioned outside of the city, where  $T_{Air}$  is typically cooler than in the city center. This can cause an error (see Figure A1 for Berlin as example).  $T_{GW}$  data were obtained from authorities or by own measurements. At Zürich #1 and Zürich #2  $T_{GW}$  was measured directly below the UCP in wells located inside the buildings on the first and second level, respectively.

Figure 3.1. Map of the study sites. Cities with studied UCP sites are indicated by dots. Berlin is represented by the city area.



### Data Analysis

The workflow for determining the heat fluxes from the measured UCPs into the groundwater and the linear regressions is shown in Figure 3.2 in the left part.

The vertical conductive heat transport from the UCP through the slab into the groundwater was calculated as follows:

$$q_{slab} = U \cdot \Delta T \quad (3.1)$$

where  $q_{slab}$  is the heat flux through the slab in  $W/m^2$ , which quantifies the rate of heat transfer per unit area,  $\Delta T$  is the difference between  $T_{UCP}$  and  $T_{GW}$  in K, and  $U$  is the thermal transmittance in  $W/(m^2 \cdot K)$ . The thermal transmittance measures the heat transfer through solid matter between two fluids and is derived from the reciprocal value of the thermal resistance ( $R$ ):

$$U = \frac{1}{R} \quad (3.2)$$

The thermal resistance indicates the resistance of a material or structure to heat flow and is calculated according to the following formula (DIN EN ISO 6946, 2018):

$$R = \frac{1}{\alpha} + \frac{d_{slab}}{\lambda_{concrete}} + \frac{d_{soil}}{\lambda_{soil}} \quad (3.3)$$

This equation adds up the resistances of every permeated layer, which in this case are the slab of the UCP and the unsaturated soil beneath. The thermal resistance of each layer is obtained by dividing the permeated layer's thickness ( $d$ ) and its thermal conductivity ( $\lambda$ ). Nowadays, UCPs are typically built with spread foundations with a thickness between 0.4 and 0.6 m. Older UCPs also have strip foundations, where deeper foundations were constructed in trenches and a thinner slab of 0.2 to 0.25 m carries only the load of the cars. Since there is no information about the age of construction, we assumed for all UCPs spread foundations with  $d_{slab} = 0.5$  m. Unsaturated soil thickness was derived from the distance between the UCP base and local groundwater tables. For the thermal conductivity of the concrete and the soil, typical values were chosen based on VDI 4640 (2010) and the geology of the soil (see Table A2). For the UCPs that reach the groundwater, only the thermal resistance of the slab was calculated. Furthermore, the reciprocal value of the heat transfer coefficient ( $\alpha$ ) is added. This value, which integrates the energy transfer between concrete and air inside the UCP, was adopted from (Guo et al., 2011), assuming a low wind velocity in UCPs of 0.1 m/s:  $\alpha = 8.75$   $W/m^2 \cdot K$ . The resulting reciprocal value is 0.114  $W/m^2 \cdot K$ , which is slightly lower than the standard value for the inner surface resistance of 0.13  $W/m^2 \cdot K$  by DIN EN ISO 6946 (2018). We prefer this experimental value of Guo et al. (2011) because it additionally considers wind velocity. In UCPs, there is typically either a natural or a mechanical ventilation system because of car exhaust fumes, as required by law in many countries (e.g., §11 GaVo, 2022). In Equation 3.1,  $\Delta T$  was

calculated temporally resolved to consider seasonal fluctuations. For Zürich #1 and Zürich #2, no groundwater time series was available. Instead, we used the mean of all temperature-depth-profiles at 20 m below ground surface (bgs) as a constant value.

For the correlation of  $T_{UCP}$  and  $T_{Air}$ , we used the Pearson correlation coefficient ( $r$ ). The average linear regression and correlation coefficient per level was calculated with the mean values of the individual sites of the respective levels and the total regression with the mean values of all sites. No average regression was calculated for levels five and six since there is only one UCP representing each of these levels.

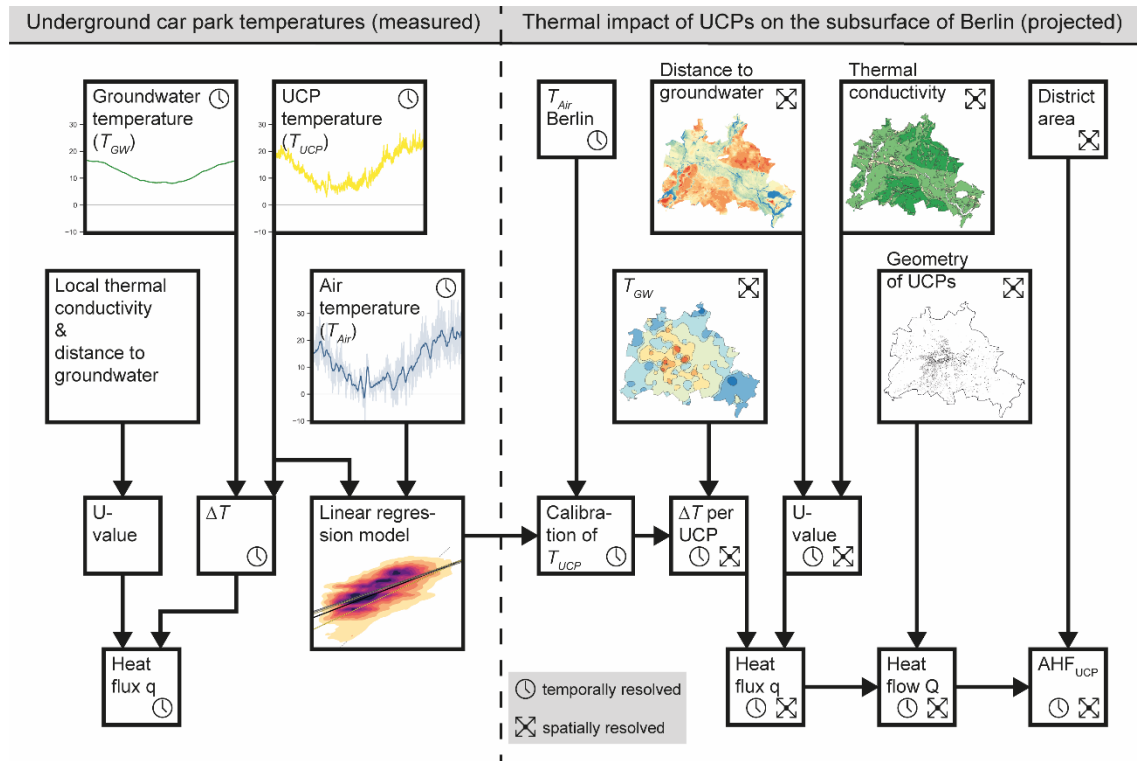


Figure 3.2. Workflow chart of the calculation of heat fluxes from the measured UCPs (left) as well as the heat fluxes and heat flows for UCPs in Berlin and the anthropogenic heat flux of UCPs ( $AHF_{UCP}$ ) per district (right). Detailed versions of the maps on the right can be seen in Figure A2.  $\Delta T$ : temperature difference, U-value: thermal transmittance.

### 3.3.2 Impact of underground car parks on subsurface warming of Berlin

#### Study area

For the spatial analysis of heat fluxes from UCPs, we chose the city of Berlin as case study site, because it offers a well-curated open data service and has a large number of UCPs in different geological settings. With >3.5 million inhabitants and an area of 891.1 km<sup>2</sup>, Berlin is Germany's largest city and capital. The district of Pankow was excluded due to a lack of data at this specific location. Parts of the districts of Reinickendorf and Mitte were also excluded because there is no shallow aquifer in these areas and therefore no meaningful distance to the groundwater can be calculated (Geoportal Berlin, 2023). The arithmetic mean of  $T_{Air}$  at the weather station of Berlin-Tempelhof between 1990 and 2021 is  $10.4 \pm 0.8$  °C (DWD, 2023). The city is located in a transitional climate zone between maritime and continental influences.

However, Berlin's climate is also strongly influenced by anthropogenic land use and forms an urban heat island. The average  $T_{Air}$  is between 1.5 and 2 K warmer than in the surrounding rural areas (Vogel & Afshari, 2020; Ward et al., 2016).

The shallow subsurface of north-eastern Germany was shaped by glacial periods and the morphology of Berlin was primarily by the Weichselian glaciation. The Warsaw-Berlin glacial valley cuts from southeast to northwest through the Barnim and Teltow plateaus, which are located in northeast and southwest Berlin. The valley, which hosts the Spree River today, consists mainly of glacial and fluvial sands, while the plateaus are mainly built up of glacial till and sand (Geoportal Berlin, 2023).

The hydrogeology in Berlin is complex due to the glacial genesis; several aquifers are separated by aquitards (Limberg & Thierbach, 1997). The groundwater level in the glacial valley, where the city center is located, is <10 m bgs in most parts. On the plateaus, the distance to the groundwater table is 10 to 40 m bgs, except for some morphological depressions, where it can be less (Hannappel & Limberg, 2007).  $T_{GW}$  is highest in the central parts (~14 °C) and decreases with distance from the city center, thus forming the typical subsurface urban heat island (Menberg et al., 2013a). At the outer parts,  $T_{GW}$  was found to be around 10 to 11 °C (Geoportal Berlin, 2023).

#### Input Data

For the spatial analysis of heat fluxes, the most recent datasets which are freely accessible via the online open data portal of Berlin were used (Geoportal Berlin, 2023):

- $T_{GW}$  of 2020 at 20 m bgs interpolated from 223 wells.
- Depth to the groundwater table for May 2009 interpolated from 1750 wells.
- Geological sketch of the surface lithology, based on various geological maps.
- Geometry of buildings in Berlin including information about the geometry of the UCPs and the number of subsurface levels. The height of the UCP levels is assumed to be 3 m.
- District and city quarter area.

The thermal conductivity of the soil was derived from the surface lithology data of the geological sketch using literature values (VDI 4640, 2010). For the soil, the average value between dry and moist material was used (for till and peat the recommended value, for concrete 1.6 W/m·K). For the building dataset, we expect that a small fraction of the private UCPs is not registered at the municipality and that the actual number of UCPs in the study area is even higher. The spatial datasets applied in the calculation are shown in Figure A2.

$T_{UCP}$  is derived from  $T_{Air}$  by the linear regressions from own measurements at 31 UCPs for each level.  $T_{Air}$  was calculated as monthly long-term averages (1990–2021) with data from the DWD (2023), measured at the Berlin-Tempelhof weather station (location shown in Figure A2d). The UCPs are distributed over the entire area of Berlin and, due to the size of the city, they can be up to 23 km away from the weather station. The urban heat island effect likely affects the  $T_{Air}$  data used in this approach (Dugord

et al., 2014; Kottmeier et al., 2007) and microclimatic variations in the study area are not considered. Comparing the other weather stations in Berlin to the one in Berlin-Tempelhof, the annual mean  $T_{Air}$  deviation is always  $<1$  K (see Figure A1). Therefore, we can assume a maximum error of  $\pm 1$  K for  $T_{Air}$ .

All input parameters applied in the spatial analysis are listed in Table A2.

### Spatial analysis

In order to extrapolate the thermal impact of UCPs to the city-scale, we projected the results from the UCP temperature analysis of the measured sites on all UCPs in Berlin (Figure 3.2, right part). For each UCP in the study area, we calculated the heat flux through the slab using Equations 3.1, 3.2, and 3.3. For the UCPs that reach into the groundwater, heat transfer of all walls below the water table is determined. The heat flux through the walls in the unsaturated soil can be neglected as most of the heat escapes to the surface (Emery et al., 2007; Thomas & Rees, 1999). The heat flux through the wall is calculated only using the resistance of the concrete as there is no soil obstructing the heat flow into the groundwater. We assumed a wall thickness of 0.3 m, which results from the typically used 0.25 m wide sheet metal strips with additional concrete cover. The mean heat flux through the slab and wall per district is calculated as a weighted mean with the heat flux and area of the individual UCPs.

Furthermore, we calculated the heat flow ( $Q$ ) from the UCP into the groundwater as follows:

$$Q = q_{slab} \cdot A_{UCP} + q_{wall} \cdot A_{wall} \quad (3.4)$$

where  $A_{UCP}$  is the area of the slab and  $A_{wall}$  is the area of the walls inside the groundwater.

Consequently, we determined the anthropogenic heat flux that is emitted into the shallow urban aquifer by various anthropogenic sources (Benz et al., 2015b; Menberg et al., 2013b). In this case, we calculated the anthropogenic heat flux of UCPs ( $AHF_{UCP}$ ) in Berlin, normalized to the area of the district ( $A$ ):

$$AHF_{UCP} = \sum q \cdot A_{UCP} / A \quad (3.5)$$

## 3.4 Results and discussion

### 3.4.1 Underground car park temperatures

#### Thermal impact on groundwater

UCPs are known to cause warming of the surrounding soil and groundwater (Becker & Epting, 2021; Zhu et al., 2015). Figure 3.3 shows temperature logs measured at groundwater monitoring wells inside a public (Zürich #1) and a private UCP (Zürich #2). Both UCPs have a well inside the building, Zürich #1 at the first level, Zürich #2 at the third level. Since the groundwater tables are higher than the UCP foundations,  $T_{GW}$  can be measured at the depths of the lower levels. Zürich #1 shows a significant

influence on  $T_{GW}$  due to the high  $T_{UCP}$ . The heat comes from above, which is reflected in the warm  $T_{GW}$  at the upper meters. Only in the winter months, when  $T_{UCP}$  is colder than  $T_{GW}$ , there is no heating effect. The  $T_{GW}$  at 20 m bgs is 16.6 °C and 2.7 K cooler than the average  $T_{UCP}$ . It should be noted that the third level is used as a nuclear shelter and no cars are parked there. In comparison, Zürich #2 is a private car park with more levels. Similar to Zürich #1, levels three and four are reserved as a nuclear shelter without traffic. Although  $T_{GW}$  in the top five meters below the structure is slightly warmer in summer and autumn, there is no significant influence over the course of the year.  $T_{GW}$  at 20 m bgs is 13.7 °C and 1.8 K cooler than the average  $T_{UCP}$ . This indicates that there is still a heating effect on the groundwater due to the thermal gradient between the UCP and the groundwater, however, it is not as pronounced as at Zürich #1.

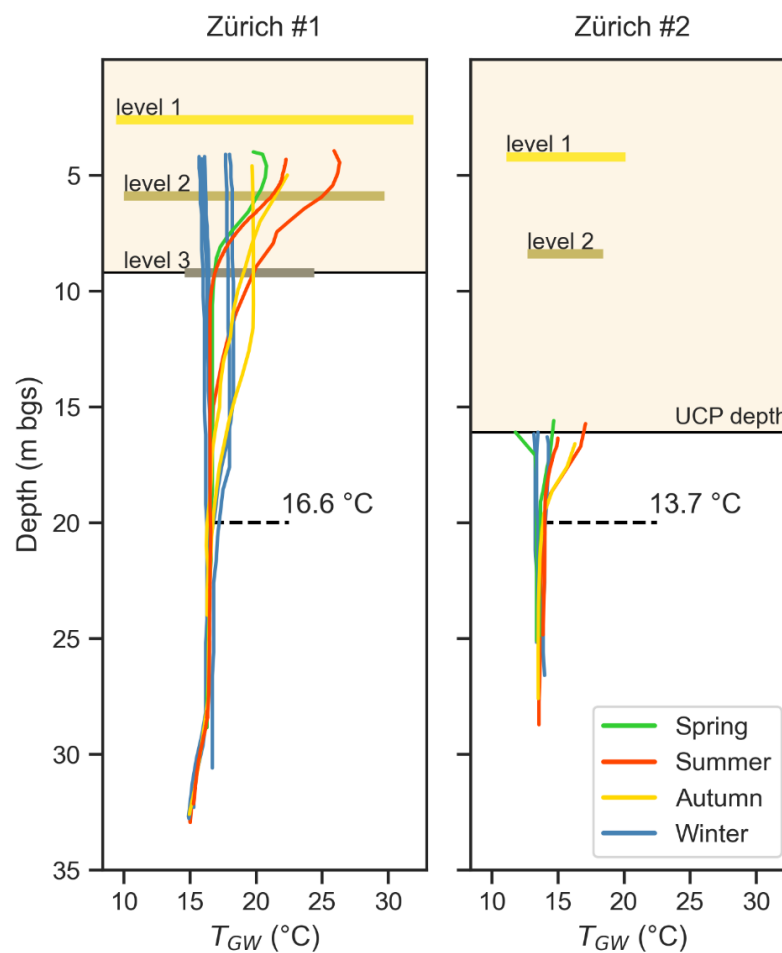


Figure 3.3. Temperature-depth-profiles of a public (Zürich #1) and a private UCP (Zürich #2), measured in observation wells inside the UCP. At the top, the UCP temperature range per level is shown with a bar, while the average groundwater temperature at 20 m bgs is indicated with a dashed line.

As indicated by the seasonal variance of the temperature logs at Zürich #1 and #2 the heat flux depends on seasonal variations of both  $T_{UCP}$  and  $T_{GW}$ . Figure 3.4 shows a time series of  $T_{GW}$ ,  $T_{UCP}$ ,  $T_{Air}$ , as well as the heat fluxes over time and as boxplots for each site based on the observed temperature data. The heat fluxes show different patterns and vary in intensity and even direction throughout the seasons. Zürich #1 shows that  $T_{UCP}$  in the upper two levels responds rapidly to  $T_{Air}$ , which indicates a good

connection to surface air. In Zürich #2, the opposite can be observed. Here,  $T_{UCP}$  hardly responds to  $T_{Air}$ . The high heat fluxes at both sites in Zürich can be attributed to the direct connection of the UCPs to the groundwater.  $T_{UCP}$  of Basel #4 is higher in all seasons than  $T_{GW}$ . The UCP is surrounded by groundwater and has the largest impact on the groundwater of the studied UCPs, with an average heat flux of  $15.5 \pm 3.3 \text{ W/m}^2$ . The development of temperatures at Basel #5 is similar to those of Basel #4, and its base is also in the saturated zone, but the surrounding groundwater is 4.1 K warmer on average. This results in a smaller mean heat flux of  $4.3 \pm 6.3 \text{ W/m}^2$  and a reverse of the flux direction in winter and spring seasons.

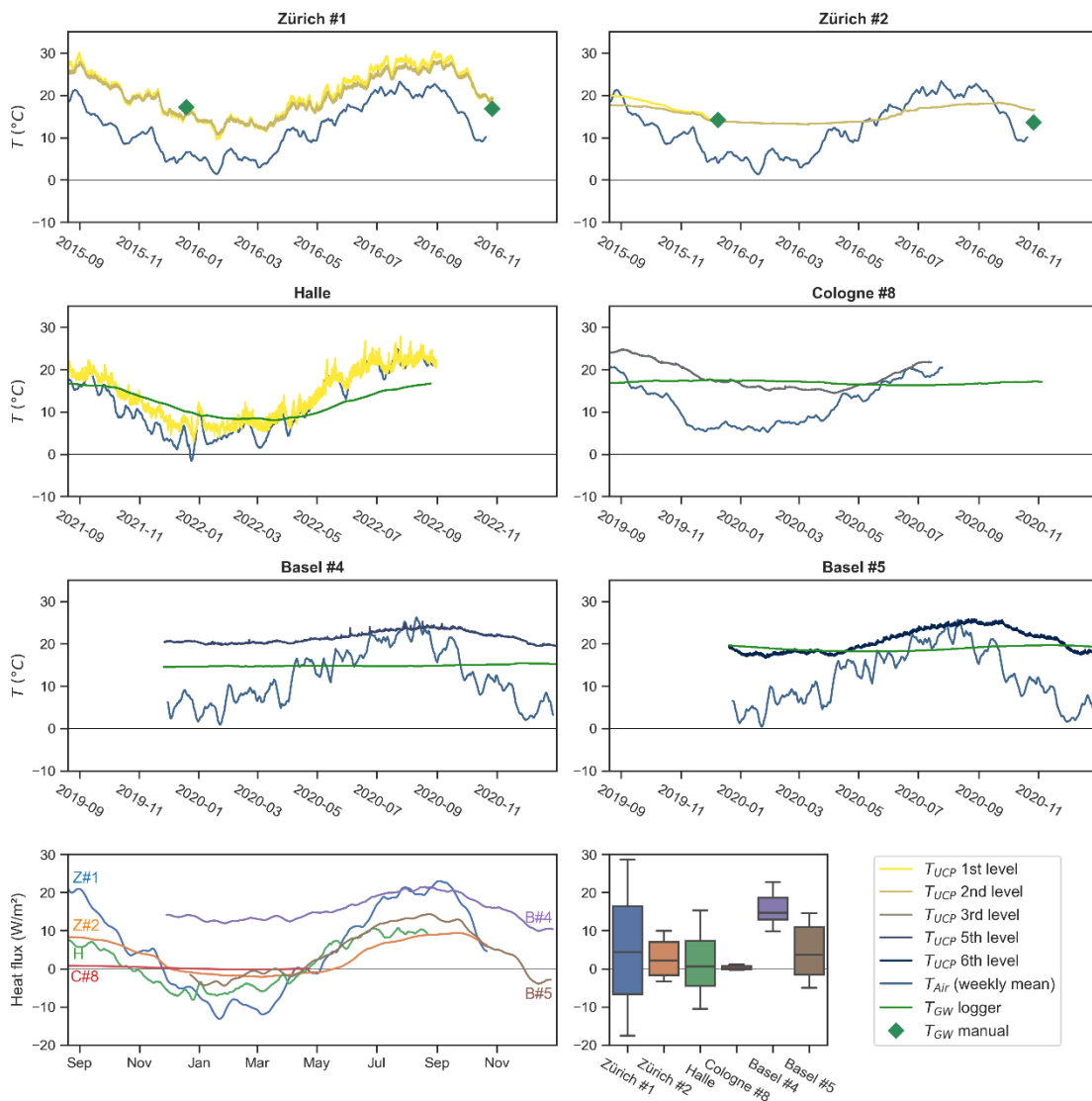


Figure 3.4. Time series of groundwater temperature ( $T_{GW}$ ), UCP temperature ( $T_{UCP}$ ), and surface air temperature ( $T_{Air}$ ) for six UCPs as well as temporally resolved heat fluxes through the slab into the groundwater.

Although the UCP Cologne #8 is considerably warm with an average  $T_{UCP}$  of  $19 \pm 3.2 \text{ }^\circ\text{C}$ , no significant net heat flux into the groundwater occurs (mean  $0.3 \pm 0.5 \text{ W/m}^2$ ). This can be attributed to the already high  $T_{GW}$  ( $17 \pm 0.4 \text{ }^\circ\text{C}$ ) and higher distance to the groundwater (6 m below the UCP base). In contrast to the publicly used UCPs, the shallow and privately used UCP in Halle is well connected to the surface air and



therefore only 1.4 K warmer than the groundwater on average. Although groundwater is found only 0.5 m below the structure, the UCP has almost no thermal impact ( $1.4 \pm 6.2 \text{ W/m}^2$ ).

Overall, mean heat flux intensities ranging between 0.3 and 15.5  $\text{W/m}^2$  are highly sensitive to the distance to the groundwater and pre-altered thermal groundwater conditions. Furthermore, the variation in the placement of the device may impact the results as temperatures within the same level can vary. In Figure A4, we show the high relevance of  $T_{UCP}$  to the results, as this parameter has the highest sensitivity.

#### Correlation of UCP and air temperature

The relationship between  $T_{UCP}$  and  $T_{Air}$  for the six individual UCPs with  $T_{GW}$  information is shown in Figure 3.5. Furthermore, the mean for all 31 monitored UCPs is plotted at the bottom of the figure. Scatter plots for all individual sites are given in the appendix in Figure A3. All sites exhibit a positive linear correlation with weaker correlation coefficients and lower gradients at deeper UCP levels. This indicates that the influence of  $T_{Air}$  (e.g., through ventilation) decreases with increasing depth. For example, at the deepest levels in the UCPs Basel #4 at 10 m bgs and #5 at 16 m bgs seasonal variation of  $T_{UCP}$  is negligibly low with a seasonal amplitude below 5.8 and 9.2 K, respectively, whereas the seasonal amplitude of  $T_{Air}$  is 29.6 K. In 84.9% of all data pairs,  $T_{UCP}$  is warmer than  $T_{Air}$ , which is represented by values above the dashed identity line. However, some UCPs appear to be better connected to the surface air and show a weaker deviation from  $T_{Air}$ , like in Halle, where only 66.8% of the time  $T_{UCP}$  exceeds  $T_{Air}$ .

The average regression of all UCPs ( $y = 0.42x + 13$ ,  $r = 0.78$ ) is in line with the findings of Rotta Loria et al. (2022), who also report a positive linear relation ( $y = 0.6x + 10.2$ ,  $r = 0.75$ ) between  $T_{UCP}$  and  $T_{Air}$ . The steeper gradient indicated that the UCPs in Chicago are better connected to surface air and adjust better to  $T_{Air}$ . This may be caused by differences in construction or higher ventilation. Note that in contrast to our approach, Rotta Loria et al. (2022) computed the regression for all UCPs at once using local above-ground air temperature data and within the same period. In this study, a regression is calculated for each individual dataset, temperatures are recorded at variable times, and  $T_{Air}$  is taken from meteorological monitoring that is typically located in the outskirts of the city. Applied to our data, the correlation coefficient would be weaker if calculated for all available data ( $r = 0.65$ ). The average regression lines of the respective levels, which are also shown in the bottom plot in Figure 3.5, show a decreasing correlation coefficient with increasing level. In particular, the first level, which has a correlation coefficient of  $r = 0.84$ , seems to respond well to  $T_{Air}$  change. However, it should be noted that the number of measurements decreases with increasing level as there are fewer UCPs with three or more levels available.

A source of the heat in UCPs seems to be the frequently parked cars. Especially at public UCPs, parked cars are often replaced several times a day, and heat from the engines of the parked cars warms the UCP (Becker & Epting, 2021). This is also clearly visible in Figure 3.6, where the bar plots on the right show the daily average  $T_{UCP}$  at all sites. While private UCPs are generally warmer during working days, the public ones gradually get warmer with each working day until Friday. They then significantly cool down on Sundays due to the reduced traffic. Becker and Epting (2021) made the same observation for the UCPs in Basel and also showed this effect for public holidays. In addition, the weekly averaged time series of  $T_{UCP}$  is plotted on the left. The private UCPs are on average  $16.6 \pm 5.1$  °C warm, while the public UCPs are  $19.5 \pm 4.6$  °C warm. The mean  $T_{UCP}$  of all studied sites is  $18.8 \pm 4.9$  °C. Private UCPs typically have fewer levels and car exchange, which may be the reason for lower  $T_{UCP}$  in comparison to public UCPs. The locations of the UCPs may influence the results as well. Public UCPs are often located in the city centers, where  $T_{Air}$  is typically higher than in residential areas, in which private UCPs are commonly found.

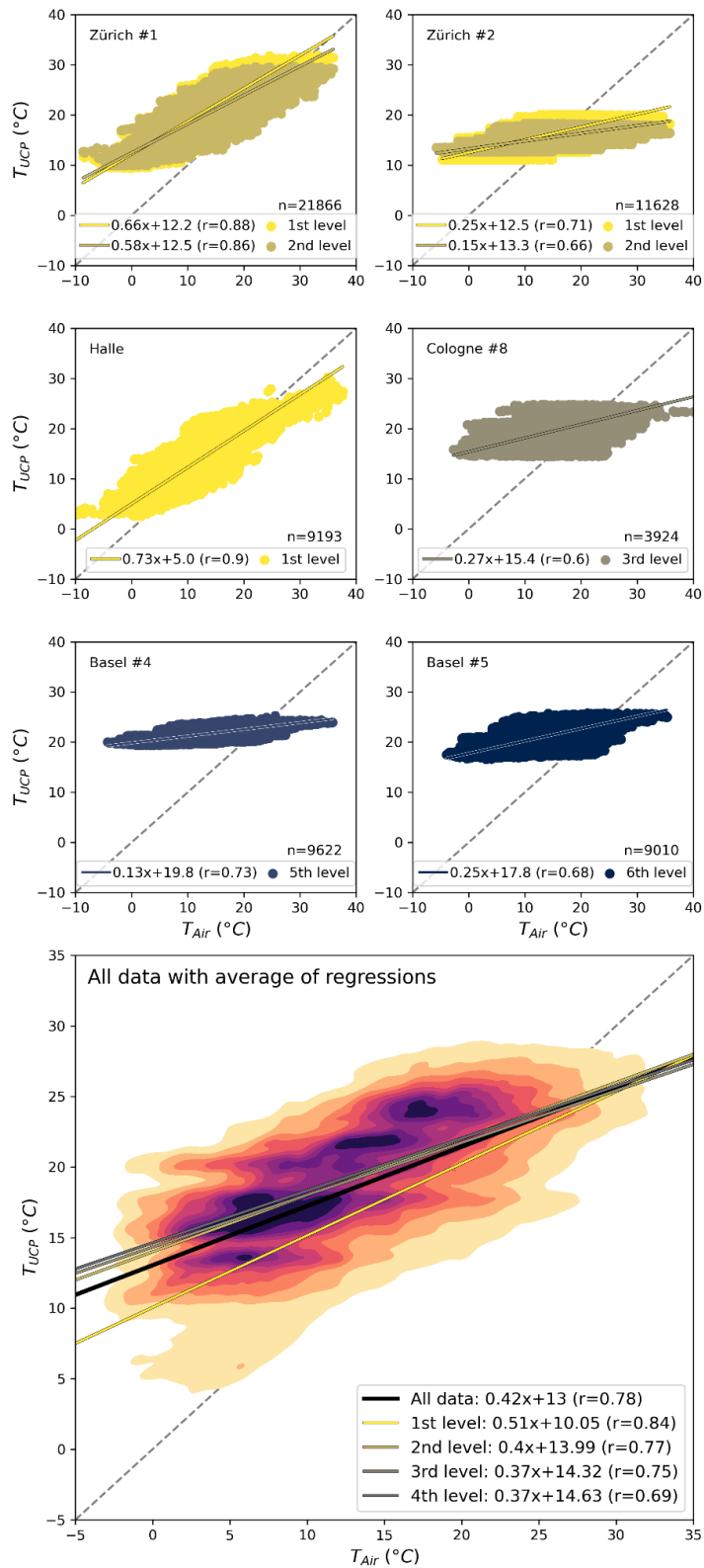


Figure 3.5. UCP temperature ( $T_{UCP}$ ) and surface air temperature ( $T_{Air}$ ) correlation for six selected sites. The colors indicate the level of the UCP at which the measurement was taken. The bottom diagram contains the data for all 31 sites and the average of the results of each individual regression for the respective levels. All plots have a dashed identity line as reference. The number of measurements is marked with an  $n$ .

Figure 3.7 shows violin plots of the temperature difference between  $T_{UCP}$  and  $T_{Air}$  for each level. At all sites,  $T_{UCP}$  is warmer than  $T_{Air}$  on a long-term average and the temperature difference increases towards deeper levels. In particular, there is a significant increase of 2.8 K in the temperature difference between the first and second level. Furthermore, at the first level, almost 25% of all values are negative, showing that  $T_{UCP}$  is colder than  $T_{Air}$  at these times. However, less data is available at deeper levels and additional data from deeper UCPs is needed to validate the observations.

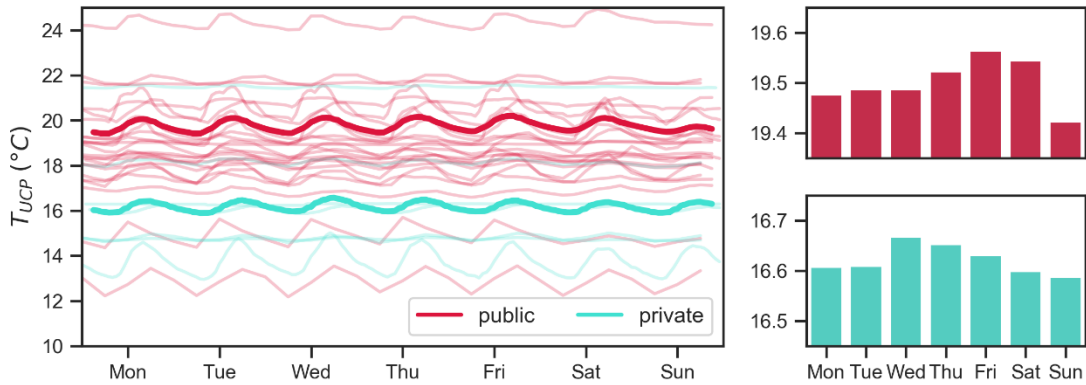
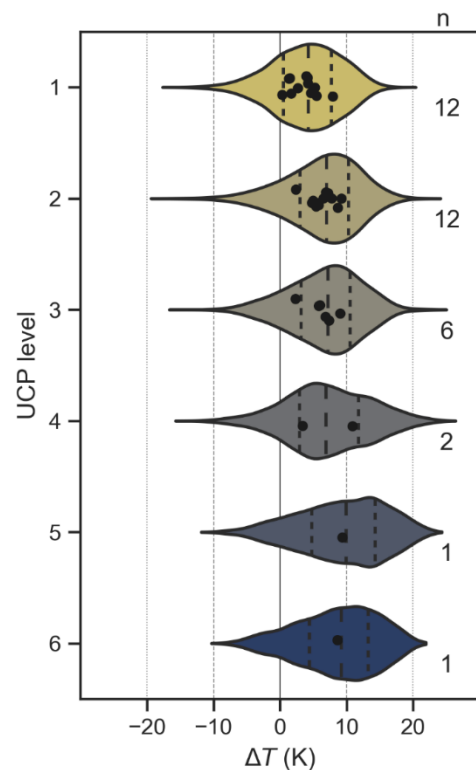


Figure 3.6. Weekly averaged time series of the UCP temperature ( $T_{UCP}$ ) and daily mean values for public (red) and private (green) UCPs. Thick lines represent a rolling mean (6 h) of all publicly and privately studied sites.

The comparison of  $T_{UCP}$  and  $T_{Air}$  also shows that, particularly in the winter season, UCPs are warmer than the outside air. The deeper, public UCPs, such as Cologne #8, Basel #4, and #5, have  $T_{UCP}$  continuously  $>15^{\circ}\text{C}$  in the winter season, as seen in Figure 3.4. This suggests that UCP air could itself be a sustainable energy source; i.e., integrating heat pumps in existing ventilation systems might be a way to utilize waste heat energy from UCP air. Harnessing this potential can supply nearby residential or commercial buildings with sustainably generated heat energy and, at the same time, reduce thermal impact on the subsurface.

Figure 3.7. Violin plots of the temperature difference ( $\Delta T$ ) between UCP and surface air at each level. The dots represent mean values of the individual UCPs. The number of UCPs is marked with an  $n$ .



### 3.4.2 Impact of underground car parks on subsurface warming of Berlin

#### Spatial and seasonal analysis of heat fluxes

The heat flux from UCPs in Berlin exhibits a high spatial variance that is mainly driven by the distance to the groundwater, local  $T_{GW}$ , and for the accumulated heat fluxes the density of UCP per area. Principle statistics of the UCP heat flux for each city district are provided in the Appendix in Table A3. In total, 0.7% of the study area is covered by 5040 UCPs that produce an average heat flux through slab and walls of  $3.7 \text{ W/m}^2$ . The highest density of UCPs per surface area is found in the districts of Mitte (3.6%) and Friedrichshain-Kreuzberg (3.5%), with all other districts being lower than 1.5%, down to 0.1% in Reinickendorf. The distance to the groundwater is tightly linked to geological features and is the major controlling factor for the heat flux (Figure 3.8a). In the glacial valley the groundwater distance is typically below 10 m and a high fraction of UCPs are in direct contact with groundwater (up to 35% in Treptow-Köpenick). The two districts with the highest UCP density, Mitte and Treptow-Köpenick, are also in the valley region and have the highest heat fluxes at  $4.8$  and  $6.8 \text{ W/m}^2$ , respectively. In Mitte, 21.4% of the heat flux is through the walls due to the high groundwater levels. In Treptow-Köpenick, only 2.9% of the heat is emitted through walls, although 35.1% of the UCPs are in contact with groundwater. This is because, in contrast to Mitte, the UCPs in Treptow-Köpenick typically have fewer levels and do not reach as deep in the groundwater. Still, heat fluxes in Mitte are on average lower than in Treptow-Köpenick because of the higher  $T_{GW}$  in the city center which results in a lower thermal gradient. Likewise, the districts of Spandau, Reinickendorf, and Friedrichshain-Kreuzberg are also located in the glacial valley and therefore have comparably high heat fluxes between  $3.8$  and  $4.2 \text{ W/m}^2$ . On the Teltow (southwest) and Barnim (northeast) plateaus the distance to groundwater is typically above 10 m and in districts that are exclusively on the plateaus like Steglitz-Zehlendorf UCPs are not in direct contact with groundwater. Consequently, those UCPs which are on the plateaus have low heat fluxes  $<1 \text{ W/m}^2$ .

For the sum of the heat flows from all UCPs per city quarter the UPC density and size are the dominant factors, and groundwater depth and temperature play a subordinate role (Figure 3.8b.) The by far highest overall impact on TGW occurs in Mitte with  $8.2 \text{ MW}$  and  $259.5 \text{ TJ}$  of heat energy emitted annually into the groundwater, which corresponds to 40% of the total heat flow of Berlin ( $20.7 \text{ MW}$ ;  $652.6 \text{ TJ/a}$ ). Marzahn-Hellersdorf on the other hand has the lowest number of UCPs (122), which results in the smallest total heat flow of  $<0.1 \text{ MW}$  and  $3.2 \text{ TJ}$  per year.



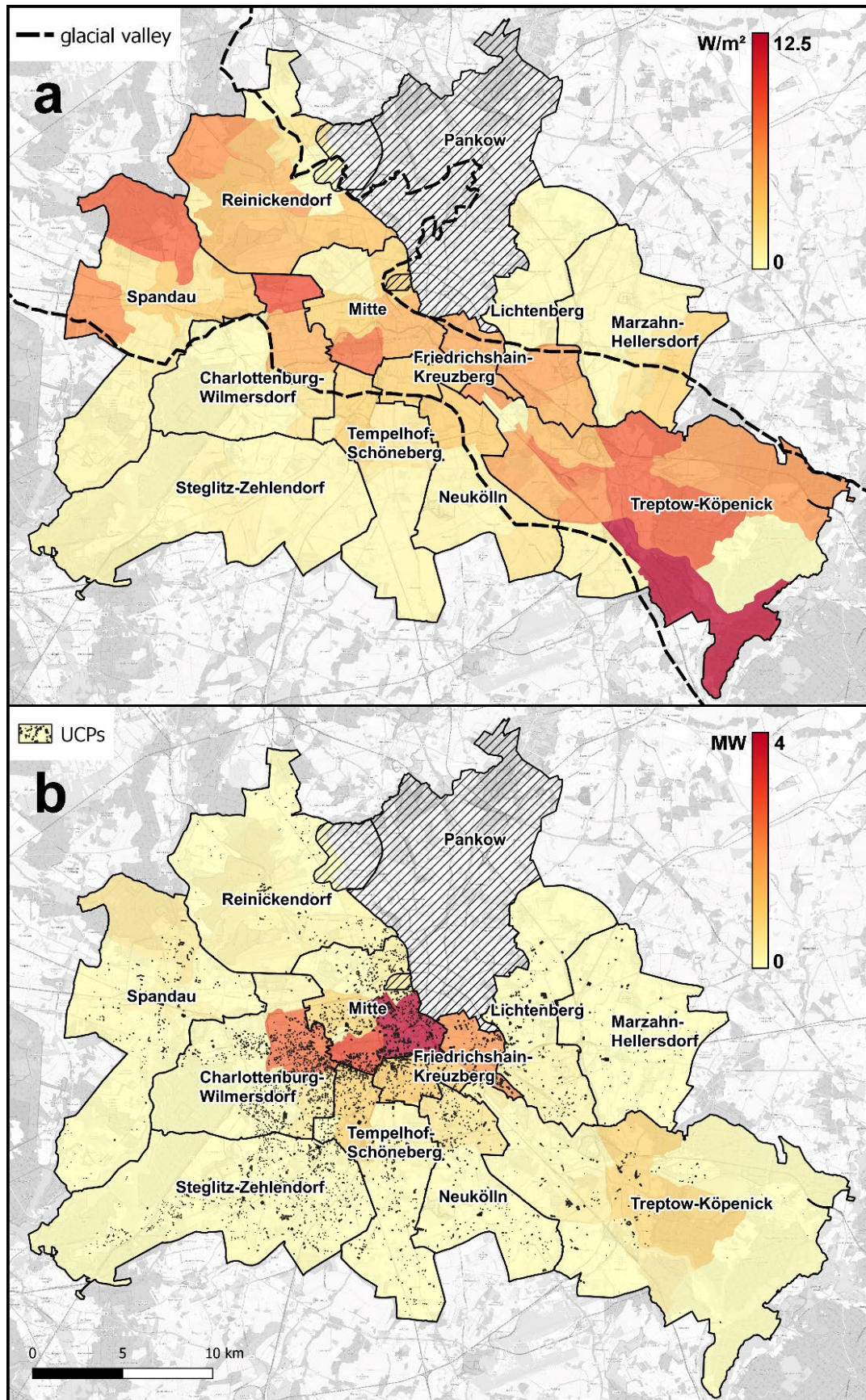


Figure 3.8. (a) Map of Berlin showing the mean heat flux through slabs ( $q_{slab}$ ) into the groundwater per city quarter. The dashed line shows the approximate boundary of the glacial valley. (b) Map of the total heat flow ( $Q$ ) from UCPs into the groundwater per city quarter. The black polygons represent the UCPs. Districts are labeled and delimited with black lines. Hatched areas have insufficient data. Background map source: OpenStreetMap.

The heat flux through the UCP slab and walls shows a strong seasonal behavior in response to the seasonal oscillation of  $T_{UCP}$  (Figure 3.9). While all UCPs heat the groundwater between April and October, differences in thermal behavior are observed for March and November. In particular in regions with high  $T_{GW}$  like the city center UCPs cool the surrounding subsurface. In the winter months, between December and February, about 75% of the UCPs cool the groundwater. Conversely, this means that the remaining 25% of UCPs heat the groundwater all year round. The annual average shows that 76% of the UCPs have a heat flux between 0 and 5 W/m<sup>2</sup>. However, some outliers appear to be highly effective heat sources with an average heat flux of 17 W/m<sup>2</sup> and up to 26.3 W/m<sup>2</sup> in July. These UCPs are located in Mitte close to the Spree River and urban green areas, where groundwater levels are relatively high and  $T_{GW}$  cool (11–12 °C). Considering a full annual cycle, all UCPs in Berlin have a net positive heat flux and therefore act as heat sources for the groundwater.

The heat fluxes of the measured UCPs are in line with the spatial analysis for Berlin. Five of the six reference UCPs seen in Figure 3.4 also have an average heat flux between 0 and 5 W/m<sup>2</sup>. With Basel #4, we have identified a UCP that is similar to the positive outliers in the spatial analysis and acts as a highly effective heat source throughout the year. The mean heat flux of the six sites presented in the UCP temperature analysis (Figure 3.4) is 4.8 W/m<sup>2</sup>, which is higher than the mean value of the UCPs in Berlin (3.2 W/m<sup>2</sup>). This is because the six measured sites, with the exception of Cologne #8, all have a very small distance to the groundwater of 0.5 m or less.

To address the parameter sensitivity of this approach additionally to Table A4, where the uncertainties of the spatial analysis are given, we applied the minimum and maximum values for each assumed parameter from Table A2 one at a time and show the error ranges in Figure A4. The most sensitive parameters appear to be  $T_{UCP}$  and  $T_{GW}$ , as a variation of 1 K changes the mean  $q_{slab+wall}$  from 3.7 to 2.6 W/m<sup>2</sup>. Furthermore, the thermal conductivity of concrete has a high sensitivity, especially the lower-end value of 0.9 W/m·K reduces the mean  $q_{slab+wall}$  to 2.5 W/m<sup>2</sup>. This shows the high impact insulation of the slab can have on the heat loss to the ground.

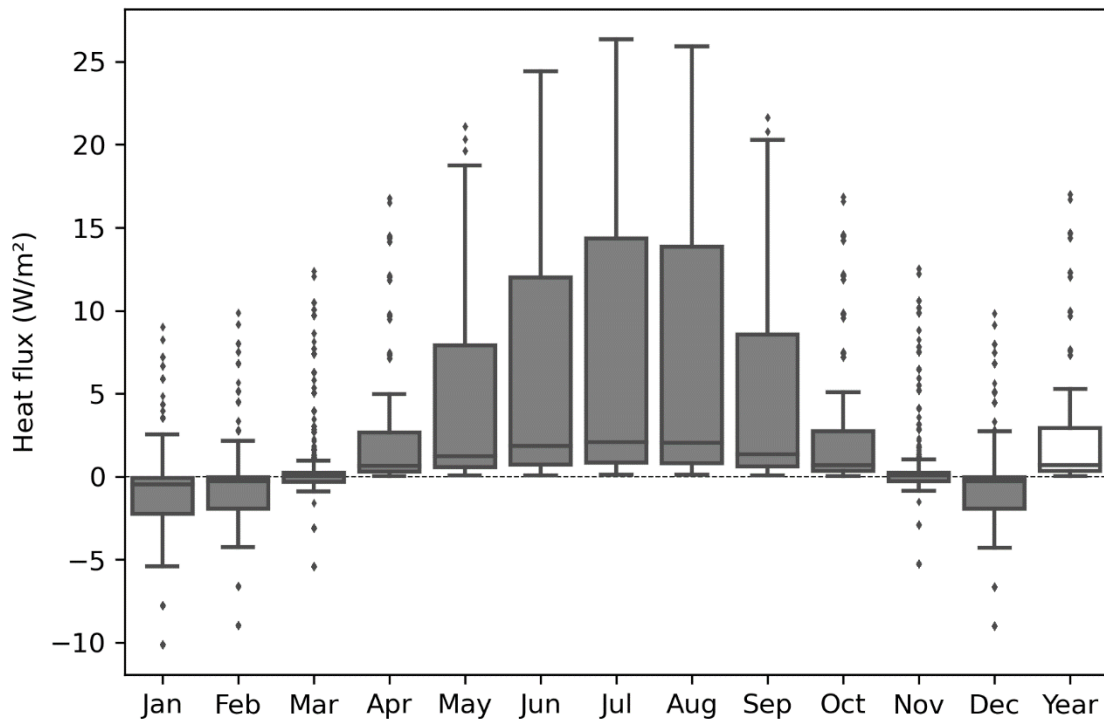


Figure 3.9. Monthly heat flux through slab and wall and average annual heat flux from each UCP in Berlin ( $n = 5040$ ).

#### Relation to other studies and heat sources

Tissen et al. (2021) determined a heat flow from various sources as a heat supply rate for shallow geothermal units for a city quarter in Vienna, Austria. They determined a total heat flow of  $0.02 \pm 0.01$  PJ/a from UCPs in Vienna based on 12 UCPs. In comparison, the impact from UCPs in Berlin is much larger at 0.65 PJ/a which accumulates from 5040 UCPs. As the total numbers are not comparable based on the number of UCPs considered, a better comparison can be made based on the average heat flux from UCPs. Tissen et al. (2021) calculated a mean value of  $15.4 \pm 5.2$  W/m<sup>2</sup>, which is significantly larger than in Berlin with  $3.7 \pm 2.2$  W/m<sup>2</sup>. This discrepancy could be caused by a different approach in the heat flux calculation. Tissen et al. (2021) used Fourier's laws to calculate the conductive heat transport between groundwater and UCP air, but do not consider the thermal properties of the slab and heat transfer coefficients.

Becker and Epting (2021) show mean heat fluxes of 0.3–4.0 W/m<sup>2</sup> for 5 UCPs in Basel. They used the same sites that are also used in this study but found noticeably smaller heat fluxes for the UCPs of Basel #4 (0.5 vs. 4.3 W/m<sup>2</sup>) and Basel #5 (4.0 vs. 15.5 W/m<sup>2</sup>). This discrepancy is caused by different values for the thermal transmittance of the UCP wall. Becker and Epting (2021) calculated with insulated UCPs, whereas in this study we assume that walls and slabs in UCPs are not insulated, since UCPs are generally unheated rooms and insulation is not legally required in Germany (§2 GEG, 2020). Hence, the thermal transmittance in our study for the same UCPs is higher than

in Becker and Epting (2021). This discrepancy also shows the magnitude of impact insulation of UCPs and basements has on mitigating heat losses into the ground.

Benz et al. (2015b), who generalized the anthropogenic heat flow for all buildings and basements in Karlsruhe and Cologne, found impacts of  $1.5 \pm 1.4$  PJ/a and  $0.3 \pm 0.1$  PJ/a, respectively. The reason for the low heat flow in Cologne is the high distance to groundwater. The resulting small heat fluxes were also observed for the UCP Cologne #8 in Figure 3.4. The heat flow of UCPs in Berlin is more than double ( $0.65$  PJ/a) than in Cologne. This amount of energy corresponds to the heating demand of 14,660 average German households, or 29,639 people, respectively (Destatis, 2023).

Compared to the heat flux induced by Earth's energy imbalance due to atmospheric warming, which is  $550\text{--}890$  mW/m<sup>2</sup> for the period 1993–2018 (Forster et al., 2021), the heat emission of Berlin's UCPs is with an average AHF<sub>UCP</sub> of  $26.7$  mW/m<sup>2</sup> still relatively low. However, the terrestrial heat flux is about  $67.1$  mW/m<sup>2</sup> (Lucazeau, 2019), which is exceeded by the AHF<sub>UCP</sub> in the districts of Mitte ( $214.5$  mW/m<sup>2</sup>) and Friedrichshain-Kreuzberg ( $148.2$  mW/m<sup>2</sup>), where the heat flux normalized to the area of the district is highest due to the high UCP density. In the district of Marzahn-Hellersdorf, on the other hand, we found both a low number of UCPs (122) and a high distance to groundwater, resulting in the lowest AHF<sub>UCP</sub> of  $1.6$  mW/m<sup>2</sup>. Considering that other heat sources, such as sewer and district heating pipes, tunnels, and surface sealing, yield an additional anthropogenic impact on subsurface temperatures, urban subsurface warming trends are expected to increase, resulting in rising  $T_{GW}$  in cities.

In comparison to the thermal impact of other structures, UCPs create stronger local anomalies but have a smaller overall contribution to subsurface warming. For example, our findings of the average heat flux from UCPs in Berlin ( $3.7 \pm 2.2$  W/m<sup>2</sup>) are higher than the heat fluxes from basements in Basel ( $0.20\text{--}0.89$  W/m<sup>2</sup>), numerically modeled for different settings (Epting et al., 2017b), or in Winnipeg, Canada, with  $\sim 2$  W/m<sup>2</sup> (Ferguson & Woodbury, 2004). The normalized heat flux per area, however, is typically higher for basements and buildings as the area covered by these heat source types is larger. Compared to the low AHF<sub>UCP</sub> of  $26.7$  mW/m<sup>2</sup> in Berlin, the AHF of buildings in Osaka, Japan, is one order of magnitude greater with  $320 \pm 180$  mW/m<sup>2</sup> (Benz et al., 2018a) and two orders of magnitude in Basel ( $5900$  to  $8000$  mW/m<sup>2</sup>) (Mueller et al., 2018).

Thermal alteration of groundwater is assumed to impact groundwater ecology and quality (Becher et al., 2022). In Berlin, special attention must be paid to areas in the Warsaw-Berlin glacial valley when it comes to groundwater protection since areas of small groundwater depth are most vulnerable to thermal pollution of aquifers (Blum et al., 2021b). However, a moderate increase in  $T_{GW}$  of 5 to 10 K yields only a minor impact on groundwater chemistry, microbiology, and fauna (Griebler et al., 2016). To date, only local thermal anomalies of highly effective heat sources (e.g., power plants or landfills) or accumulations of heat sources in dense urban areas exceed these limits.



Nonetheless, mitigation of high  $T_{GW}$  by extracting heat with geothermal applications not only protects groundwater ecosystems and urban freshwater resources but also has the potential to sustainably supply local infrastructure and buildings with green energy (Epting et al., 2020b). The heated urban environment therefore benefits geothermal applications economically in contrast to a cooler rural setting. So-called energy geostructures, which integrate heat exchanger in foundations of buildings, might be a solution for harnessing subsurface waste heat in areas of limited available space (Brandl, 2006; Loveridge et al., 2020). For example, heat exchanger can be implemented in the slab of an UCP (Lee et al., 2023). In comparison to unheated basements, publicly used UCPs have particularly high indoor temperatures and hence high local impacts on  $T_{GW}$ , which increases the efficiency of geothermal heat pumps. However, an increasing number of geothermal applications in cities raises the need of managing geothermal potential (Attard et al., 2020; Epting et al., 2017a; García-Gil et al., 2020a).

While the methods can be applied to any urban area as it accounts for climatic and hydrogeological parameters, the results of this study should not be generalized to other settings. For example, Mediterranean cities have higher natural  $T_{GW}$  and  $T_{Air}$  and therefore different environmental conditions and energy demands. Recycling of waste heat is only meaningful when the heating demand is high.

### 3.5 Conclusions

In this study, we investigated the thermal impact of underground car parks (UCPs) on groundwater. For this purpose, we collected data from 31 sites in Germany, Austria, and Switzerland. The dataset includes time series of  $T_{UCP}$ ,  $T_{Air}$ , and at six sites  $T_{GW}$ . In order to evaluate the impact on a regional scale, we expanded our analysis to 5040 UCPs in Berlin, Germany, and assessed the patterns and influencing factors of their heat fluxes.

We found the mean  $T_{UCP}$  on all investigated sites to be  $18.8 \pm 4.9$  °C. However,  $T_{UCP}$  varies significantly from site to site based on the depth and usage type of the UCP. We identified cars to be potential drivers of  $T_{UCP}$ , as public UCPs, which generally have more traffic, are on average 2.9 K warmer than private UCPs. In addition, we observed that  $T_{UCP}$  is cooler on Sundays when the traffic is reduced. Towards deeper levels the deviation between  $T_{Air}$  and  $T_{UCP}$  increases. For example, the temperature difference at the second level is on average 2.8 K higher than in the first level and subsequently hotter in the levels below. The evaluation of repeated recordings of temperature-depth-profiles confirms our understanding that public UCPs yield a higher impact on  $T_{GW}$  than private ones. All six sites with  $T_{GW}$  time series can be considered as net heat sources, with their heat fluxes into the groundwater ranging between 0.3 and 15.5 W/m<sup>2</sup> and seasonal variations in intensity and direction. For the UCP of Basel #4, which has the largest impact, we detected temporally continuous heat fluxes of

$>10 \text{ W/m}^2$ . Finally, we computed the mean of the individual linear regression from all sites to be able to derive  $T_{UCP}$  from  $T_{Air}$  to upscale the effect UCPs have at the city-scale.

Together with other open data, the regressions were used to estimate the  $T_{UCP}$  of 5040 UCPs in Berlin. The average heat flux from UCP slabs into the groundwater in the study area is  $3.2 \text{ W/m}^2$ . However, if the walls within the saturated zone are considered, the rate increases to  $3.7 \text{ W/m}^2$ . The average  $AHF_{UCP}$  of UCPs in Berlin is  $26.7 \text{ mW/m}^2$ , which is still lower than the heat flux induced by atmospheric warming ( $550\text{--}890 \text{ mW/m}^2$ ) and the terrestrial heat flux ( $67.1 \text{ mW/m}^2$ ). The district of Mitte has the highest impact with an  $AHF_{UCP}$  of  $214.5 \text{ mW/m}^2$  and a total heat flow of  $8.2 \text{ MW}$ , which corresponds to 40% of the total heat flow of Berlin ( $20.7 \text{ MW}$ ). This is due to the high UCP density and shallow groundwater in Mitte and despite the already heated groundwater. Besides the density and size of UCPs, we determined the shallow (hydro-)geological conditions as the driving factor for the distribution of heat flows. On the Barnim and Teltow plateaus in the northeast and southwest of Berlin, heat fluxes are typically lower than in the Warsaw-Berlin glacial valley (southeast to northwest). Therefore, we identified the glacial valley as most vulnerable to thermal pollution. On the other hand, the higher  $T_{GW}$  likewise enables higher efficiency of geothermal applications that utilize subsurface waste heat. Furthermore, harnessing the heat energy that is retained in UCP air through heat pumps in existing ventilation systems might be another solution for generating sustainable energy while reducing the thermal footprint on the subsurface. When looking at the individual UCPs in Berlin, we found that all UCPs heat the groundwater between April and October and the majority (about 75%) cool the groundwater between December and February. On an annual average, all UCPs in Berlin act as heat source. Ultimately,  $652.6 \text{ TJ}$  of thermal energy is emitted into the groundwater in the study area annually. This amount of energy is equivalent to the heating demand of 14,660 average German households or 29,639 people, respectively.

## 4 Estimation of shallow groundwater temperatures in Saxony-Anhalt, Germany

This chapter is translated from its original version in German language:

Noethen, M., Hemmerle, H., Meyer, L., & Bayer, P. (2024). Prognose der oberflächennahen Grundwassertemperatur in Sachsen-Anhalt. *Grundwasser – Zeitschrift der Fachsektion Hydrogeologie*, DOI: <https://doi.org/10.1007/s00767-024-00570-z>.

The original version is in Appendix B.

## 4.1 Abstract

Information on groundwater temperature (GWT) is often sparse and only available as point data from monitoring wells. For large-scale spatially distributed estimates of GWT, satellite data are a suitable complement to conventional interpolation. This method utilizes thermal coupling between land surface and the shallow subsurface. In this study, the distribution of GWT in Saxony-Anhalt is characterized. Based on remote sensing data and measurements from 436 wells, the GWT field is estimated with a spatial resolution of 500 m. In addition to the GWT and the land surface temperature, further variables are used, which influence the GWT and thus increase the accuracy of the estimation. Compared to previous studies, the results show the highest resolution and accuracy (RMSE = 0.74 K) for current GWT estimates. The methodology produces good results for all land cover classes (RMSE = 0.55–1 K). However, outliers show that a higher resolution is needed to detect local hotspots more reliably.

## 4.2 Introduction

Groundwater temperatures (GWT) play an important role in the efficient supply of green energy from shallow geothermal energy (Bayer et al., 2019; Yasukawa et al., 2009; Zhu et al., 2010). For example, a 5 K increase in GWT can elevate the output of geothermal systems by up to 40% (Rivera et al., 2017). The raising demand for geothermal energy resources increases the need for groundwater monitoring and spatially high-resolution site knowledge. A reliable supply of high-quality drinking water is even more important. In times of climate change, not only does the supply of sustainably available groundwater change, but the GWT is also subject to change as it adapts to rising air temperatures (Kurylyk et al., 2014). Increased GWT can impair groundwater ecosystems with their important purification function and thus reduce groundwater quality (Bonte et al., 2011; Brielmann et al., 2009; Griebler et al., 2016). The species diversity of stygobiont groundwater fauna, which is adapted to constant conditions, can decrease with increasing GWT (Becher et al., 2022; Blum et al., 2021b; Koch et al., 2021; Spengler & Hahn, 2018). In addition, higher underground temperatures lead to increased bacterial growth, especially in urban drinking water networks (Agudelo-Vera et al., 2017; Gunkel et al., 2022; van den Bos, 2020).

The comprehensive determination of the GWT is often difficult in practice due to the strong variability of the temperature distribution in the subsurface. As only point data can be collected at groundwater monitoring wells, the interstitial spaces are usually interpolated (e.g., Böttcher & Zosseder, 2022; Previati & Crosta, 2021b; Tissen et al., 2021). A large error can occur with low spatial density. For example, if cool, rural wells include a typically warmer built-up area in which no measured values were collected, the heat anomaly of the built-up area is not reflected in the result. To circumvent this weakness of point interpolation, it is possible to use remote sensing data. These can

incorporate the various factors that influence the GWT with spatial resolution in the calculation of an estimated groundwater temperature (eGWT). For example, the dependence of the near-surface GWT on the air temperature can be utilized. The satellite-based land surface temperature is used as a proxy for the air temperature (Čermák et al., 2014). As the GWT is also determined by other influences in addition to climatic conditions, the estimation of the GWT benefits from the inclusion of further information in addition to the land surface temperature (e.g., Benz et al., 2017a; Hemmerle et al., 2019). GWT is significantly influenced by land cover; in particular, locally increased temperatures in groundwater have been detected in areas with high building density (Böttcher & Zosseder, 2022; Epting et al., 2017b; Ferguson & Woodbury, 2007; Menberg et al., 2013a). However, evapotranspiration and the proportion of snow days can also have an effect on the offset between land surface temperature and GWT due to evaporative cooling or insulation and thus improve the results of an estimation (Shukla & Mintz, 1982; Sun et al., 2016; Zhang, 2005).

Previous approaches to calculating GWT using remote sensing data have focused on urban areas, with the exception of a study by Benz et al. (2017a), in which a global dataset was used. For cities in Germany (Benz et al., 2015a; Hemmerle et al., 2020), France (Hemmerle et al., 2019) and China (Zhan et al., 2014), subsurface urban heat islands (Ferguson & Woodbury, 2007; Menberg et al., 2013a) have been characterized using satellite-based datasets. However, little research has been conducted into how well the methodology can be applied to rural areas and how great the influence of land use is on the accuracy of the estimation.

The aim of this study is to describe and analyze the GWT distribution in the federal state of Saxony-Anhalt for the first time and then to calculate the eGWT using satellite and measurement data. The results will be analyzed with regard to the influence of land use on the GWT and the reliability of the methodology.

## 4.3 Materials and methods

### 4.3.1 Study area

The study area covers the German state of Saxony-Anhalt and is 20,452 km<sup>2</sup> in size. The three largest cities are Magdeburg, Halle (Saale) and Dessau. To the west lies the Harz low mountain range with the Brocken as its highest point (1141 m above sea level). The dominant river is the Elbe, which flows 302 km through the state from south-east to north.

Saxony-Anhalt has a temperate transitional climate between maritime and continental influences. The average annual mean temperature for the years 2007-2022 on the outskirts of Magdeburg was 10.6 °C (DWD, 2023). While the air temperatures in the higher altitudes of the Harz are significantly lower, for example an average of 4.7 °C at the Brocken (DWD, 2023), the temperatures in urban agglomerations typically rise

by 1–2 K compared to the surrounding area due to the dense development (Tzavali et al., 2015).

#### 4.3.2 *Measurement and remote sensing data*

The GWT data used originates from groundwater quality measurements by the Saxony-Anhalt State Office for Flood Protection and Water Management (LHW, 2023) and from measurements carried out by members of the group of Applied Geology of the University of Halle. The selected LHW data was collected between 2007 and 2022. In the groundwater quality measurements, the groundwater is pumped until physicochemical parameters are stable, but at least twice the well volume has been pumped. The temperature of the pumped groundwater is then measured in a flow-through cell on the surface. With this method, the measuring depth of the GWT corresponds approximately to the average depth of the filter section. Our own measurements were carried out in the cities of Magdeburg (Feb., Jun., Nov. 2021), Halle (Feb., Jun. 2020; Jan., Jun., Nov. 2021) and Dessau (Mar., Jun. 2020; Jan., Jun., Nov. 2021) as well as the Saalekreis (Jun., Aug. 2021). Depth profiles were measured with the help of temperature cable light meters from HT Hydrotechnik and SEBA. Both devices have a measurement accuracy of <0.1 K.

The available groundwater data was limited to the depth range of 10 to 50 m below ground level in order to minimize the influence of seasonal temperature fluctuations and the geothermal gradient. Wells with a distance of less than 3 m to each other were summarized. From a total of 1098 wells, 436 were selected for further evaluation, 325 of which were sampled by the LHW and 111 of which were sampled in our own measurements. The frequency of the measurements varied, and each of the selected monitoring sites was sampled an average of twelve times. A visualization of the measurement repetitions per measuring point can be found in Figure C1 for the quality measurements of the LHW. The number of measurement repetitions is highly heterogeneous, with 15 wells being sampled only once and a maximum of 32 repetitions being achieved. Figure C1 also shows the distribution of measurement times. This shows a focus on spring and autumn. The temperature data from the selected wells were summarized consecutively as monthly, quarterly, and annual averages, as well as averages between the years 2007 and 2022.

Remote sensing data of land surface temperature (Wan et al., 2021), evapotranspiration (Mu et al., 2014) and the proportion of snow days (Hall et al., 2006) with a ground resolution of approximately 1 km (land surface temperature = MODIS/061/MOD11A1 and MODIS/061/MYD11A1, evapotranspiration = MODIS/006/MOD16A2) or 500 m (proportion of snow days = MODIS/MOD10A1) were used to calculate the eGWT. These were converted to a resolution of 500 × 500 m as an average for the period 2007–2022. Four representative locations were used to estimate the temporal variability of the land surface temperature. During this period, the land surface temperature shows a linear trend of 0.13 K/a (Halle: 0.13 K; Brocken:

0.12 K; Altmark: 0.14 K; Börde: 0.14 K) and a variance from the annual means of 1.44 K (Halle: 1.31 K; Brocken: 1.13 K; Altmark: 1.71 K; Börde: 1.60 K). The spatial variance of all pixels in Saxony-Anhalt is 0.42 K. The proportion of snow days was additionally masked with regard to the distribution of surface waters (MODIS/061/MCD12Q1). The building density was averaged from the latest impervious built-up data from 2018 (European Environment Agency, 2023) to the 500 m grid of the other datasets. CORINE Land Cover (CLC) data from Copernicus was used for further analysis (European Environment Agency, 2023). Figure 4.1 shows all datasets used as maps.

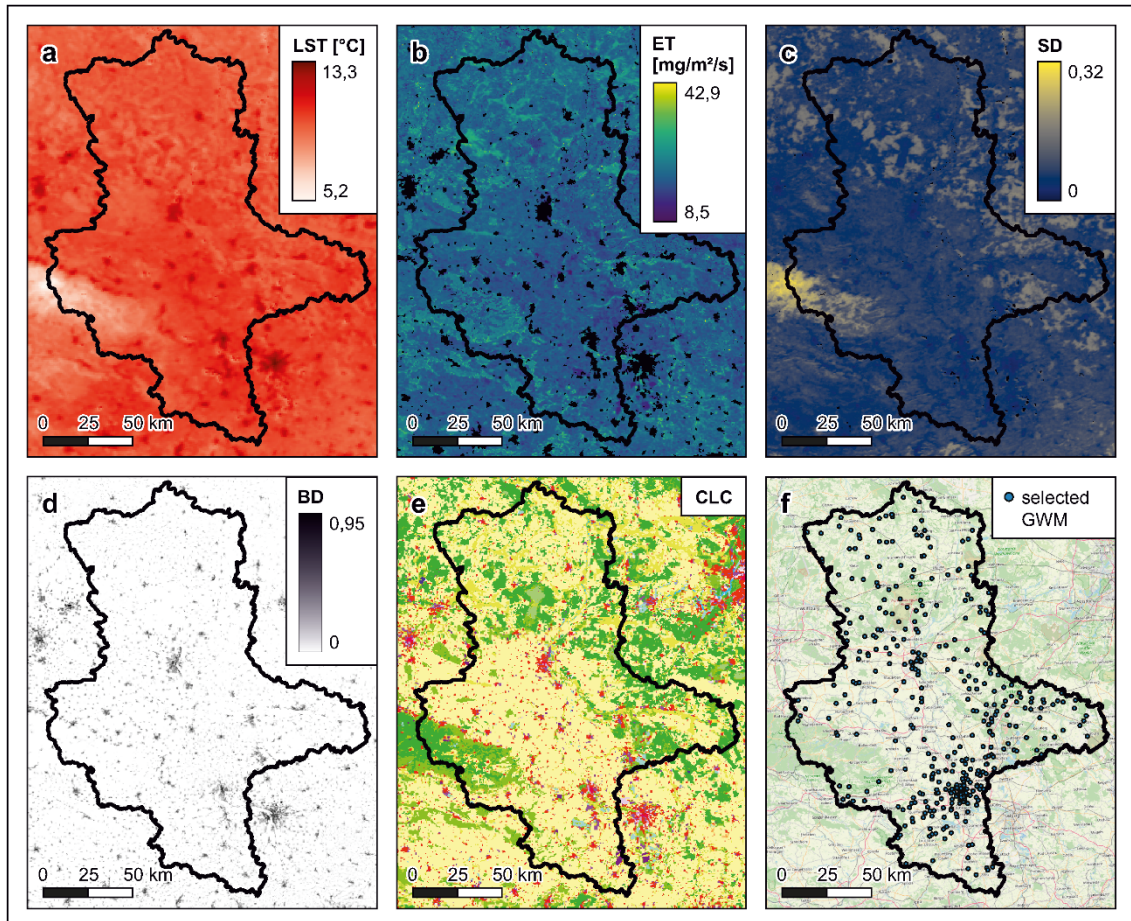


Figure 4.1. Maps of Saxony-Anhalt with the datasets used: (a) raster data of the Land Surface Temperature (LST); (b) raster data of Evapotranspiration (ET); (c) raster data of Snow Days (SD); (d) raster data of Building Density (BD); (e) raster data of CORINE Land Cover (CLC); (f) point data of selected monitoring wells (GWM).

### 4.3.3 Current state of research

An initial investigation of the relationship between ground temperatures and satellite-based land surface temperature was carried out by Zhan et al. (2014), but only included depths down to 3.2 m below ground level and was validated with measurement data at only nine points. This approach was further developed by Benz et al. (2015a) for the four German cities of Berlin, Munich, Cologne, and Karlsruhe by additionally considering building density and basement temperature to better reflect the heat flux from anthropogenic sources. A Spearman correlation coefficient of 0.8 was achieved, with particularly high correlations for older cities. Nevertheless, the

GWT was warmer than the land surface temperature in 95% of the pixels, with an average underestimation of the annually averaged GWT by 1.5 K. The study shows that GWT cannot be estimated using land surface temperature alone, although there is a significant correlation. Other influencing factors, such as underground anthropogenic heat sources, warm the groundwater in cities additionally (Menberg et al., 2013b). (Benz et al., 2017a) introduced a methodology that establishes an empirical relationship between evapotranspiration and the proportion of snow days with the difference between GWT and land surface temperature and applied this to a global dataset. This allowed the root mean square error (RMSE) of the GWT estimation to be reduced by 0.5 K to 1.4 K compared to an estimation based solely on the land surface temperature. (Hemmerle et al., 2019) combined the approaches from Benz et al. (2017a) for rural areas with the proposals from Benz et al. (2015a) for urban areas to produce a GWT estimation for Paris. Based on GWT measurement data from 377 wells, an estimate was made with a further reduction of the RMSE to 0.96 K. In a further study, Hemmerle et al. (2020) applied the approach of Benz et al. (2017a) with the additional consideration of building density for the city of Cologne. The GWT estimation was able to achieve the most accurate results to date with an RMSE of 0.86 K.

#### 4.3.4 Calculation and evaluation of the groundwater temperature

In the previous studies, the calculations of the eGWT were carried out using multiple linear regression. For the present study, we compared the results for various alternative approaches in advance (Table C1). However, as the more complex methods only provided a small reduction in the forecast error, we only present the established multiple linear regression method for calculating the eGWT in the main text (Benz et al., 2017a; Hemmerle et al., 2019).

The methodology for calculating the eGWT follows Hemmerle et al. (2020) using the land surface temperature (LST), evapotranspiration (ET), the proportion of snow days (SD) and the building density (BD). The following equation was applied for each spatially discretised pixel:

$$eGWT = LST + 0.02 \left[ K \frac{m^2 \cdot s}{mg} \right] \cdot ET + 7.47 [K] \cdot SD + 2.23 [K] \cdot BD + 0.29 [K] \quad (4.1)$$

While the y-axis intercept adds an offset of 0.29 K for each pixel, the remaining regressors contribute to the eGWT to varying degrees, depending on the derived regression coefficients and the regressors. Averaged over the area of Saxony-Anhalt, evapotranspiration has the strongest influence at 0.33 K. The influences of snow cover and building density are about half as large at 0.17 K and 0.16 K, respectively. However, the building density shows the greatest local changes of up to 1.66 K. The distribution of the contributions of the regressors is shown in Figure 4.2.



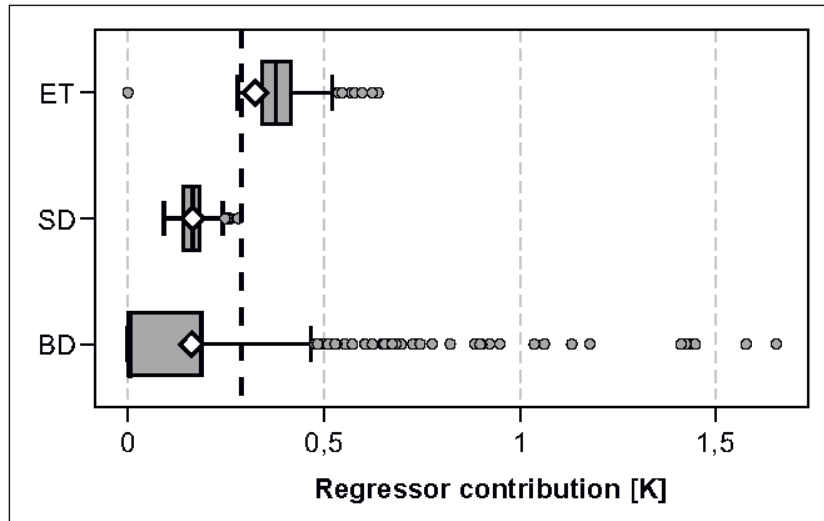


Figure 4.2. Regressor contributions for the calculation of the estimated groundwater temperature per monitoring well, shown as box plots. The dashed line shows the contribution of the y-axis intercept. The mean values are marked with diamonds. ET = Evapotranspiration, SD = Snow days, BD = Building density.

## 4.4 Results and discussion

### 4.4.1 Spatial distribution of groundwater temperature

First, the distribution of the measured GWT is considered (points in Figure 4.3). The coldest GWT of 8.7 °C was recorded in a forest area near Rottleberode in the southern Harz Mountains. At higher altitudes in the Harz Mountains, where even colder temperatures are to be expected, there are no wells in the hard rock in the monitoring network. The elevated temperatures in the cities of Magdeburg, Halle, and Dessau of up to 17 °C (15.7 and 16.6 °C, respectively) are noticeable. The high GWTs are generally attributable to anthropogenic sources, as in the case of the warmest well sampled, which is located in the immediate vicinity of a medical facility with a basement in the south of Magdeburg. The heat emission from the basement could have a direct influence on the high GWT here. The fact that the highest temperature in Magdeburg was not measured in the city center, where the buildings are the densest, shows the strong influence of local heat sources on the thermal field of the subsurface and the resulting strong variability of groundwater temperatures. The respective CLC class was assigned to each well for further evaluation. This allows the influence of land use on the GWT to be investigated. To simplify matters, the classes were combined into groups (Table C2).

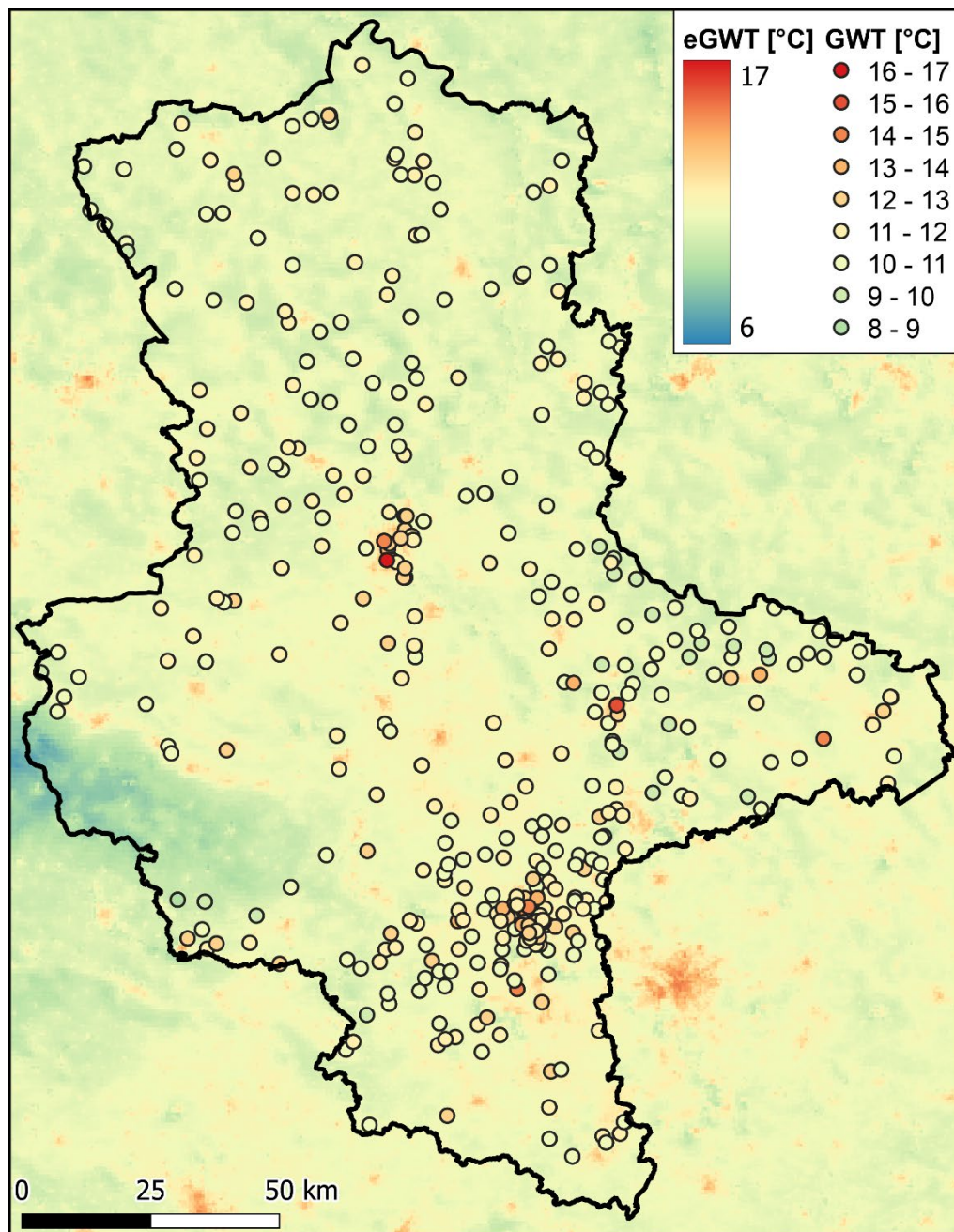


Figure 4.3. Estimated groundwater temperatures (eGWT) in Saxony-Anhalt with the measured groundwater temperatures (GWT) as points.

The arithmetic mean of the measured GWT in Saxony-Anhalt is 11.2 °C, with a spatial variance of 1.08 K. The temporal variance that occurs between the individual measurements, on the other hand, is lower at 0.87 K. The mean vertical variance of the GWT within the monitoring wells is 0.03 K. It was calculated from all temperature profiles between 10 and 50 m depth ( $n = 100$ ), whereby it must be noted that the profiles cover different depth ranges. At 81% of the sampled wells, the GWT is below 12 °C and can therefore be considered natural under the prevailing climatic conditions. Results of other studies that have evaluated the distribution of GWT in a region or country show similar values. However, comparability is limited by differing climatic conditions and differences in data collection. For example, Riedel (2019)

describes an average GWT of 10.6 °C for Baden-Württemberg between 2000 and 2015, while Benz et al. (2018b) state an average GWT of 11.4 °C for the year 2013 in Austria.

Even though an attempt was made in this study to cover all regions of the country by conducting additional measurement campaigns in urban areas, agricultural areas and forest and natural areas (79% of the monitoring sites) are represented more strongly than urban areas due to the LHW's monitoring network, which is based on the Water Framework Directive. The high altitudes of the Harz Mountains are also not represented in this study. In addition, the different number of samples per monitoring site as well as the uneven distribution of monitoring times may have an influence on the results (Figure C1). A dependence of the GWT on the measurement depth is not apparent within a depth of 10 to 50 m (Figure 4.4). The error due to seasonal temperature fluctuations in the near-surface area is generally <1 K below 10 m (Anderson, 2005; Böttcher & Zosseder, 2022; Kurylyk et al., 2019) and is additionally reduced in this study by the repeated measurements. The different measurement methods and measuring devices also represent a possible source of error. Temperature values in groundwater quality measurements could be slightly higher compared to in-situ measurements due to the pumping process. However, this has not yet been systematically investigated. As no accompanying in-situ measurements were carried out in Saxony-Anhalt, we are also unable to determine this error here. However, data from a study by Hemmerle et al. (2022) show that the temperature in groundwater quality measurements in Cologne was overestimated by 0.29 K on average.

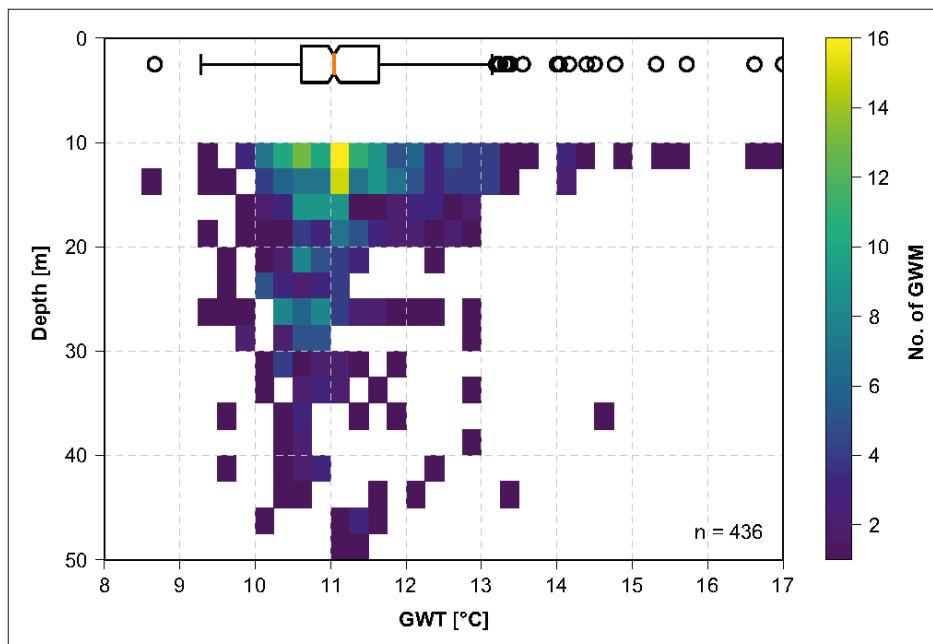


Figure 4.4. Average measurement depth and groundwater temperature (GWT) of all monitoring wells, shown as a scatter plot with boxplot of GWT distribution at the top. The colour of the pixels indicates the number of monitoring wells (GWM).

It is also possible that suspending the pump at the medium height of the filter section does not guarantee that the pumped groundwater originates from this depth. Due to the heterogeneity of the hydraulic permeability of the sediments in the area of the filter section, the true extraction depth may deviate from the average filter section depth.

#### 4.4.2 Comparison between measured and estimated groundwater temperature

The estimated groundwater temperatures are shown as a grid in Figure 4.3. The distribution depicts the expected patterns of land surface temperature, showing an increase in eGWT in urban areas and the coldest eGWT of below 8 °C in the Harz Mountains. To assess the quality of the eGWT calculated from the satellite images, the results are compared with the measured GWT. Figure B5 shows scatter plots that illustrate the correlations of eGWT/GWT and land surface temperature/GWT. An estimation based solely on the land surface temperature would have an RMSE, i.e., the deviation of the measured value from the estimated value, of 1.22 K and would underestimate the true GWT by an average of 0.94 K. A better estimate would be provided by the mean value of the measured GWT of 11.2 °C alone (RMSE 0.84 K). The estimation using a single additional remote sensing parameter reduces the RMSE considerably to 0.77 K (evapotranspiration; proportion of snow days) and 0.75 K (building density).

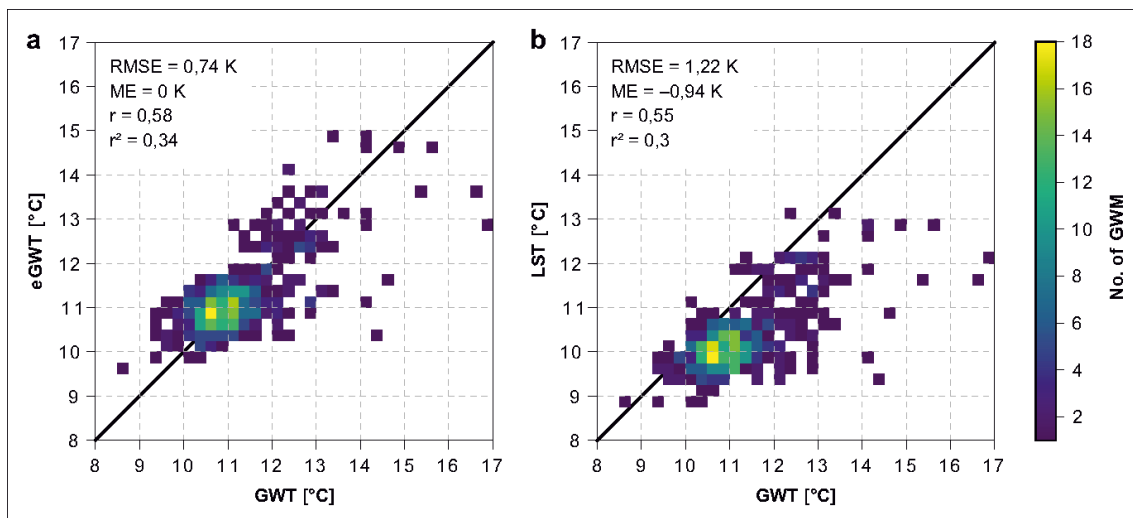


Figure 4.5. Scatter plots showing the correlation of (a) estimated (eGWT) and measured groundwater temperature (GWT); (b) Land Surface Temperature (LST) and GWT. The color of the pixels indicates the number of wells (GWM). The errors are indicated by the Root Mean Square Error (RMSE) and the Mean Error (ME). The Spearman correlation coefficient is indicated by  $r$  and the coefficient of determination by  $r^2$ .

The accuracy of the estimation with all regressors was improved by an RMSE of 0.74 K compared to previous work. Previous studies for a global dataset, for Cologne and for Paris (Benz et al., 2017a; Hemmerle et al., 2020; Hemmerle et al., 2019) show higher RMSEs of 0.86–1.4 K. The slightly improved result can be attributed, among other things, to the high number and wide distribution of wells. Furthermore, fewer

outliers with high GWT caused by local heat sources can be observed in rural areas. As a result, a higher error is to be expected for studies in urban areas, such as Paris and Cologne, where groundwater is more frequently influenced by buildings.

The three highest positive and negative outliers are summarized in Table C3. Strong underestimates of the GWT in Magdeburg ( $-4.2$  K) and Dessau-Roßlau ( $-3.1$  K) are due to local temperature anomalies caused by building development. In Klöden, the lower estimation ( $-3.9$  K) is presumably due to the proximity to the Elbe and the associated infiltration of warmer surface water. An overestimation of the GWT by the model can be observed in particular for green areas (agricultural areas or city parks) within or near urban structures. In this study, the measured GWT in various cases in Halle (Saale) is lower than the estimation ( $1.5$ – $1.8$  K). Green areas in cities generally show lower GWT than surrounding built-up areas. The satellite data, on the other hand, with a resolution of 500 m, is in some cases too coarse to capture smaller green areas in cities. This shows the general problem of GWT estimations with low-resolution satellite data, namely that regional effects such as subsurface urban heat islands can be reproduced well, but local anomalies are only inadequately mapped. This effect also results in the relatively low coefficient of determination of 34% in the estimation. In addition, there are influences from the averaging of the input data over several years, the averaging over depth and the measurement errors in determining the groundwater temperature, which have a negative impact on the accuracy of the model results. For example, an error due to the warming of the water during the pumping process can be assumed in the groundwater quality measurements, which is included with the other uncertainties in the high residual error of the estimation and partially justifies it.

#### 4.4.3 Influence of land use on groundwater temperature

In order to better evaluate the influence of land use on the GWT and eGWT, which was already evident in the outliers of the estimation, the CLC classifications of the wells is evaluated. The average values for the GWT and eGWT of the respective CLC groups and the resulting RMSE (Table C4) provide information on the suitability of the methodology for the different land use classes (Figure 4.6).

As expected, lower GWTs can be measured in rural areas than in urban areas. Forest and natural areas have the lowest average GWT in Saxony-Anhalt with  $10.7$  °C and a variance of  $0.48$  K, followed by agricultural areas ( $11.0$  °C  $\pm$   $0.44$  K). In urban areas, urban green spaces are the coldest at  $11.7$  °C  $\pm$   $4.01$  K, while in urban and industrial areas the GWT rises to  $12.3$  °C  $\pm$   $1.21$  K and  $12.6$  °C  $\pm$   $0.85$  K, respectively. The difference between the coldest and warmest CLC group is therefore  $1.9$  K.

The best results are obtained for the wells in forest and natural areas (RMSE =  $0.55$  K,  $n = 78$ ) and on urban green spaces (RMSE =  $0.62$  K,  $n = 8$ ). This is due to the lower influence of local heat sources in forest and nature areas. Only eight wells were classified as urban green spaces. Due to the low number of data points and therefore

low representativeness, the result for urban green spaces must be assessed critically. At the same time, wells that are actually located on green spaces or strips fall into the urban structure class. As a result, the true value of the average GWT is probably higher than the calculated 12.3 °C.

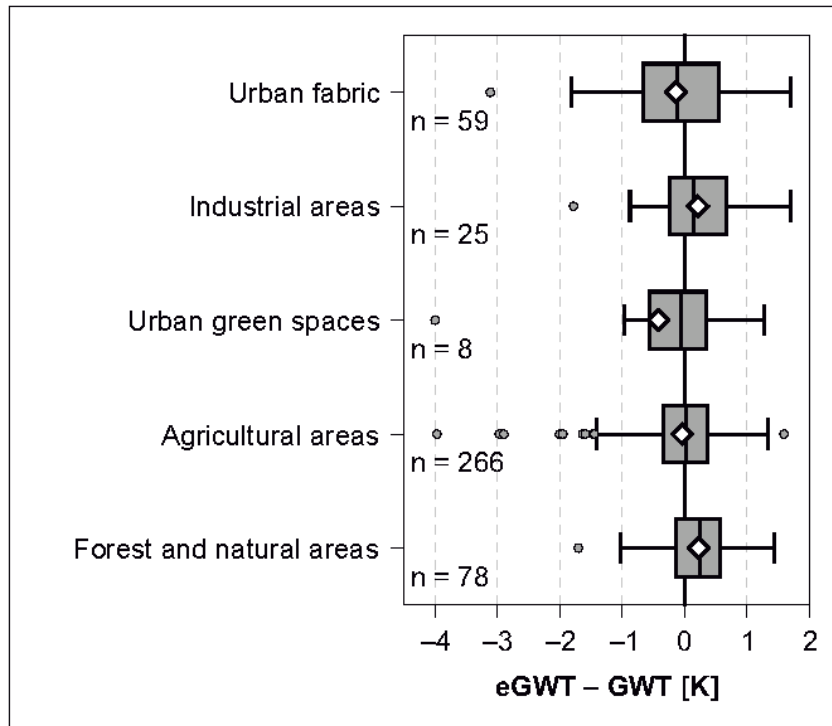


Figure 4.6. Difference between estimated (eGWT) and measured groundwater temperature (GWT) as boxplot per land use group. The number of measured wells in the respective land use group is indicated by n. The mean values are marked with diamonds.

For agricultural areas, on which 61% (n = 266) of the wells are located, the RMSE is 0.71 K. Here too, it can be assumed that there is little anthropogenic influence and therefore a more homogeneous temperature distribution compared to urban areas. The heterogeneity of the temperature field in cities is reflected in the errors for the CLC groups “urban structure” and “industrial areas”, which are higher than the average at 0.95 and 1.00 K, respectively. Urban GWT additionally depend on underground heat sources, which cannot be mapped with this methodology, and are less strongly coupled to the land surface temperature. In addition, the locally strongly varying GWT in cities can be poorly reproduced at a spatial resolution of 500 m.

The estimation error can be reduced in future, in particular through a higher resolved spatial and temporal discretization of the input data. The consideration of anthropogenic heat sources such as wastewater and district heating networks or tunnels would also enable more accurate estimates than with building density alone but requires detailed datasets. Similar approaches as used by Menberg et al. (2013b) or Benz et al. (2015b) to determine heat fluxes into urban aquifers could be used by resolving different heat sources in detail for model areas. If the GWT for smaller areas is to be estimated with high resolution, however, numerical models are suitable,

which can also take aquifer properties into account in addition to anthropogenic influencing factors, but are correspondingly more complex to parameterize and calculate (Epting et al., 2013; Makasis et al., 2021). Satellite-based calculations, as presented in this study, are suitable for making reliable regional-scale estimates of GWT using publicly available data. The procedure represents a reliable alternative to the commonly used interpolation methods, especially in areas with lower data density or uneven distribution of wells. The results of the eGWT distribution can be used, for example, to map geothermal potential (Hemmerle et al., 2022).

## 4.5 Conclusions

The distribution of shallow GWT in Saxony-Anhalt is characterized for the first time in this study. The arithmetic mean GWT is 11.2 °C, with a spatial variance of 1.08 °C and based on repeated measurements at 436 monitoring wells. The range of GWT values from 8.7 to 17.0 °C shows the variability in the spatial distribution between natural areas and cities.

The presented calculation of the eGWT was carried out using multiple linear regression and on the basis of satellite data and the measured GWT data. The result shows a low error (RMSE = 0.74 K) and represents an improvement compared to previous studies. After evaluating the land use, the warmest GWTs can be found in urban areas (12.3 °C ± 1.21 K) and industrial areas (12.6 °C ± 0.85 K), as well as the largest errors in the calculation of the eGWT (RMSE = 0.95 and 1.00 K). The coldest GWTs were measured in forest and natural areas and agricultural areas (10.7 °C ± 0.48 K; 11.0 °C ± 0.44 K), which corresponds to the expected temperature distribution in the subsurface. The methodology used is most reliable for forests and natural areas with an RMSE of 0.55 K. Regional trends such as urban heat islands in the subsurface are reliably mapped, while local heat anomalies are generally poorly detected due to the pixel size. The poorer applicability in urban areas that can be derived from the errors is due to the greater heterogeneity of the GWT due to small-scale changes in land use and the large number of anthropogenic heat sources. A smaller pixel size of the satellite data and the inclusion of other factors such as underground anthropogenic heat sources would offer potential for improvement for use in urban areas.

The methodology used can be easily and cost-effectively transferred to other regions and offers an alternative to the simple interpolation of point data, which requires a high number and homogeneous distribution of wells. A higher resolution of the estimation can be achieved with numerical groundwater models, which are therefore particularly suitable for small-scale issues. However, numerical approaches are comparatively complex to parameterize and calculate. The results of this study can be used, for example, to map the potential for near-surface geothermal energy.

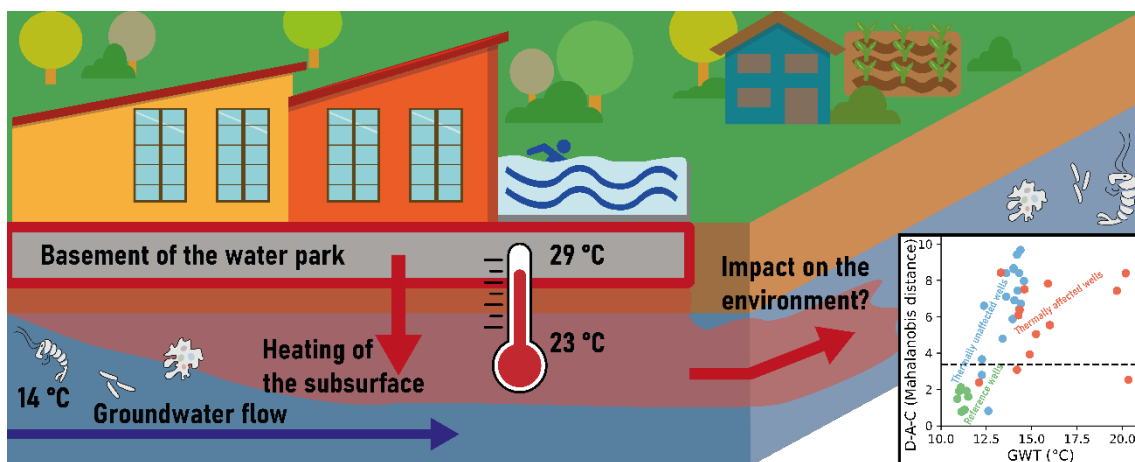


## 5 Environmental impact of an anthropogenic groundwater temperature hotspot

This chapter is reproduced from:

Noethen, M., Becher, J., Menberg, K., Blum, P., Schüppler, S., Metzler, E., Rasch, G., Griebler, C., & Bayer, P. (2024). Environmental impact of an anthropogenic groundwater temperature hotspot. *Science of the Total Environment*, 955, 177153.

### Graphical abstract





## 5.1 Abstract

Heat emitted by buildings and other infrastructure accumulates in the subsurface. This additional heat can cause a pronounced shift in thermal boundary conditions of the important groundwater ecosystem. Shallow groundwater systems in Central Europe are often inhabited by communities of fauna adapted to cold and stable conditions as well as microorganisms, whose activity is dependent on ambient temperatures. At a local groundwater temperature hotspot of up to 23 °C, caused by a water park, we assessed the environmental impact of this thermal alteration on the shallow groundwater system. The results show that the overall groundwater quality at the site is influenced by anthropogenic land use, compared to wells in a nearby water protection zone. However, neither hydrochemical nor ecological characteristics of groundwater from wells in the vicinity of the water park indicate any significant dependence on temperature. Hence, we conclude that in this eutrophic and anoxic aquifer moderate heat stress does not lead to significant alterations in terms of hydrochemistry as well as microbiological properties. Due to the overall low oxygen concentrations (<1 mg/l), stygofauna is present only occasionally and cannot be used as bioindicators. These results have to be verified for other aquifer types and would benefit from a more in-depth analysis of microbial community composition.

## 5.2 Introduction

The shallow subsurface is increasingly utilized by geothermal applications, altering groundwater temperatures (GWT) especially in densely populated areas (Epting et al., 2017b; Menberg et al., 2013a; Vienken et al., 2019). Beside these wanted interventions, many other unintended heat sources cause increased subsurface temperatures (Noethen et al., 2022). The most prominent and impactful is the anthropogenically induced climate warming as atmospheric temperatures delineate the natural state of shallow GWT (Benz et al., 2024; Hemmerle & Bayer, 2020; Loeb et al., 2021). Typically, shallow subsurface temperatures can be approximated by the annual average air temperature + 1–2 K, depending on hydrogeological factors as well as land cover (Benz et al., 2017a, 2017b; Molnar, 2022; Stauffer et al., 2013). Hence, a rise in air temperatures directly impacts GWT with a temporal delay. Additionally, other heat sources, such as buildings with basements (Benz et al., 2015b; Makasis et al., 2021), tunnels (Epting et al., 2020a), and district heating networks (Tissen et al., 2021), contribute unintentionally to subsurface warming by various processes, like conductive heat transport from underground car parks (Noethen et al., 2023), leakage of warm waste water in sewage networks (Benz et al., 2015b), or biochemical heat generation in municipal solid waste landfills (Coccia et al., 2013). This heat can accumulate and ultimately form subsurface heat islands of typically up to 7 K in cities where the underground space is heavily used (Hemmerle et al., 2022; Previati & Crosta, 2021a).

Additional heat can affect groundwater chemistry, for example, through enhanced carbonate precipitation (Griffioen & Appelo, 1993), increased mobility of heavy metals (Bonte et al., 2013), or reduced oxygen concentrations (Figura et al., 2013; Riedel, 2019). Furthermore, shallow aquifers host ecosystems that deliver valuable services, such as biological water purification (Griebler & Avramov, 2015). Increasing GWT might affect these ecosystems as groundwater fauna and microbiological communities are adapted to stable conditions. Additionally, urban aquifers are already stressed by various factors, such as salt and heavy metal pollution or oxygen depletion (Becher et al., 2022). A good indicator for adverse changes in groundwater quality is the abundance of prokaryotic cells (Fillinger et al., 2019; Retter et al., 2021), which may increase with rising temperatures (Lienen et al., 2017). While higher water temperatures stimulate microbial metabolism, bacterial growth in clean and oligotrophic groundwater systems is limited due to restricted energy availability (Briemann et al., 2009). Hartog et al. (2013) found no correlation between bacterial quantities and temperature at a monitored aquifer thermal energy storage (ATES) site (11–35 °C). Microbial biodiversity, on the other hand, is expected to change already at a moderate GWT increase, not only in eutrophic aquifers (Briemann et al., 2011; Griebler et al., 2016). Additionally, a negative relationship was observed between water temperature and both biodiversity of groundwater fauna (Briemann et al., 2009; Spengler & Hahn, 2018) and the lethality of individual crustacean species (Briemann et al., 2011). The impacts of a locally confined heat plume caused by thermal energy discharge on shallow groundwater ecosystems was previously studied by Briemann et al. (2009). They measured GWT of up to 17 °C and detected no significant correlation between temperature and bacterial and faunal abundances. However, they could associate an increase in bacterial diversity and, at the same time, a decrease of faunal diversity with the thermal anomaly. This could be due to the fact that microbial communities are generally ubiquitous and less adapted taxa can easily be replaced by others as environmental conditions change, whereas stygofauna are mainly cold stenotherms with a small thermal tolerance (Briemann et al., 2011). Loss of species is hardly compensated by new ones. In most countries, thermal alterations of the subsurface by geothermal applications are not regulated (Hähnlein et al., 2010) while the unintended impacts of anthropogenic structures are not yet considered (Blum et al., 2021b).

In this study, we present a holistic field investigation, aiming to (1) quantify the thermal impact on the groundwater caused by a public water park (“Aquadrom Hockenheim”) and its associated basements and (2) investigate the environmental impact of the induced local heat plume on groundwater quality and ecology. By repeatedly sampling nine wells in the immediate vicinity of the water park and three wells in a nearby water protection zone, we are able to determine possible deviations from the natural state and a deterioration between thermally unaffected wells and those affected by the thermal plume of the water park. Evaluation of the ecological

state of the groundwater is done by the D-A-C index based on different microbial measures, namely the prokaryotic cell density, activity, and bioavailable carbon (Fillinger et al., 2019). In addition, occurrence of groundwater fauna was evaluated. Insights gained about temperature-induced ecological changes will help uncover possible consequences of unintended thermal impacts of anthropogenic heat sources to groundwater communities and in consequence to groundwater quality. The findings will also support knowledge-based decision making of policy makers and authorities, for example, for the utilization of the subsurface by geothermal applications or low-temperature thermal energy storage systems, such as subsurface thermal energy storage systems (Bott et al., 2024; Fleuchaus et al., 2018).

## 5.3 Materials and methods

### 5.3.1 Study site

The site of investigation is located in the north-western part of the German state of Baden-Württemberg (Figure 5.1a) with the water park called “Aquadrom” at the southern border of the city of Hockenheim. The land use of the surroundings is a mixture of residential and agricultural areas. Three reference wells (RE1–RE3) are embedded in the Reilingen forest, approximately 3–4 km south of the water park (Figure 5.1b). Since the wells are located in a water protection zone II, the condition of the groundwater can be considered close to natural and thermally undisturbed. The depth of the three wells is between 30 and 33 m.

The water park itself consists of an indoor and outdoor area. The basement is located mainly underneath the indoor area, but also extends north to the outdoor pools. One extraction well (P9) and three observation wells (GWM1–GWM3) are placed in the south-eastern corner of the property in an upstream location. One observation well is drilled through the basement slab, allowing the groundwater beneath the building to be studied (P8). Four observation wells are in different downstream locations on the property (P1, P2, P4, P5; Figure 5.1c). All wells have a depth of 7–10 m, except for P9 which is 15 m deep. In the north-eastern area of the property there is an oil-fueled cogeneration plant, which supplies the water park with heat and power.

The thermal impact of the Aquadrom was investigated earlier in the context of a feasibility study for a thermal energy storage of waste heat in the upper aquifer (Blum et al., 2021a). The results of this study show a limited suitability for aquifer thermal energy storage due to the relatively high groundwater velocity and shallow groundwater depth, which can reduce the recovery rate.

Hockenheim is located on the Lower Terrace of the Upper Rhine Graben which consists of fluvial Late Pleistocene deposits and extensive fluvial flood deposits and channel fillings (HGK, 2001). Drillings at the study site show sandy gravels to medium sands as well as peaty layers and clayey-silty lenses, deposited by the small River Kraichbach, which is located about 250 m to the east.

The direction of groundwater flow at the study site is approximately north-west towards the Rhine River (Figure 5.1c). A previous pumping test on this site published in Blum et al. (2021a) resulted in a hydraulic conductivity of  $2.1 \cdot 10^{-3}$  m/s and a groundwater velocity of about 0.5 m/d. The groundwater has a seasonally fluctuating depth of 3–5 m and is only about 1 m below the base of the Aquadrom.

The water quality in the water protection zone at the Reilingen forest is generally good. Except for the flocculation of iron and manganese, no further treatment is required to achieve drinking water quality in accordance with German law (Stadtwerke Hockenheim, 2023). However, the presence of reduced iron and manganese in the produced water clearly indicates hypoxic to anoxic conditions.

Hockenheim has a transitional climate between maritime and continental influences. The mean air temperature in the period of 1991–2020 at the weather station Waghäusel-Kirrlach in about 7.5 km distance is 11.4 °C (DWD, 2023).

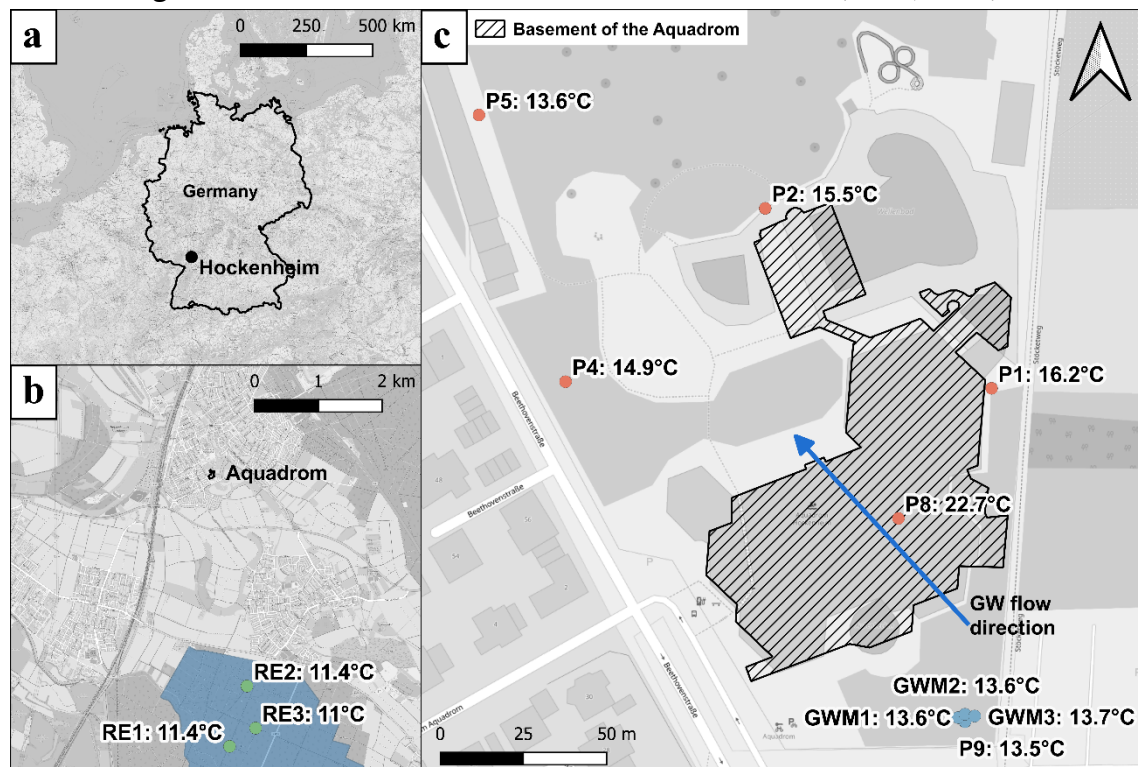


Figure 5.1. (a) Location of Hockenheim in Germany. (b) Location of the Aquadrom in Hockenheim and the position of the three reference wells in the Reilingen forest. The water protection zone II is indicated by the blue area. (c) The Aquadrom Hockenheim with all observation wells which were used in this study. The temperature labels represent the arithmetic mean over the course of a year in 5 m depth. Colors indicate reference wells (green), thermally unaffected wells (blue), and thermally affected wells (red). Basemap: OpenStreetMap.

### 5.3.2 Temperature monitoring and sample collection

The data for the temperature time series were recorded in the period from May 2022 to May 2023. HOBO data loggers of the type U20L-01 were placed at a depth of 5 m below surface level in all wells shown in Figure 5.1. They monitored the water level as well as the GWT with an accuracy of  $\pm 0.37$  K and a resolution of 0.1 K. Additionally, four temperature data loggers of the type U22-001 (accuracy:  $\pm 0.21$  K, resolution: 0.02 K) were deployed, one of them in P8 at 2.5 m depth below surface level and the

others in P9 at 2.5 (attached above groundwater surface), 10 and 15 m depth. Two data loggers of the type MX2201 (accuracy:  $\pm 0.5$  K, resolution: 0.04 K) monitored the basement air temperature and one of the same type monitored the outdoor air temperature in a covered and shaded area at 2 m above ground level. All loggers were deployed with a temporal resolution of 1 h.

Sampling was performed every three months, starting in May 2022, and ending in May 2023, resulting in a total of five field campaigns. Before sampling, temperature depth profiles were taken with an RBR*duet*<sup>3</sup> T.D temperature data logger (accuracy:  $\pm 0.002$  K, resolution: 0.00005 K). It was attached to a contact gauge and lowered slowly through the well. By measuring water pressure and temperature in 0.5 s time steps, we were able to create quasi-continuous temperature profiles. Subsequently, a multiparameter probe (KLL-Q-2 with MPS-D8, SEBA), which was calibrated prior to application, was used to measure profiles of key physico-chemical parameters (pH, electrical conductivity [EC], redox potential [Eh], concentration of dissolved oxygen, oxygen saturation) in wells wider than two inches diameter. However, this applied only to the following wells: RE1, RE2, RE3 and P9.

The sampling routine involved the collection of well water and freshly pumped groundwater for both chemical and microbial analysis. Well water samples were retrieved using a bailer, while pumping was conducted with a Grundfos MP1 submersible pump. Prior to sampling from the aquifer, the well water underwent pre-purging twice the well volume and until key physico-chemical parameters stabilized. For chemical and adenosine triphosphate (ATP) analysis, samples were collected in sterilized glass bottles. Samples intended for the bacterial abundance (BA) analysis, also referred to as total cell counts, were filled into sterile 15 ml Falcon tubes supplemented with glutardialdehyde fixative (final conc. of 0.5%). Finally, samples for dissolved organic carbon (DOC) analysis were filtered through 0.45  $\mu\text{m}$  polyvinylidene fluoride (PVDF) syringe filters directly at the sampling site. Before pumping, fauna samples were taken with a modified Cvetkov net according to the procedure described in Hahn and Fuchs (2009).

Due to clogging, pumping was not possible at the wells P2 and P4 and therefore, only well water samples could be obtained here. The clogging was likely caused by iron and manganese deposits in the filter section of the wells. However, further analysis as described in Chapter 5.3.4 requires aquifer water samples. We have therefore considered P2 and P4 for the temperature analysis, but not for the ecological evaluation.

### 5.3.3 Sample analysis

Laboratory analysis of the chemical parameters of both well and aquifer water involved identifying major anions and cations by means of ion chromatography, alongside quantifying DOC with a TOC analyzer. Laboratory analysis of the chemical parameters of both well and aquifer water Evaluating the microbiological properties

of the water comprised determining BA (in cells/ml) and the concentration of cellular ATP (in pM) of prokaryotic cells. Prokaryotic cell counts were obtained utilizing flow cytometry (Cytomics FC500 Flow Cytometer by Beckman Coulter), with a detailed methodology described by Fillinger et al. (2019).

For ATP measurements, the BacTiter-Glo Microbial Viability Assay Kit (Promega) was used, following the method outlined by Hammes and Egli (2010), with adjustments as detailed by Fillinger et al. (2019). Sample preparation and measurements were conducted at room temperature and all measurements were carried out in technical triplicates. Luminescence emitted from the ATP-dependent oxidation of luciferin catalysed by luciferase was detected using the GloMax 20/20 luminometer (Promega). An ATP calibration curve was established using an external ATP standard (100 nM, BioThema) dissolved in ATP-free water (Invitrogen™ UltraPure™, Fisher Scientific). Furthermore, cellular ATP concentrations were derived by subtracting external ATP from total ATP concentrations. Measurements conducted on unfiltered samples reflected the total ATP content (Hammes & Egli, 2010). To isolate extracellular ATP by removing cells, samples aliquotes were filtered (Millex® 33 mm PVDF, 0.1 µm), enabling the assessment of luminescence solely from the extracellular ATP fraction.

#### *5.3.4 Classification of the ecological state*

On behalf of the Federal Environment Agency (Umweltbundesamt) of Germany, Griebler et al. (2014) created an assessment scheme that enables the evaluation of the ecological state of a groundwater body, named GESI. In an ideal case, this assessment is based on the proportion of the crustacea and oligochaeta populations. If not enough fauna is found, when the concentration of dissolved oxygen is regularly below 1 mg/l, or the wells are ochred, the scheme proposes an evaluation based on chemical and microbiological parameters only as living conditions are considered hostile for animals. Overall, at least five criteria have to be assessed from a number of parameters.

However, since there are no suitable reference values provided in the data set, a level 2 assessment has to be conducted (Griebler et al., 2014). This is achieved by firstly defining the natural background values of the local aquifer. The data obtained at the reference wells RE1–3 in the Reilingen forest is suitable to define the natural background since the wells are located in a water protection zone II, where no direct anthropogenic influences are to be expected. The hydrogeological conditions in this area are similar to those at the water park. Furthermore, the groundwater extracted in this forest undergoes no treatment except for the flocculation of iron and manganese, since in its natural state it already meets the chemical criteria defined in the German drinking water guideline (Stadtwerke Hockenheim, 2023). Ideally, these background values are used to evaluate at least two criteria from the following categories: (1) physico-chemical, (2) microbiological and, (3) faunistic criteria. However, faunistic criteria can only be applied to oxic aquifers, where there is a regular

presence of stygophile or stygobite fauna. The range of background values is calculated by the minimum and maximum of the mean values of each well. The ecological state of each well at the study site is then calculated by dividing the number of parameters within the reference values ( $P_{pos}$ ) with the total number of parameters ( $P_{tot}$ ), thus obtaining a quality grade between 0 and 1:

$$GESI = \frac{P_{pos}}{P_{tot}} \quad (5.1)$$

As an additional assessment scheme, the D-A-C index offers a method to identify environmental disruptions through the assessment of microbiological parameters ATP, BA, and dissolved organic carbon (Fillinger et al., 2019). The D-A-C index is calculated with the Mahalanobis distance, facilitating a multivariate outlier analysis by combining these parameters. This multivariate approach exhibits greater resilience and sensitivity in outlier detection compared to univariate analyses (Retter et al., 2021). In this multivariate space, normally distributed data forms an elliptical cloud defined by the mean values of the variables, while the covariance matrix shapes the ellipse's form and orientation (Retter et al., 2021). The Mahalanobis distance from each sample to the centroid of the ellipse serves as an indicator of disturbances if this distance exceeds distances attributable to random variation. In an unguided scenario, no specific reference groups are designated, and the analysis comprises the entire dataset. Conversely, a guided approach includes the establishment of a reference group, with outliers identified as significantly divergent from these references. The reference group comprises samples collected from wells RE1–RE3, located within the water protection zone of the Reilingen forest. To identify outliers, we defined the critical value at a 99% confidence level of a chi-squared distribution with three degrees of freedom, following the methodology of Fillinger et al. (2019). Samples with Mahalanobis distances exceeding this threshold are therefore considered as disturbed. Computations were executed using the programming language R, with variables subjected to log10 transformation prior to analysis.

## 5.4 Results and discussion

### 5.4.1 Thermal impact on groundwater

As a water park with several swimming pools and an extensive basement, the Aquadrom yields an impact on the thermal regime of the subsurface. Extent, intensity, and seasonality of this impact are to be analyzed here. Due to the monitoring not only of groundwater, but also of air temperatures over the course of a year, we are able to identify seasonal variations. The spatial distribution of the GWT at a depth of 5 m is depicted in Figure 5.1c. Figure 5.2a shows the time series of the GWT in all wells. Additionally, the temperature evolution of surface and basement air is plotted with dashed lines. The outdoor air temperature shows the typical seasonal pattern with an arithmetic mean of 14.1 °C (SD: 7.9 K). The placement in a roofed area close to a

building possibly influences the temperature. In the basement, we observed 29.4 °C on average, however the SD is much smaller with 1.7 K, since the basement air is heated by the machines and pools throughout the year. The heat is distributed unevenly. Especially the secluded and only seasonally used northern part is cooler in the winter months (Blum et al., 2021a).

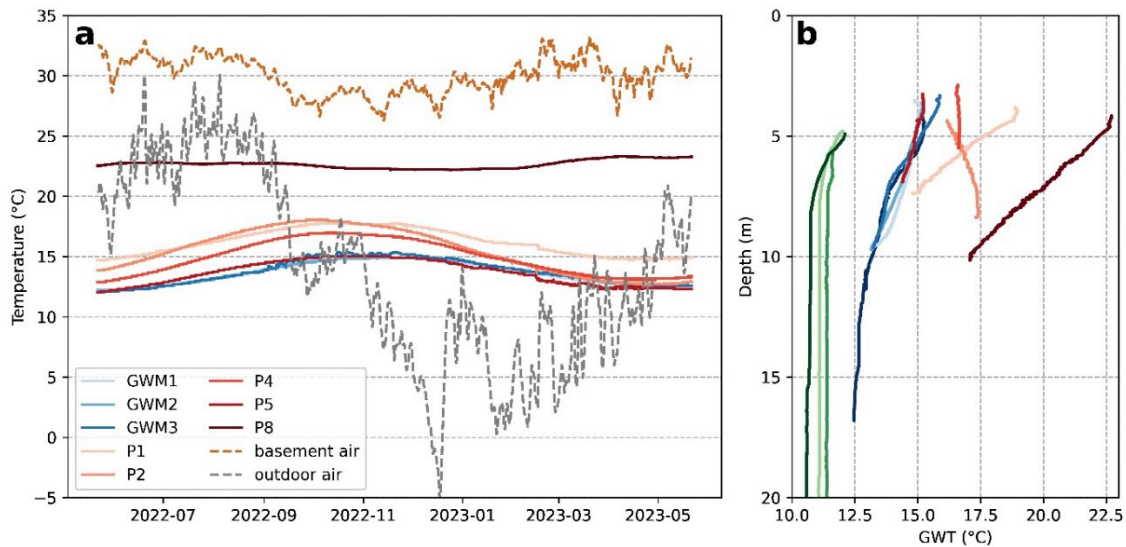


Figure 5.2. (a) Time series of monitored groundwater and air temperatures. Groundwater temperatures were recorded in 5 m depth below surface level except at P9, where the logger was installed at a depth of 15 m. All time series were smoothed with a 24 h rolling mean. (b) Temperature depth profiles of all wells, taken in November 2022. The color groups indicate the position relative to the heat source: reference wells (green), thermally unaffected wells (blue), and thermally affected wells (red). Temperature depth profiles of all campaigns are depicted in Figure D1.

The wells GWM1–GWM3 are thermally unaffected by the site and show the expected patterns at 5 m depth of elevated GWT in fall and lower GWT in spring. Arithmetic means of the GWT are 13.6–13.7 °C, with SD of 0.9–1.0 K. The GWT of well P9, on the other hand, was recorded at a depth of 15 m and shows significantly less seasonal variation (mean:  $12.6 \pm 0.1$  °C). These GWT in the upstream are already higher than the expected range of 11–12 °C for this region, as it can be seen exemplarily at the reference wells which are located in a forest (11.0–11.4 °C). This difference might be caused by the semi-urban setting and the resulting subsurface urban heat island of Hockenheim. Due to the high groundwater velocity (0.5 m/d), it is unlikely that the Aquadrom directly influences the GWT at the upstream wells.

Directly influenced by the heated basement, the well P8 shows high GWT during the whole year (mean:  $22.7 \pm 0.3$  °C), thus overlaying the natural seasonal variations. In Figure 5.2b, it can be seen that the heat at P8 comes from above and decreases with depth. The other thermally affected wells show similar seasonal patterns as the unaffected wells. The GWT at these wells is increased by up to 2.6 K. Interestingly, the monitoring well P1 has the highest GWT of the downstream wells with 16.2 °C on average although it lies laterally to the building in groundwater flow direction. This strong impact is due to the small distance of only 1 m to the basement wall. The direct



influence of the water park on well P1 is also evident by the temperature-depth-profile in Figure 5.2b, which shows the same shape as the one of the well P8. The monitoring well P5, which is located about 100 m downstream from the basement, has a mean GWT of 13.6 °C. Because this value is equal to the GWT at the upstream wells, we assume the thermal plume to be dispersed at this point. Thus, the water park yields a local thermal anomaly in subsurface temperatures (see Figure 5.1c).

Applying Fourier's law of heat conduction (Fourier, 1888), a simple assessment of the rate of subsurface warming by the water park can be carried out. The equation is applied using the measured data of the thermally unaffected wells, P8 and the basement air temperature. The resulting heat flux into the aquifer is about 44 W/m<sup>2</sup> at the upstream facing building part and 19 W/m<sup>2</sup> around the well P8, where the groundwater is already heated. This suggests that spatially and temporally resolved analysis, for example with numerical modeling, would provide more detailed insights into the distribution of the water park's heat losses into groundwater. However, this first evaluation shows that the emitted energy of the basement slab amounts to 3–7 MWh.

Similar to district heating networks, leakage from pools or pipes can be prominent additional sources of heat input. However, this is difficult to detect and distinguish from the general conductive heat flux as leakages act as point sources. Only few other publications mentioned subsurface thermal anomalies due to swimming pools. (Menberg et al., 2013a) recorded around 20 °C warm groundwater downstream to a heated public swimming pool in Frankfurt, Germany, while Tissen et al. (2019) detected 16 °C in a well 4 m away from a municipal swimming pool in Germany. In comparison to other regular heat sources, such as residential basements, underground car parks, and tunnels, swimming pools yield higher impacts on the subsurface thermal regime as they are typically filled with heated water instead of air. Geothermal applications, on the other hand, can cause even higher thermal impacts (García-Gil et al., 2020b; Mueller et al., 2018). These, however, are regulated by law in many countries (Hähnlein et al., 2010). The heat flux emitted from the water park's basement is on the upper end compared to the fluxes of other heat sources (Noethen et al., 2022). This is probably due to the small distance to the groundwater of about 1 m from the basement's slab and the comparatively high temperature difference between the basement and the groundwater.

#### *5.4.2 Environmental impact of groundwater heating*

##### Groundwater chemistry

The chemical groundwater data both at the Reilingen forest and the Aquadrom site indicates that the aquifer has reducing conditions since mean concentrations of oxygen ( $0.71 \pm 0.75$  mg/l) and nitrate (87% below detection limit of 0.125 mg/l) are low, while mean concentrations of DOC ( $10.6 \pm 9.4$  mg/l) and iron ( $5.7 \pm 3.8$  mg/l; Blum et al. (2021a)) are high. Some chemical parameters measured in groundwater at the

study site differed from the natural background, for example pH is lower, with a mean of 6.8 for thermally unaffected wells and 7.3 for the reference wells, and EC is higher (mean 1.5 and 0.7 mS/cm, respectively) as shown in Figure 5.3. Possible reasons for these deviations are the greater depths of the wells in the Reilingen forest as well as increased releases of nutrients and pollutants into the subsurface due to anthropogenic activities in the urban area of Hockenheim. Especially the high concentrations of sulphate at the test site, with 369 mg/l on average (natural background: 133 mg/l), point at systematic differences. Sulphate concentrations are higher than the threshold defined by the German drinking water regulations of 250 mg/l. High sulphate concentrations may originate from construction waste (e.g., bricks) buried in the shallow subsurface of urban areas. In addition, high sulphate is typical for organic rich aquifers, aquifers containing old saline waters or experience the upwelling of deeper thermal waters. Finally, fertilization of agricultural land upstream of the test site could have contributed to elevated levels (Kaown et al., 2009; Spoelstra et al., 2021). Chloride concentrations are most likely not affected by the chlorination of pool water, since the difference between up- and downstream wells is insignificant (mean 101 and 97 mg/l, respectively). Possible sources for increased chloride contents in comparison to the reference wells are deicing of streets with salt and fertilization of agricultural land in upstream areas (Kelly et al., 2012; Perera et al., 2013).

However, none of the chemical parameters are correlated with GWT or altered in the thermally affected wells (Figure 5.3). In addition, Spearman correlation coefficients ( $\rho$ ) range between 0.08 and 0.48 ( $P=0.01-0.69$ ). Only EC shows a moderate correlation with GWT ( $\rho=0.48$ ,  $P=0.01$ ). Although the sulphate concentration is higher in the thermally affected wells than in the unaffected wells (412 and 334 mg/l, respectively), the correlation with GWT is weak and not significant ( $\rho=0.21$ ,  $P=0.23$ ). Mean values of relevant parameters at the reference wells, the thermally unaffected, and affected wells are given in Table D1, alongside thresholds defined by the German drinking water regulations, if applicable. Furthermore, no seasonal temporal trends were observed within the study period.

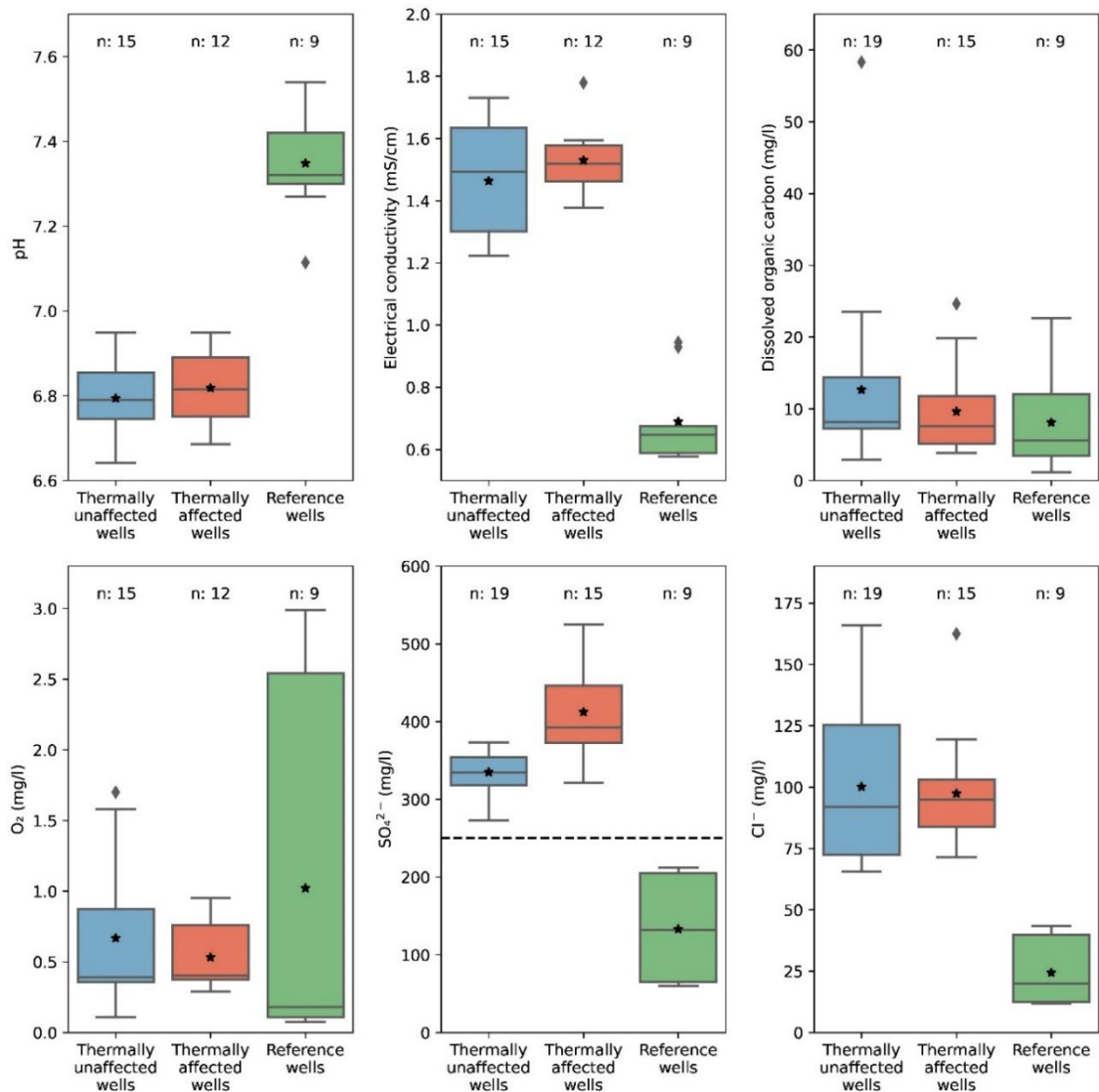


Figure 5.3. Selected chemical parameters of groundwater samples taken in the wells at the Aquadrom Hockenheim (thermally unaffected/affected wells) and in the Reilingen forest (reference wells). Mean values are indicated by stars. sulphate concentration threshold defined by the German drinking water regulations is shown with a dashed line. Other threshold values are outside the data ranges and are given in Table D1.

### Groundwater microbiology and fauna

The mean BA of groundwater from wells at the study site ranged from  $9.5 \cdot 10^4$  cells/ml at P5 to  $1.5 \cdot 10^5$  cells/ml at GWM3. Mean values in groundwater from the reference sites were lower ( $1.5 \cdot 10^4$  to  $9.0 \cdot 10^4$  cells/ml) which can be explained by the natural, non-urban setting and consequently less import of organic compounds and nutrients, as well as by the greater depth of the wells. However, there is no direct correlation between BA and GWT ( $\rho = 0.09$ ,  $P = 0.60$ ). Thermally unaffected wells in the upstream have a slightly lower mean BA value compared to those which are affected in the downstream of the structure ( $1.4 \cdot 10^5$  and  $1.1 \cdot 10^5$  cells/ml) as shown in Figure 5.4. This underlines the sensitivity of BA as an indicator to discriminate between anthropogenically impacted from close to natural groundwater quality, although temperature alone does not seem to be an exclusive driver.

Similar patterns can be observed with the cellular ATP values which differed significantly between the single wells. The highest mean cellular ATP concentration was found in GWM1 (195 pM), the lowest value in P9 (32 pM). Again, the reference wells showed lower values on average (25–88 pM). Statistically, there is no direct significant relation between GWT and cellular ATP ( $\rho = 0.11$ ,  $P = 0.53$ ). Thermally unaffected wells in the upstream had on average similar cellular ATP values as those in the downstream of the Aquadrom (133 and 108 pM, respectively).

Generally, both the BA and cellular ATP in groundwater sampled at the study site are in the upper concentration range when compared to other non-contaminated and close-to-natural shallow aquifers in Germany (Fillinger et al., 2019). This can be explained by the reducing conditions and high DOC concentrations. Anoxic groundwaters generally exhibit higher BA and ATP values due to elevated DOC and phosphate levels (Griebler et al., 2014). Increased inputs of nutrients from agricultural and residential areas are probably additional drivers for microbial abundance and activity. What may be expected, but has not been addressed in this study, is a shift in microbial community composition. Previous studies have shown a community change and an increase in bacterial diversity with groundwater warming (Briellmann et al., 2009; Griebler et al., 2016).

The abundance of fauna in groundwater was generally low both at the study site with 2.0 and in the Reilingen forest with 1.8 individuals per sample on average (Figure 5.4). Most samples were either completely devoid of fauna (68%) or revealed only a small number of 1–3 individuals (25%), while few outlier samples contained up to 48 individuals. The sample that contained 48 animals was taken in May 2023 in GWM3 and did not show any anomalies in groundwater chemistry (e.g.,  $O_2 = 0.35$  mg/l). The samples from well P8, which is located beneath the Aquadrom's basement and showed the highest GWT, contained only one animal (Nematoda) throughout all five campaigns.

The low abundance or even absence of fauna in groundwater was expected due to the low amount of oxygen in the shallow aquifer. In consequence, the use of groundwater fauna taxa as indicators for the ecological status of the aquifer at the test site was not applicable. At the prevailing conditions, the absence of fauna in groundwater does not necessarily indicate a poor ecological status (Griebler et al., 2014). An earlier study by Fuchs (2008) on groundwater fauna in Baden-Württemberg has already found that only one of three wells in the city of Hockenheim was colonized.

Bathynellacea (total counts: 6) and Cyclopoida (1), both taxa belonging to the crustaceans, were only found in the reference wells. No crustaceans could be found in wells at the water park. A single individual of the stygophile Cyclopoida genus *Diacyclops languidooides* was found in RE2 in May 2023. Acari (26) were found in most of the wells. Oligochaetes (42) were identified in three samples only, despite the high number of total counts. The majority of them occurred in a single sample in GWM3 in May 2023 and were identified as the stygophile species *Marionina argentea* (32). Other

Oligochaetes were identified as *Dorydrillus/Trichodrilus* (7) in the well RE2 in February 2023. Only one Gastropoda was found in P1 and Nematoda (17) were scarce as well, except for GWM3, where 14 individuals were found in total in five samples.

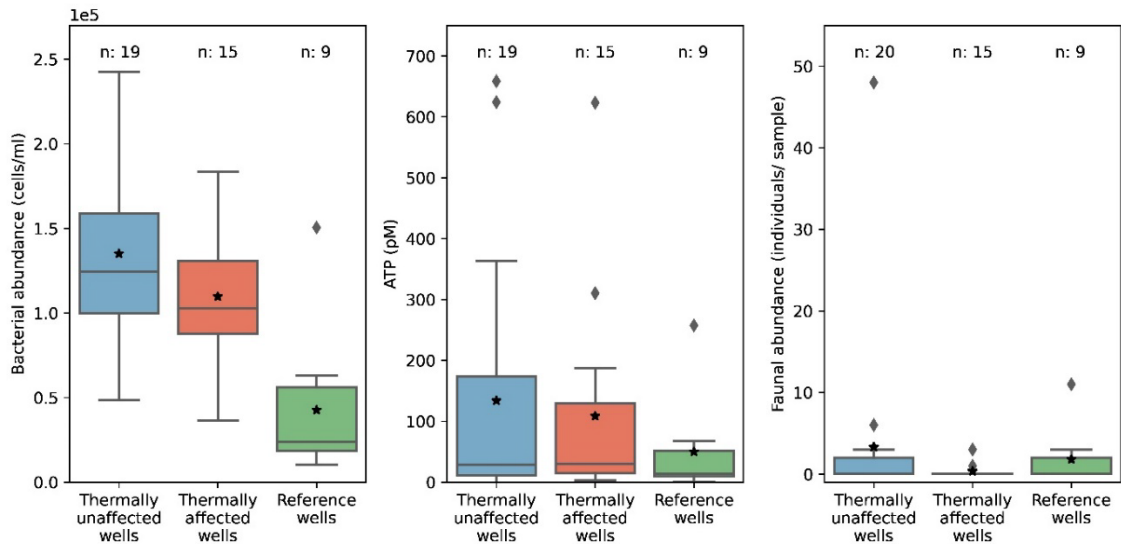


Figure 5.4. Biotic parameters of groundwater samples taken in the wells at the Aquadrom Hockenheim (thermally unaffected/affected wells) and in the Reilingen forest (reference wells). Mean values are indicated by stars. ATP = adenosine triphosphate.

### Ecological assessment schemes

For the groundwater ecosystem status index (GESI), introduced by Griebler et al. (2014), different abiotic and biotic parameters are assessed integratively against the natural background at reference sites. As already mentioned above, groundwater faunal parameters could not be considered for the index, since living conditions (low or no oxygen) are hostile at both the study site and the reference site. Hence, the Groundwater Fauna Index (Hahn, 2006) could not be applied as well. On a qualitative level, the occurrence of crustaceans at the reference sites and the absence of crustaceans in the Aquadrom area, hints at additional pressures at the test side besides the low oxygen conditions.

With the chosen parameters, the results for the GESI show a heterogenous distribution, ranging from 0.2 to 0.6, as it is shown in Table 5.1. According to Griebler et al. (2014), the ecological state of all wells at the water park is either considered *severely affected* (GESI  $\geq 0.2-0.4$ ) or *affected* (GESI  $\geq 0.4-0.6$ ), which means a significant deviation from the natural reference values. This is explained by the higher GWT but also due to a greater microbiological abundance. These results were expected since the upper aquifer is influenced by agricultural and residential land use. Furthermore, a decrease of the GESI for the thermally affected wells could not be observed.

In order to detect disturbances in the ecological state of the upper aquifer, we applied another groundwater health assay, the D-A-C index. The results of this multivariate analysis are expressed as the distances of the individual samples in a

three-dimensional space (Mahalanobis distance) and plotted against the GWT in Figure 5.5.

For this approach, 83% of the samples taken at the water park exceed the critical value of the chi-squared distribution at a 99% confidence level with three degrees of freedom. Hence, all samples except for five can be considered as disturbed in comparison to the natural background values. This can mainly be attributed to the previously described increased microbiological features, i.e., the cellular ATP and BA values. Four of the five samples that did not exceed the critical value were taken in May 2022, where the lowest average DOC concentrations were measured (May 2022 mean: 4.6 mg/l, tot. mean: 11.5 mg/l). There is no significant difference in the D-A-C index between samples from thermally unaffected (6.7) and affected wells (5.7) within the urban area. Considering all samples taken at the Aquadrom, there is no correlation between GWT and the ecological state ( $\rho = 0.18$ ,  $P = 0.32$ ). If we exclusively correlate the samples taken at the thermally unaffected wells, there is a moderate to strong positive correlation with GWT ( $\rho = 0.60$ ,  $P = 0.01$ ). From this, it can be concluded that temperature is one but not the only driving factor of microbial abundance in groundwater. All thermally unaffected wells are in close proximity to each other, while the thermally affected wells are distributed over the whole plot, leading to a broader variation of chemical parameters, possibly overruling the sole impact of groundwater warming. Although temperature is without doubt a parameter influencing groundwater ecology, we could not detect any direct significant deterioration of the ecological state by temperature in this case study.

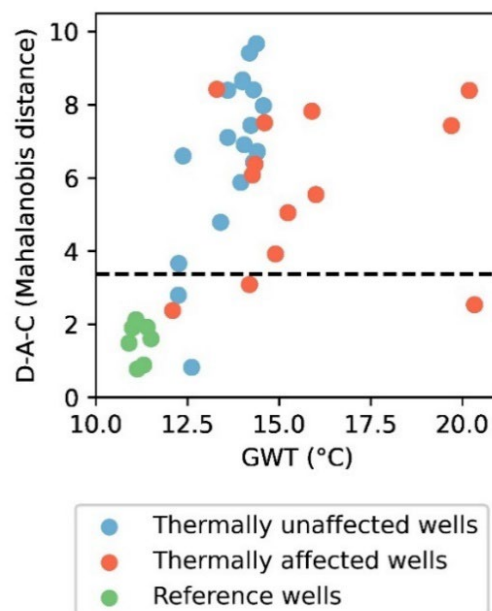


Figure 5.5. D-A-C index of all samples, computed following a guided approach and correlated to the groundwater temperature (GWT). The dashed line shows the critical value of the chi-squared distribution at a 99% confidence level with three degrees of freedom.

Table 5.1. Parameters included in the Groundwater Ecosystem Status Index (GESI) and results, determined according to Equation 5.1. Mean values for each well are displayed. DOC = dissolved organic carbon; ATP = adenosine triphosphate; BA = bacterial abundance.

Criteria (unit)	Natural background	Thermally unaffected wells				Thermally affected wells			
		GWM1	GWM2	GWM3	P9	P1	P5	P8	
<b>GWT</b> (°C)	11.0–11.4	13.6	13.6	13.7	13.5	16.2	13.6	22.7	
<b>O<sub>2</sub></b> (mg/l)	0.1–2.8	0.7	0.6	0.7	0.7	0.5	0.5	0.6	
<b>DOC</b> (mg/l)	4.7–12.4	11.9	21.4	9.3	7.2	11.4	9.2	8.2	
<b>ATP</b> (pM)	25–88	195	95	194	32	106	148	71	
<b>BA</b> (cells/ml)	1.5 · 10 <sup>4</sup> – 9.0 · 10 <sup>4</sup>	1.4 · 10 <sup>5</sup>	1.3 · 10 <sup>5</sup>	1.5 · 10 <sup>5</sup>	1.2 · 10 <sup>5</sup>	1.1 · 10 <sup>5</sup>	9.5 · 10 <sup>4</sup>	1.2 · 10 <sup>5</sup>	
<b>GESI</b> (-)	-	<b>0.4</b>	<b>0.2</b>	<b>0.4</b>	<b>0.6</b>	<b>0.4</b>	<b>0.4</b>	<b>0.6</b>	

## 5.5 Conclusions

In this study, a water park in south-western Germany was identified as the source of a local groundwater heat plume of up to 23 °C (9 K increase), induced by the basement with an average air temperature of 29 °C. The main objective, whether this hot spot affects groundwater quality and ecology, was investigated by comparing data from thermally unaffected and affected wells and by applying the ecological assessment schemes GESI and D-A-C index.

Chemical parameters have shown no significant changes due to heat. Increased sulphate and chloride concentrations in comparison to reference wells in a water protection zone imply that groundwater chemistry at the water park is already influenced by anthropogenic impacts due to residential and agricultural land use. Furthermore, analysis of ecological parameters as well as the assessment schemes underlined clear differences between the chosen reference site and the water park. However, GWT might be one driver of the differences but not the only one. This is most likely due to the fact that the influence of GWT is masked by other factors such as the influence of contamination from urban and agricultural land use. Despite the low oxygen concentration with a mean of only 0.71 mg/l, it could be shown that the aquifer still is inhabited by a small number of stygophile fauna which move regularly and actively into the groundwater ecosystem. Impacts from GWT on fauna, however, could not be analyzed due to the overall low oxygen concentrations and the consequently small number of animals. Assessment based on microbial indicators, on the other

---

hand, allowed to clearly discriminate between groundwater from reference sites and samples from the Aquadrom. Within the facility area, the microbial criteria selected were not sensitive enough to reliably separate GWT affected and unaffected from each other. We may speculate that microbial community composition analysis would have delivered a more detailed picture. Also, it is important to note that the insights gained in this case study are transferable to other sites and aquifer types only with caution. Microbial and faunal communities in oxic aquifers, for example, might react differently to heat stress. Hence, we propose to verify our results at other sites and improve our understanding about the impact of heat stress to groundwater ecosystems for other aquifer systems with different microbial and faunal compositions as well.



## 6 Synthesis

### 6.1 Conclusions: Findings in the field of subsurface warming

In times of rapidly changing climate, the associated worldwide warming of the subsurface is often overlooked. Benz et al. (2024) project an average global groundwater warming of 2.1 K between the years 2000 and 2100 under a medium emissions pathway. This is a drastic change of one of the most critical environmental variables, temperature, given the normally very stable conditions beneath the seasonally influenced zone of about 15 m below the Earth's surface.

Changes in groundwater temperature (GWT) affect various biogeochemical processes that modify groundwater quality (Riedel, 2019), besides little-researched effects on groundwater ecology (Griebler, 2015). The projected warming is additionally increased on local and regional scales by individual anthropogenic heat sources.

The overall aim of this thesis was to analyze the anthropogenic sources for local subsurface warming in respect to their thermal impact and environmental implications at different scales.

The first objective of this work was to identify and classify sources of subsurface warming according to their characteristics. This was achieved by providing a comprehensive literature review and a novel categorization based on a description of key characteristics and similarities in **Chapter 2**. These four characteristics are

- (i) the scale of the thermally affected zone (global, regional, and local),
- (ii) the geometry of the heat source from an aerial perspective (polygonal, linear, and punctual),
- (iii) the heat-generating process (climatic, actively heated, passively heated, leakage, and chemical), and
- (iv) the intention of heat release (intended and unintended).

Typical intensities of GWT changes and heat fluxes were compiled from the literature and discussed comparatively. While sources with a geochemical heat generation, such as landfills and heaps, induce the highest absolute GWT, atmospheric warming and buildings/basements create the relatively highest thermal impact. Furthermore, in this chapter, a detailed analysis of potential implications by heated groundwater was provided. These include changes in physicochemical groundwater parameters (e.g., oxygen saturation, pH), reduced faunal biodiversity, and enhanced shallow geothermal potential for heating (in contrast, reduced shallow geothermal potential for cooling).

The second objective was to research the thermal impact and the significance for subsurface warming of *underground car parks* (UCP) on the city scale. This heat source type was chosen exemplarily because of the good data availability in comparison to other source type, e.g., sewage pipes or infiltration. Furthermore, UCPs are a

prominent but little-researched heat source type in urban areas. Hence, in **Chapter 3**, temperature data from six cities in Austria, Germany, and Switzerland were compiled and analyzed to calculate the heat flux of 31 UCPs into groundwater. These insights into the controlling factors and temporal patterns of UCP indoor temperatures were then applied to broader geological datasets from Berlin, Germany. This analysis estimated the overall thermal impact of 5,040 UCPs, revealing that the annually emitted thermal energy amounts to 0.65 PJ — equivalent to the average heating demand of 14,660 German households. This finding proves that recovering the waste heat — either directly from UCP air or indirectly from groundwater using geothermal heat pumps — may be a viable sustainable heating alternative, particularly in already heated urban settings. In this regard, this work attracted widespread media interest and has been featured in various articles online, radio, and in podcasts (e.g., MDR, 2023; Wöhrle, 2023).

Following the evaluation of UCPs' contribution to local-scale and city-wide subsurface warming, in **Chapter 4**, the third objective was further developing an approach to estimate shallow GWT with the help of remote sensing data. With this approach, the shallow GWT was estimated for the federal state of Saxony-Anhalt, Germany, with a spatial resolution of 500 × 500 m. Compared to previous studies, this publication achieved the highest estimation accuracy (RMSE = 0.74 K). Further, it revealed the high dependency of GWT on anthropogenic land use and verified expected patterns of heat accumulation in urban areas. Advancing this methodology helps providing comprehensive GWT data on a large scale. However, limitations in estimating local GWT anomalies were identified, primarily due to the limited spatial resolution of remote sensing data. As a result, while this technology is most suitable for regional investigations, local information is still best obtained through direct, on-site measurements or hydrogeological modeling.

Finally, in **Chapter 5**, the last objective was to research the implications of local thermal anomalies for the environment. In a case study, GWT data from a water park in Hockenheim, Germany, was analyzed in context with environmental variables. The results showed a local heat plume induced by the water park's basement with an intensity of up to 9 K. However, an evaluation of hydrochemical and ecological data revealed that this GWT hotspot has no significant impact on the environment. This mostly anoxic aquifer (mean oxygen concentration: 0.71 mg/l), inhabited by a small number of animals, thus seems to be resilient against heat stress. Although the results have to be verified for other aquifer types, this finding is a helpful insight for planners and decision-makers considering the environmental impact of anthropogenic heat discharge, caused by, e.g., geothermal systems for cooling.

## 6.2 Outlook

### 6.2.1 *Relevance of local heat sources*

Anthropogenic heat sources not only create strong local thermal anomalies but also contribute to subsurface urban heat islands. While it is difficult to measure the thermal impact directly in a dense urban fabric as observation wells are often scarce, the heat flux can be determined instead. However, extensive datasets are needed to calculate the impact on a city scale, as demonstrated for UCPs in Chapter 3. The same methodology can be applied to other heat sources, with the exception of sources involving additional processes such as leakage and geochemical heat generation. Sewage leakage is considered by Benz et al. (2015b) and Menberg et al. (2013b) as a contribution to subsurface urban heat islands. However, the required information about leakage volume and temperature is usually not available for swimming pools, sewage, and district heating networks and can only be estimated. Additionally, such leakages are not equally distributed over a line source but rather occur in single spots. Since there is typically no information on this effect, only the conductive heat loss can be considered for most sources, although leakage yields a higher overall impact (Benz et al., 2015b; Menberg et al., 2013b).

In practice, the required information is often not available. Hence, a quantitative assessment of the impact of the individual heat source types can hardly be made.

As a recommendation, municipalities and federal states should better implement open data laws in the future to provide researchers and citizens with access to data. Berlin can currently serve as a role model in this respect. Building on the publications included in this thesis and other studies (e.g., Becker & Epting, 2021; Benz et al., 2015b; Menberg et al., 2013b), higher (temporally and spatially) resolved geospatial and infrastructure data can be used in the future to conduct detailed studies for model areas, incorporating the heat flux from all source types. Ideally, a numerical approach that also considers thermal interactions and temporal resolution should be chosen for case studies, rather than the typically used analytical approach (e.g., based on Fourier's law). With this, the comparative relevance of all heat sources can be determined for a model area. Such numerical modeling approaches can also be useful for municipal authorities that want to manage the use of shallow geothermal energy since development scenarios can be simulated.

### 6.2.2 *Utilization of waste heat*

Researching local heat sources enables the identification of suitable locations for geothermal energy use. Rivera et al. (2017) showed that borehole heat exchangers in urban settings reach up to 40% higher efficiency compared to those in rural areas, assuming a 5 K higher GWT in a city. Considering that local heat plumes can reach even higher temperatures (e.g., 9 K at the water park investigated in Chapter 5), an ideal placement can increase the system's efficiency drastically.

Continuous heat emission from subsurface structures ensures the longevity of the system by counteracting the cooling of the adjacent ground. Therefore, it is recommended to place boreholes for geothermal applications downstream of anthropogenic structures that are known to have a high local heat release, e.g., heated basements, tunnels, swimming pools, or multi-level UCPs. In this respect, research activities need to focus on developing tools for the identification of hotspots in GWT and the implementation in the municipal management of shallow geothermal resources.

Another way to recover the waste heat of anthropogenic structures is by installing heat exchangers in building parts that are in contact with the subsurface. These so-called energy geostructures can be integrated with different building types, such as tunnels (Barla & Di Donna, 2018; Epting et al., 2020a), sewer pipes (Adam & Markiewicz, 2009; Cipolla & Maglionico, 2014), and common building slabs and foundations (Loveridge et al., 2020; Rammal et al., 2020). These technologies are tested in case studies (Zito et al., 2021) but often lack market maturity due to uncertainties in material behavior and the complexity of planning and construction. However, utilizing subsurface waste heat may not only provide green energy but also yield a positive side effect by mitigating subsurface urban heat islands, thus counteracting the negative implications of subsurface warming.

### 6.2.3 *Environmental response to subsurface warming*

Regarding the environmental impact of subsurface warming in general, and particularly for local hotspots the current state of knowledge is still limited. This is mostly due to a general lack of information about groundwater ecosystems. Therefore, it is necessary to research the temperature dependency of groundwater faunal and microbiological communities. It is still unknown how rising temperatures affect community composition and abundance.

Researching this topic contains many complications, such as (i) the limited access to environmental data, (ii) the complexity of field study execution due to technical limitations in measuring ecological parameters and coarse distribution of observation wells, and (iii) the locally highly endemic ecosystems. Therefore, tools to quantify the ecological state of an aquifer need to be developed that can be carried out without expert knowledge. To reveal potential GWT dependencies, it is required to conduct field studies, as provided in Chapter 5, at different scales (local and regional), for different intensities of heat stress, and different aquifer types. In particular, long-term field studies are lacking. Furthermore, the behavior of contaminants under elevated GWT needs to be researched.

Research needs to investigate generally applicable threshold values for thermal alteration and answer the most pressing question of how much GWT change is “acceptable”. Although temperature is known to be a key parameter for groundwater quality, especially in urban areas there seem to be several other factors overruling temperature effects, e.g., contaminations or oxygen depletion (Becher et al., 2022;

Koch et al., 2021). Past research could not find major deteriorations of ecological parameters due to GWT increases, although some parameters, such as bacterial abundance and faunal diversity, correlate with GWT (Briemann et al., 2009; Griebler, 2015; Retter et al., 2020). Therefore, Griebler et al. (2016) state that a moderate rise in GWT (5–10 K) has only a minor impact on groundwater quality. However, they also note that temperatures of >30 °C — usually only reached by geothermal systems for cooling or heat storage applications — are likely to cause significant changes in water quality, especially for areas contaminated with organics, nutrients, and heavy metals.

#### 6.2.4 *Legislation and recommendations for mitigation strategies*

For water law enforcement, the water authorities in particular would profit from instruments and well-founded decision-making support for the approval or rejection of applications for shallow geothermal systems. In the future, thermal resources will need to be managed alongside groundwater resources in order to guarantee the efficient and environmentally compatible use of geothermal energy.

It is essential to find a balance between the public interests of groundwater and drinking water protection, climate and environmental protection, and a sustainable energy supply (Hähnlein et al., 2010). This requires concepts for measuring, evaluating, and monitoring thermal changes in the subsurface and especially in groundwater, as well as for the efficient management of geothermal potential (Kabuth et al., 2017). Ultimately, geothermal applications cause only a fraction of the thermal changes in the subsurface, so that the scope of consideration for a holistic assessment must be extended to include the unintentional heat sources that have not yet been sufficiently considered. For sources that generate heat actively, e.g., swimming pools or district heating pipes, a maximum allowable temperature difference in the surrounding soil or ground in a specific distance from the source might be recommended. In practice, this can be demonstrated by numerical modelling of the thermal field. Exemptions could be granted for sites that are already contaminated. On the other hand, for sources that emit passively generated heat, legal requirements might involve providing adequate insulation.

As healthy groundwater resources are vital for our society, groundwater extraction zones in particular are to be protected (Blum et al., 2021b). Thus, it is recommended to regard heat as a pollutant in water protection zones to ensure high water quality and in protected nature reserves to protect groundwater ecosystems. Excluding already anthropogenically influenced zones by restricting these regulations to protected areas prevents counteracting the development of geothermal resources and thus the transition toward sustainable energy supply. In general, threshold values should be based on scientific evidence. For individual buildings that are known to have high heat flows into the subsurface (e.g., tunnels, heated basements, multi-level UCPs), the possibility of waste heat recovery — either directly from indoor air or the ground as energy geostructures — should be assessed during the planning phase.

# Appendices

## Appendix A

### Appendix A-1: Temperature analysis datasets

Table A1. Information and datasets used for the UCP temperature analysis.

Name	Depth of structure (m)	No. of levels	Type of use	Device	Measuring period	Temporal resolution (h)	Assigned weather station	Distance to weather station (km)	Well distance (m)
Basel #1	9	2	public			1		2.1	-
Basel #2	11.3	3	public	EA		1		2.2	-
Basel #3	8.6	3	public	WLAN-	2019/12 –	1	BKLI, BAES <sup>a</sup>	0.6	-
Basel #4	11.3	5	private	TH+	2020/12	1		1.1	130
Basel #5	17.9	7	public			1		0.2	150
Cologne #1	3.1	1	public			1		5.6	-
Cologne #2	3.2	1	public			1		7.4	-
Cologne #3	5.6	2	public			1		6.3	-
Cologne #4	5.9	2	public			1		5.3	-
Cologne #5	5.4	2	public	DS1922L	2019/03 –	1	Köln-	6	-
Cologne #6	5.7	2	public	iButton	2020/08	1	Stammheim <sup>b</sup>	5.7	-
Cologne #7	6.4	2	public			1		5.1	-
Cologne #8	8.4	3	public			1		6	10
Cologne #9	11.5	4	public			1		6.3	-
Cologne #10	10.6	4	public			1		5.5	-
Halle	3.5	1	private	HOBO MX2201	2021/08 – 2022/08	1	Heide-Süd <sup>c</sup>	1.8	35
Karlsruhe	3	1	private	HOBO MX100	2018/06 – 2022/07	3	Rheinstetten <sup>b</sup>	7.1	-
Vienna #1	3*	1	public			6		7.8	-
Vienna #2	3*	1	public			6		8.5	-
Vienna #3	3*	1	public			6		10.1	-
Vienna #4	3*	1	private			6		5.8	-
Vienna #5	3*	1	private			6		12.4	-
Vienna #6	3*	1	private	DS1922L	2018/04 –	6	Hohe Warte <sup>d</sup>	12.6	-
Vienna #7	6*	2	public	iButton	2019/06	6		6.5	-
Vienna #8	6*	2	public			6		4.3	-
Vienna #9	6*	2	public			6		11.1	-
Vienna #10	9*	3	public			6		5.3	-
Vienna #11	9*	3	public			6		7.4	-
Vienna #12	9*	3	public			6		7.5	-
Zürich #1	9.2	3	public	DS1922L		2		1.3	0

Zürich #2	16.1	4	private	iButton	2014/12 – 2016/10	2	Schimmelstraße <sup>e</sup>	1.1	0
-----------	------	---	---------	---------	-------------------	---	-----------------------------	-----	---

\* Assumed depth;

<sup>a</sup> Research group Meteorology, Climatology and Remote Sensing, University of Basel

<sup>b</sup> DWD (2023)

<sup>c</sup> Institute of Geosciences and Geography, Martin Luther University Halle-Wittenberg

<sup>d</sup> ZAMG (2023)

<sup>e</sup> Stadt Zürich (2023)

## Appendix A-2: List of input parameters

Table A2. List of input parameters applied in the spatial analysis.

Name	Parameter	Unit	Minimum	Mode	Maximum
Thermal conductivity sand			0.4	0.9	1.4
Thermal conductivity peat	$\lambda_{soil}$	W/mK	0.2	0.4	0.7
Thermal conductivity till			1.1	2.4	2.9
Thermal conductivity concrete	$\lambda_{concrete}$		0.9	1.6	2.0
Groundwater temperature	$T_{GW}$	°C	From Geoportal Berlin (2023)		
UCP air temperature	$T_{UCP}$	°C	Derived from $T_{Air}$ , resolved by month and UCP level		
UCP depth	$d_{UCP}$	m	2.5	3	3.5
UCP slab thickness*	$d_{slab}$	m	0.4	0.5	0.6
UCP wall thickness*	$d_{wall}$	m	0.2	0.3	0.4
Soil thickness	$d_{soil}$	m	From Geoportal Berlin (2023)		
UCP area	$A_{UCP}$	m <sup>2</sup>	From Geoportal Berlin (2023)		

\* Minimum values were applied to calculate the maximum results and vice versa, as the thickness of a permeated layer is a resistance.

### Appendix A-3: Air temperature comparison

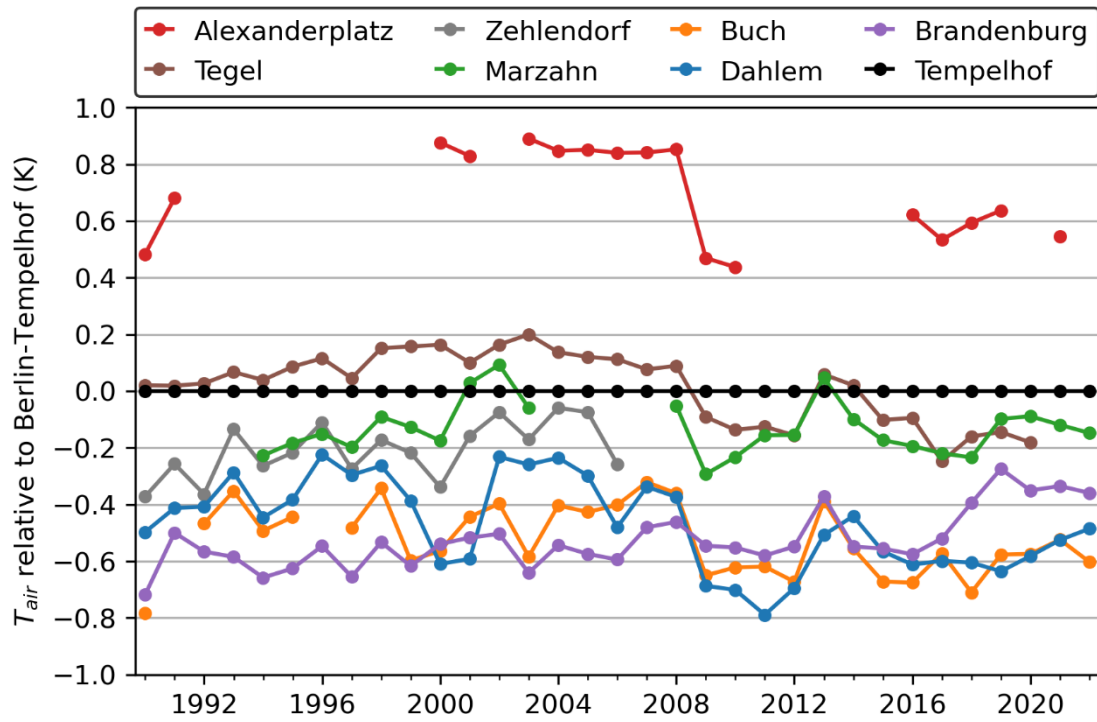


Figure A1. Annual mean surface air temperature ( $T_{Air}$ ) measured for eight weather stations in Berlin since 1990, relative to the weather station of Berlin-Tempelhof. Data source: DWD (2023).



## Appendix A-4: Maps of input data for the spatial analysis

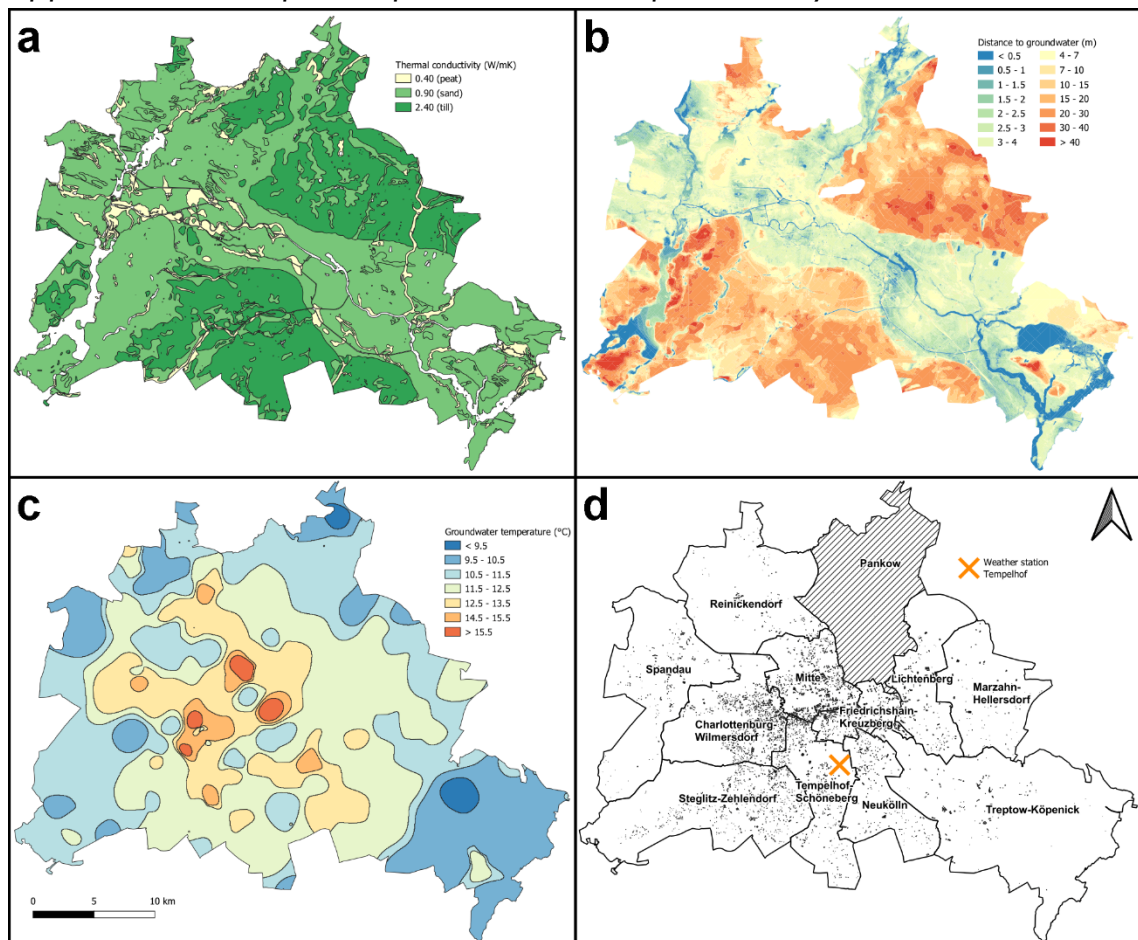


Figure A2. Maps of Berlin showing the spatial datasets used as input for the analysis of the thermal impact of UCPs on the groundwater in Berlin. (a) Thermal conductivity of the shallow soil material. (b) Distance to the groundwater from the surface. (c) Groundwater temperature in 20 m below ground surface. (d) Shapes of UCPs, district areas and location of the Tempelhof weather station.

## Appendix A-5: Temperature correlation plots for all sites

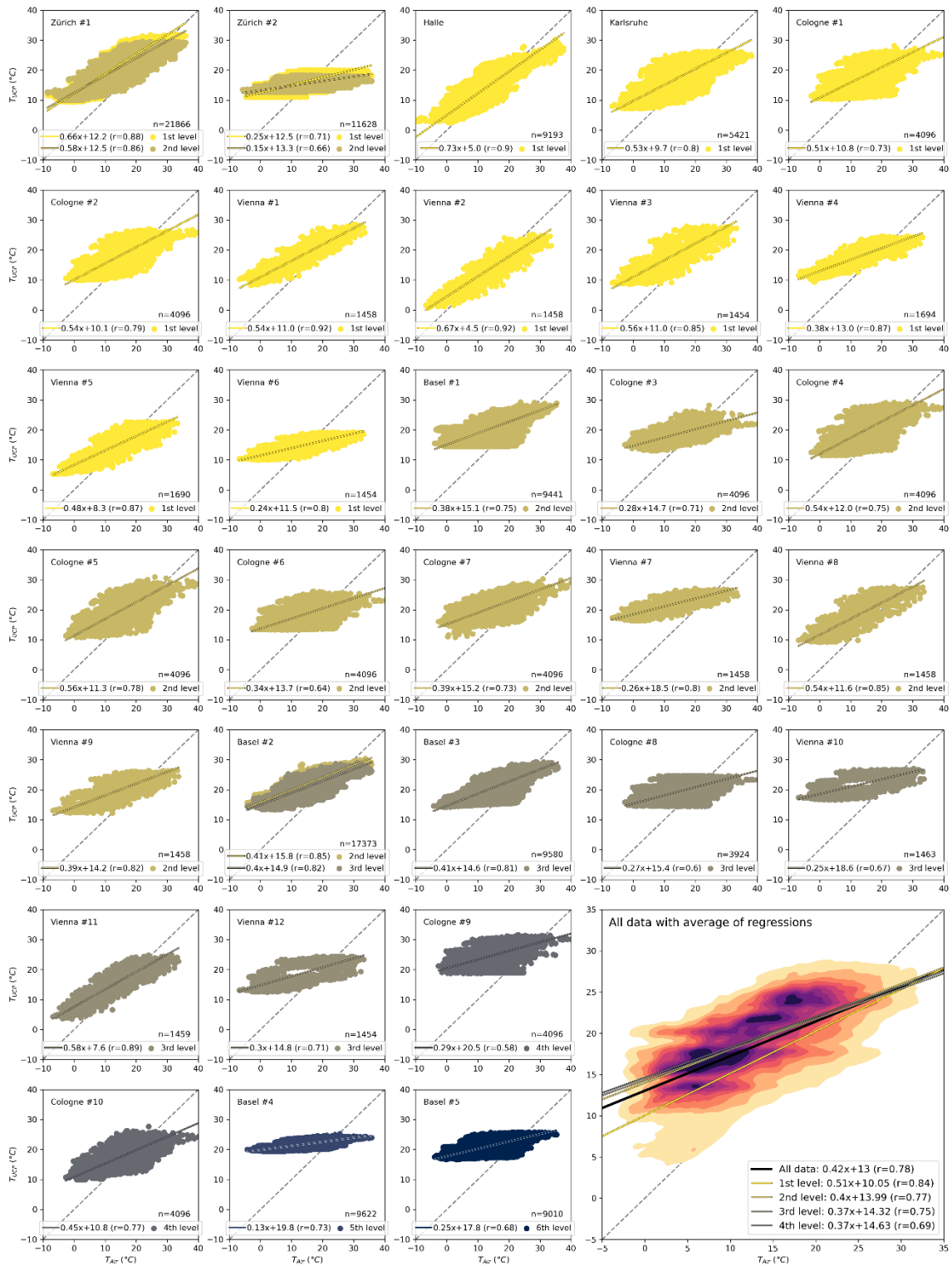


Figure A3. Scatter plots for all 31 sites to show the correlation between UCP temperature ( $T_{UCP}$ ) and surface air temperature ( $T_{Air}$ ). The colors indicate the level of the UCP at which the measurement was taken. The bottom diagram contains the data for all 31 sites and the average of the results of each individual regression for the respective levels. All plots have a dashed identity line as reference. The number of measurements is marked with an  $n$ .

## Appendix A-6: Spatial Analysis results

Table A3. Results of the spatial analysis of heat fluxes from UCPs in Berlin. The uncertainties of the results are shown in Table A4.

District	Area (km <sup>2</sup> )	UCP area (km <sup>2</sup> )	Total UCPs (in GW)	Mean $q_{slab}$ (W/m <sup>2</sup> )	Mean $q_{slab+wall}$ (W/m <sup>2</sup> )	AHF <sub>UCP</sub> (mW/m <sup>2</sup> )	Sum $Q$ (MW)	Yearly $E$ into GW (TJ/a)
Charlottenburg-Wilmersdorf	64.7	1.0	1163 (82)	2.8	3.2	48.0	3.1	98.0
Friedrichshain-Kreuzberg	20.2	0.7	349 (68)	4.2	4.5	148.2	3.0	94.2
Lichtenberg	52.3	0.4	236 (28)	1.8	1.8	13.1	0.7	21.6
Marzahn-Hellersdorf	61.7	0.2	122 (3)	0.5	0.5	1.6	<0.1	3.2
Mitte	38.4*	1.4	881 (180)	4.8	6.1	214.5	8.2	259.5
Neukölln	44.9	0.3	288 (26)	2.0	2.1	13.7	0.6	19.4
Reinickendorf	78.2*	0.1	169 (22)	3.8	4.0	6.2	0.5	15.4
Spandau	91.9	0.2	227 (21)	3.8	4.0	10.2	0.9	29.5
Steglitz-Zehlendorf	102.5	0.5	886 (0)	0.5	0.5	2.5	0.3	8.1
Tempelhof-Schöneberg	53.1	0.6	528 (18)	2.0	2.1	21.8	1.2	36.5
Treptow-Köpenick	168.4	0.3	191 (67)	6.8	7.0	12.7	2.1	67.3
<b>Berlin</b>	<b>776.4*</b>	<b>5.5</b>	<b>5040 (515)</b>	<b>3.2</b>	<b>3.7</b>	<b>26.7</b>	<b>20.7</b>	<b>652.6</b>

\* Areas without groundwater data are excluded (see Figure A2 for comparison).

## Appendix A-7: Uncertainties of spatial analysis results

Table A4. Uncertainties of the spatial analysis, shown as minimum (min) and maximum (max) values.

District	Mean $q_{slab}$ (W/m <sup>2</sup> )		Mean $q_{slab+wall}$ (W/m <sup>2</sup> )		AHF <sub>UCP</sub> (mW/m <sup>2</sup> )		Sum $Q$ (MW)		Yearly E into GW (TJ/a)	
	min	max	min	max	min	max	min	max	min	max
Charlottenburg-Wilmersdorf	1.5	3.7	1.6	4.7	24.4	70.0	1.6	4.5	49.9	142.9
Friedrichshain-Kreuzberg	2.2	5.6	2.3	6.3	77.8	210.3	1.6	4.2	49.4	133.6
Lichtenberg	0.9	2.4	0.9	2.5	6.8	18.1	0.4	0.9	11.2	29.9
Marzahn-Hellersdorf	0.3	0.7	0.3	0.7	0.8	2.1	<0.1	0.1	1.6	4.2
Mitte	2.6	6.5	3.1	9.1	107.6	320.3	4.1	12.3	130.2	387.5
Neukölln	1.1	2.7	1.1	2.8	7.1	18.9	0.3	0.8	10.0	26.7
Reinickendorf	2.1	5.3	2.1	5.8	3.2	9.0	0.3	0.7	8.0	22.2
Spandau	2.0	5.3	2.1	5.7	5.3	14.5	0.5	1.3	15.5	42.0
Steglitz-Zehlendorf	0.3	0.7	0.3	0.7	1.2	3.2	0.1	0.3	3.7	10.4
Tempelhof-Schöneberg	1.0	2.6	1.1	2.9	11.1	29.8	0.6	1.5	18.5	49.9
Treptow-Köpenick	3.7	9.2	3.7	9.9	6.7	17.9	1.1	3.0	35.8	94.9
<b>Berlin</b>	<b>1.7</b>	<b>4.4</b>	<b>1.9</b>	<b>5.4</b>	<b>13.6</b>	<b>38.6</b>	<b>10.6</b>	<b>29.9</b>	<b>333.8</b>	<b>944.1</b>

## Appendix A-8: Parameter sensitivity

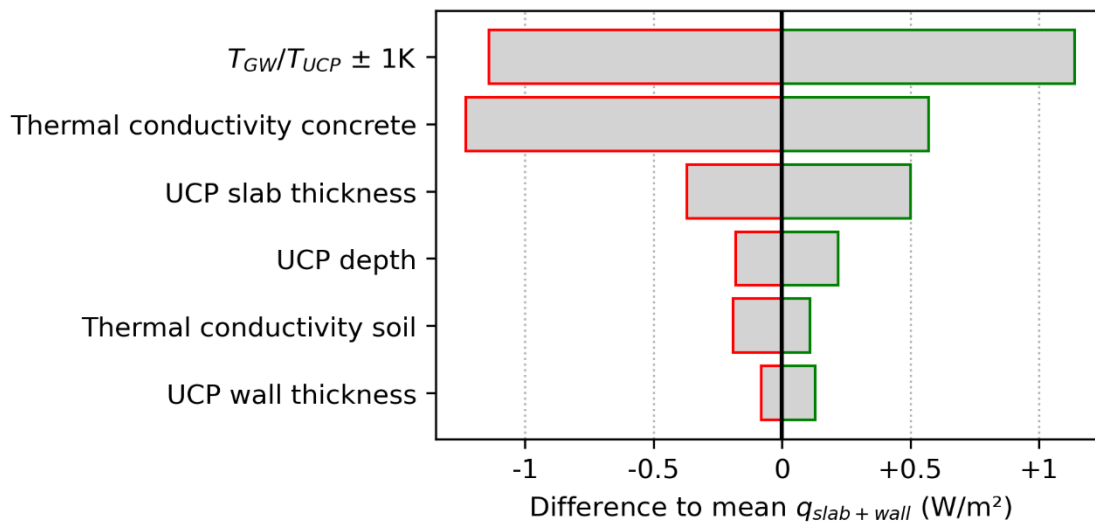


Figure A4. Barplot showing the parameter sensitivity of the spatial analysis as difference to the mean  $q_{slab+wall}$  of the total area of Berlin (3.7 W/m<sup>2</sup>). The differences were calculated with only one parameter changed to the minimum and maximum values of Table A2.

## Appendix B: Original version of chapter 4 in German language

This chapter is reproduced from:

Noethen, M., Hemmerle, H., Meyer, L., & Bayer, P. (2024). Prognose der oberflächennahen Grundwassertemperatur in Sachsen-Anhalt. *Grundwasser – Zeitschrift der Fachsektion Hydrogeologie*, DOI: <https://doi.org/10.1007/s00767-024-00570-z>.

### *Appendix B-1: Zusammenfassung*

Informationen zu Grundwassertemperaturen (GWT) sind häufig spärlich und nur als Punktdaten aus Grundwassermessstellen verfügbar. Für räumlich aufgelöste Vorhersagen der GWT bieten sich Satellitendaten als Alternative zur herkömmlichen Interpolation an. Dabei wird sich die thermische Kopplung der Landoberfläche und des oberflächennahen Untergrundes zunutze gemacht. In dieser Studie wird die Verteilung der GWT in Sachsen-Anhalt erstmals charakterisiert. Basierend auf Fernerkundungsdaten und Messdaten aus 436 Grundwassermessstellen wird eine Vorhersage mit einer flächigen Auflösung von 500 m getroffen. Zudem werden neben der GWT und der Landoberflächentemperatur als Prognoseparameter weitere Variablen genutzt, welche die GWT beeinflussen und so die Genauigkeit der Vorhersage erhöhen. Die Vorhersage zeigt im Vergleich zu vorangegangenen Studien die bisher höchste Auflösung und Genauigkeit (RMSE = 0,74 K). Die Methodik liefert für alle Landnutzungsklassen gute Ergebnisse (RMSE = 0,55 – 1 K). Ausreißer zeigen jedoch auch, dass eine höhere Auflösung nötig ist, um lokale Hotspots zuverlässiger zu detektieren.

### *Appendix B-2: Einleitung*

Grundwassertemperaturen (GWT) spielen eine wichtige Rolle für die effiziente Versorgung mit grüner Energie aus oberflächennaher Geothermie (Bayer et al., 2019; Yasukawa et al., 2009; Zhu et al., 2010). So kann eine um 5 K erhöhte GWT die Leistung von Erdwärmesonden um bis zu 40% steigern (Rivera et al., 2017). Die zunehmende Nachfrage nach der Ressource Erdwärme verstärkt den Bedarf an Grundwassermonitoring und räumlich hoch aufgelöster Standortkenntnis. Mindestens ebenso wichtig wie die Energiewende ist die zuverlässige Versorgung mit qualitativ hochwertigem Trinkwasser. In Zeiten des Klimawandels verändert sich nicht nur das Dargebot an nachhaltig verfügbarem Grundwasser, auch die GWT unterliegt einer Veränderung, die sich an die steigenden Lufttemperaturen anpasst (Kurylyk et al., 2014). Erhöhte GWT können Grundwasserökosysteme mit ihrer wichtigen Reinigungsfunktion beeinträchtigen und damit die Grundwasserqualität verringern (Bonte et al., 2011; Brielmann et al., 2009; Griebler et al., 2016). Die Artenvielfalt stygobionter Grundwasserfauna, die an konstante Bedingungen

angepasst ist, kann mit steigenden GWT abnehmen (Becher et al., 2022; Blum et al., 2021b; Koch et al., 2021; Spengler & Hahn, 2018). Zusätzlich führen höhere Untergrundtemperaturen zu vermehrtem Bakterienwachstum, insbesondere in städtischen Trinkwassernetzen (Agudelo-Vera et al., 2017; Gunkel et al., 2022; van den Bos, 2020).

Die flächendeckende Bestimmung der GWT gestaltet sich aufgrund der starken Variabilität der Temperaturverteilung im Untergrund in der Praxis oft als schwierig. Da nur Punktdaten an Grundwassermessstellen erhoben werden können, werden die Zwischenräume in der Regel interpoliert (Z.B., Böttcher & Zosseder, 2022; Previati & Crosta, 2021b; Tissen et al., 2021). Bei geringer Punktdichte kann ein großer Fehler entstehen. Wenn beispielsweise kühle, ländlichen Messstellen eine typischerweise wärmere bebauten Gegend einschließen, in der selbst keine Messwerte erhoben wurden, wird die Wärmeanomalie der Bebauung im Ergebnis nicht widerspiegelt. Um diese Schwäche der Punktinterpolation zu umgehen, ist die Nutzung von Fernerkundungsdaten möglich. Diese können die verschiedenen Faktoren, welche die GWT beeinflussen, räumlich aufgelöst in die Berechnung einer vorhergesagten Grundwassertemperatur (eGWT) mit einbeziehen. So lässt sich zum Beispiel die Abhängigkeit der oberflächennahen GWT von der Lufttemperatur nutzen. Die satellitengestützte Landoberflächentemperatur wird dabei als Proxy für die Lufttemperatur verwendet (Čermák et al., 2014). Da die GWT neben den klimatischen Bedingungen auch von anderen Einflüssen bestimmt wird, profitiert die Vorhersage der GWT davon, wenn zusätzlich zur Landoberflächentemperatur weitere Informationen einbezogen werden (Z.B., Benz et al., 2017a; Hemmerle et al., 2019). Die GWT wird maßgeblich von der Bodenbedeckung beeinflusst, insbesondere wurden in Gebieten mit hoher Bebauungsdichte lokal erhöhte Temperaturen im Grundwasser nachgewiesen (Böttcher & Zosseder, 2022; Epting et al., 2017b; Ferguson & Woodbury, 2007; Menberg et al., 2013a). Aber auch Evapotranspiration und der Anteil der Schneetage können durch Verdunstungskälte bzw. Isolierung einen Effekt auf den Versatz zwischen Landoberflächentemperatur und GWT haben und somit die Ergebnisse einer Vorhersage verbessern (Shukla & Mintz, 1982; Sun et al., 2016; Zhang, 2005).

Bisherige Ansätze, die GWT mithilfe von Fernerkundungsdaten zu berechnen, konzentrierten sich auf urbane Räume, mit Ausnahme einer Studie von Benz et al. (2017a), in der ein globaler Datensatz verwendet wurde. Für Städte in Deutschland (Benz et al., 2015a; Hemmerle et al., 2020), Frankreich (Hemmerle et al., 2019) und China (Zhan et al., 2014) wurden urbane Wärmeinseln im Untergrund, im Englischen Subsurface Urban Heat Islands (Ferguson & Woodbury, 2007; Menberg et al., 2013a), mithilfe von satellitengestützten Datensätzen charakterisiert. Es ist jedoch bislang wenig erforscht, wie gut sich die Methodik auf den ländlichen Raum anwenden lässt und wie groß der Einfluss der Landnutzung auf die Genauigkeit der Vorhersage ist.

Ziel dieser Studie sind die erstmalige Beschreibung und Auswertung der GWT-Verteilung in dem Bundesland Sachsen-Anhalt sowie anschließend die Berechnung der eGWT mithilfe von Satelliten- und Messdaten. Die Ergebnisse sollen hinsichtlich des Einflusses der Landnutzung auf die GWT und die Zuverlässigkeit der Methodik ausgewertet werden.

### *Appendix B-3: Materialien und Methoden*

#### Untersuchungsgebiet

Das Untersuchungsgebiet umfasst das deutsche Bundesland Sachsen-Anhalt und hat eine Größe von 20.452 km<sup>2</sup>. Die drei größten Städte sind Magdeburg, Halle (Saale) und Dessau. Im Westen liegt das Mittelgebirge Harz mit dem Brocken als höchsten Punkt (1141 m NHN). Dominanter Vorfluter ist die Elbe, die das Land von Südosten nach Norden in 302 km durchfließt.

In Sachsen-Anhalt herrscht ein gemäßigtes Übergangsklima zwischen maritimen und kontinentalen Einflüssen. Die durchschnittliche Jahresmitteltemperatur der Jahre 2007–2022 im Randbereich von Magdeburg betrug 10,6 °C (DWD, 2023). Während die Lufttemperaturen in den Höhenlagen des Harzes wesentlich niedriger sind, beispielsweise am Brocken durchschnittlich 4,7 °C (DWD, 2023), steigen die Temperaturen in urbanen Zentren aufgrund der dichten Bebauung typischerweise um 1–2 K im Vergleich zum Umland an (Tzavali et al., 2015).

#### Mess- und Fernerkundungsdaten

Die genutzten Daten der GWT stammen aus Grundwasserqualitätsmessungen des Landesbetriebs für Hochwasserschutz und Wasserwirtschaft Sachsen-Anhalt (LHW, 2023) sowie aus selbst durchgeführten Messungen. Die ausgewählten Daten des LHW wurden zwischen 2007 und 2022 erhoben. Bei den Grundwasserqualitätsmessungen wird das Grundwasser so lange gepumpt bis physikochemische Parameter stabil sind, mindestens aber das doppelte Pegelvolumen gefördert wurde. Die Temperatur des gepumpten Grundwassers wird dann in einer Durchflusszelle an der Oberfläche gemessen. Die Messtiefe der GWT entspricht bei dieser Methodik in etwa der mittleren Tiefe der Filterstrecke. Die eigenen Messungen wurden in den Städten Magdeburg (Feb., Jun., Nov. 2021), Halle (Feb., Jun. 2020; Jan., Jun., Nov. 2021) und Dessau (Mär., Jun. 2020; Jan., Jun., Nov. 2021) sowie dem Saalekreis (Jun., Aug. 2021) durchgeführt. Dabei wurden mithilfe von Temperatur-Kabellichtloten der Firmen HT Hydrotechnik und SEBA Tiefenprofile gemessen. Beide Geräte haben eine Messgenauigkeit von <0,1 K.

Die vorhandenen Grundwasserdaten wurden auf den Tiefenbereich von 10 bis 50 m unter Geländeoberkante beschränkt, um den Einfluss saisonaler Temperaturschwankungen sowie des geothermischen Gradienten möglichst gering zu halten. Messstellen mit einem Abstand von unter 3 m zueinander wurden zusammengefasst. Von insgesamt 1098 Messstellen wurden so 436 für die weitere Auswertung selektiert, wovon 325 vom LHW und 111 Messstellen in eigenen

Messungen beprobt wurden. Die Häufigkeit der Messungen variiert, und jede der selektierten Messstellen wurde durchschnittlich zwölf Mal beprobt. Eine Darstellung der Messwiederholungen pro Messstelle ist in Figure C1 für die Qualitätsmessungen des LHW zu finden. Es zeigt sich eine stark heterogene Anzahl der Messwiederholungen, wobei 15 Messstellen nur einmal beprobt wurden, während maximal 32 Wiederholungen erreicht wurden. In Figure C1 ist ebenfalls die Verteilung der Messzeitpunkte dargestellt. Hier zeigen sich Schwerpunkte in Frühjahr und Herbst. Die Temperaturdaten der selektierten Messstellen wurden konsekutiv als Monats-, Quartals- und Jahresmittel, sowie als Mittel zwischen den Jahren 2007 bis 2022 zusammengefasst.

Für die Berechnung der eGWT wurden Fernerkundungsdaten der Landoberflächentemperatur (Wan et al., 2021), Evapotranspiration (Mu et al., 2014) und dem Anteil der Schneetage (Hall et al., 2006) mit einer Bodenauflösung von circa 1 km (Landoberflächentemperatur = MODIS/061/MOD11A1 und MODIS/061/MYD11A1, Evapotranspiration = MODIS/006/MOD16A2) bzw. 500 m (Anteil der Schneetage = MODIS/MOD10A1) genutzt. Diese wurden als Mittel des Zeitraums 2007–2022 auf eine Auflösung von 500 × 500 m umgerechnet. Um die zeitliche Variabilität der Landoberflächentemperatur einschätzen zu können, wurden vier repräsentative Standorte herangezogen. Die Landoberflächentemperatur zeigt in diesem Zeitraum einen linearen Trend von 0,13 K/a (Halle: 0,13 K; Brocken: 0,12 K; Altmark: 0,14 K; Börde: 0,14 K) und eine Varianz aus den Jahresmitteln von 1,44 K (Halle: 1,31 K; Brocken: 1,13 K; Altmark: 1,71 K; Börde: 1,60 K). Die räumliche Varianz aller Pixel in Sachsen-Anhalt beträgt 0,42 K. Der Anteil der Schneetage wurden zusätzlich noch hinsichtlich der Verteilung der Oberflächengewässer (MODIS/061/MCD12Q1) maskiert. Die Bebauungsdichte wurde aus den aktuellsten Impervious Built-up Daten von 2018 (European Environment Agency, 2023) auf das 500 m Raster der weiteren Datensätze gemittelt. Für die weitere Auswertung wurden CORINE Land Cover (CLC) Daten von Copernicus genutzt (European Environment Agency, 2023). In Figure B1 sind alle genutzten Datensätze als Karten dargestellt.



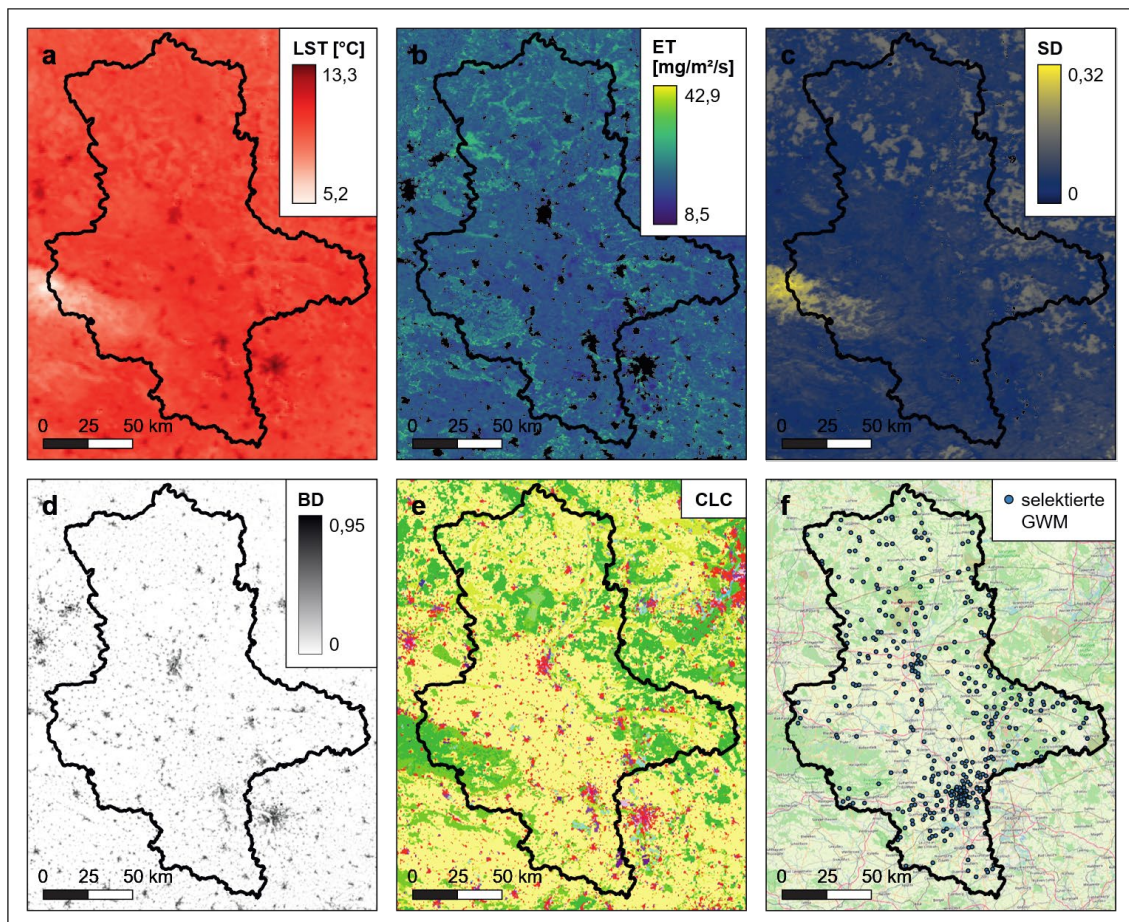


Figure B1. Karten von Sachsen-Anhalt mit den genutzten Datensätzen: (a) Rasterdaten der Land Surface Temperature (LST); (b) Rasterdaten der Evapotranspiration (ET); (c) Rasterdaten der Snow Days (SD); (d) Rasterdaten der Building Density (BD); (e) Rasterdaten der CORINE Land Cover (CLC); (f) Punktdaten der ausgewählten Grundwassermessstellen (GWM).

### Aktueller Forschungsstand

Eine erste Untersuchung des Zusammenhangs zwischen Bodentemperaturen und satellitengestützten Landoberflächentemperatur wurde von Zhan et al. (2014) durchgeführt, beinhaltet jedoch nur Tiefen bis 3,2 m unter Geländeoberfläche und wurde an lediglich neun Punkten mit Messdaten validiert. Dieser Ansatz wurde von Benz et al. (2015a) für die vier deutschen Städte Berlin, München, Köln und Karlsruhe weiterentwickelt, indem zusätzlich die Bebauungsdichte und Kellertemperatur berücksichtigt wurde, um den Wärmefluss von anthropogenen Quellen besser widerzuspiegeln. Es konnte ein Spearman-Korrelationskoeffizient von 0,8 erzielt werden, wobei besonders hohe Korrelationen für ältere Städte auftraten. Dennoch war die GWT in 95% der Pixel wärmer als die Landoberflächentemperatur, mit einer durchschnittlichen Unterschätzung der jährlich gemittelten GWT um 1,5 K. Die Studie zeigt, dass die GWT nicht allein mithilfe der Landoberflächentemperatur geschätzt werden kann, obwohl eine signifikante Korrelation besteht. Weitere Einflussfaktoren, wie unterirdische anthropogene Wärmequellen, sorgen in Städten dafür, dass das Grundwasser zusätzlich erwärmt wird (Menberg et al., 2013b). Benz et al. (2017a) führten eine Methodik ein, die einen empirischen Zusammenhang zwischen

Evapotranspiration und dem Anteil der Schneetage mit der Differenz aus GWT und Landoberflächentemperatur erstellt, und wendeten diese für einen globalen Datensatz an. Damit konnte die Wurzel des mittleren quadratischen Fehlers (RMSE) der GWT-Vorhersage im Vergleich zu einer Vorhersage, die sich ausschließlich auf die Landoberflächentemperatur stützt, um 0,5 K auf 1,4 K verringert werden. Hemmerle et al. (2019) kombinierten die Ansätze aus Benz et al. (2017a) für den ländlichen Raum mit den Vorschlägen aus Benz et al. (2015a) für urbane Flächen, um eine Vorhersage der GWT für Paris zu erstellen. Gestützt auf GWT-Messdaten aus 377 Messstellen gelang eine Schätzung mit einer weiteren Reduktion des RMSE auf 0,96 K. In einer weiteren Studie wendeten Hemmerle et al. (2020) den Ansatz von Benz et al. (2017a) mit der zusätzlichen Berücksichtigung der Bebauungsdichte für die Stadt Köln an. Die GWT-Vorhersage konnte die bisher genauesten Ergebnisse mit einem RMSE von 0,86 K erzielen.

#### Berechnung und Auswertung der Grundwassertemperatur

In den bisherigen Studien wurden die Berechnungen der eGWT mithilfe Multipler Linearer Regression durchgeführt. Für die vorliegende Studie haben wir vorab für verschiedene alternative Ansätze die Ergebnisse verglichen (Table C1). Da die komplexeren Methoden jedoch nur eine geringe Reduktion des Prognosefehlers lieferten, stellen wir im Haupttext nur das etablierte Verfahren der Multiplen Linearen Regression zur Berechnung der eGWT vor (Benz et al., 2017a; Hemmerle et al., 2019).

Die Methodik zur Berechnung der eGWT folgt Hemmerle et al. (2020) unter Nutzung der Landoberflächentemperatur (LST), Evapotranspiration (ET), dem Anteil der Schneetage (SD) und der Bebauungsdichte (BD). Dazu wurde je räumlich diskretisiertem Pixel folgende Gleichung angewendet:

$$eGWT = LST + 0,02 \left[ K \frac{m^2 \cdot s}{mg} \right] \cdot ET + 7,47 [K] \cdot SD + 2,23 [K] \cdot BD + 0,29 [K]. \quad (B.1)$$

Während durch den y-Achsenabschnitt für jeden Pixel einen Versatz von 0,29 K addiert wird, tragen die restlichen Regressoren unterschiedlich stark zur eGWT bei, abhängig von den abgeleiteten Regressionskoeffizienten und den Regressoren. Hierbei hat, gemittelt auf die Fläche von Sachsen-Anhalt, die Evapotranspiration mit 0,33 K den stärksten Einfluss. Die Einflüsse der Schneebedeckung und Bebauungsdichte sind mit 0,17 K und 0,16 K etwa halb so groß. Die Bebauungsdichte weist jedoch lokal die größten Änderungen von bis zu 1,66K auf. Die Verteilung der Beiträge der Regressoren sind in Figure B2 dargestellt.

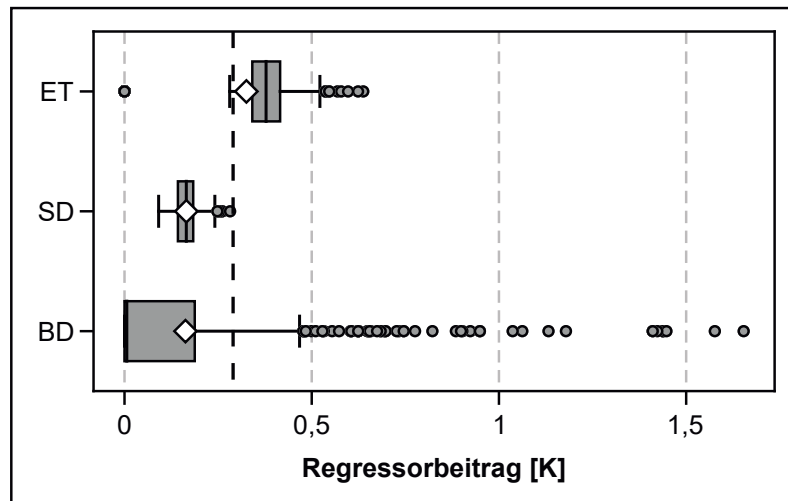


Figure B2. Beiträge der Regressoren für die Berechnung der vorhergesagten Grundwassertemperatur an jeder Grundwassermessstelle, dargestellt als Boxplots. Die gestrichelte Linie zeigt den Beitrag des y-Achsenabschnitts. Die Mittelwerte sind mit Rauten markiert. ET = Evapotranspiration, SD = Anteil der Schneetage, BD = Bebauungsdichte.

## Appendix B-4: Ergebnisse und Diskussion

### Räumliche Verteilung der Grundwassertemperatur

Zunächst wird die Verteilung der gemessenen GWT betrachtet (Punkte in Figure B3). Die kälteste GWT wurde mit 8,7 °C in einem Waldgebiet in der Nähe von Rottleberode im Südharz aufgezeichnet. In den höheren Lagen im Harz, wo noch kältere Temperaturen zu erwarten sind, sind im Festgestein keine Messstellen im Messnetz enthalten. Auffällig sind die erhöhten Temperaturen in den Städten Magdeburg, Halle und Dessau von bis zu 17 °C (bzw. 15,7 und 16,6 °C). Die hohen GWT sind in der Regel auf anthropogene Quellen zurückzuführen, wie bei der wärmsten beprobten Messstelle, die in direkter Nähe zu einer unterkellerten medizinischen Einrichtung im Süden Magdeburgs liegt. Die von der Unterkellerung ausgehende Wärme könnte hier einen direkten Einfluss auf die hohe GWT haben. Dass die höchste Temperatur in Magdeburg nicht in der Innenstadt, wo die Bebauung am dichtesten ist, gemessen wurde, zeigt den starken Einfluss lokaler Wärmequellen auf das thermische Feld des Untergrunds und die daraus resultierende starke Variabilität von Grundwassertemperaturen. Für die weitere Auswertung wurde jeder Messstelle die jeweilige CLC-Klasse zugewiesen. Dadurch kann der Einfluss der Landnutzung auf die GWT untersucht werden. Zur Vereinfachung wurden die Klassen in Gruppen zusammengefasst (Table C2).



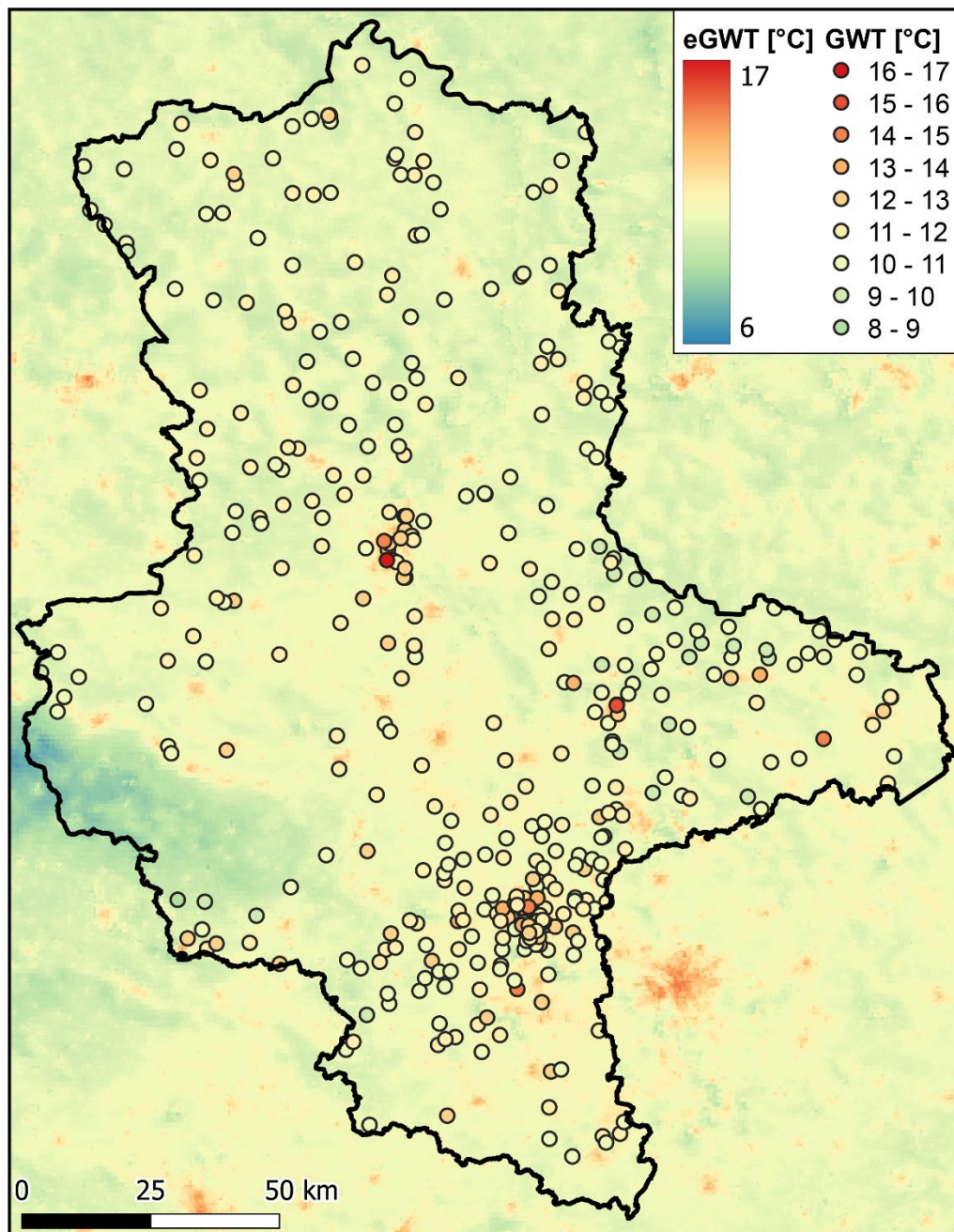


Figure B3. Vorhergesagte Grundwassertemperaturen (eGWT) in Sachsen-Anhalt mit den gemessenen Grundwassertemperaturen (GWT) als Punkte.

Das arithmetische Mittel der gemessenen GWT in Sachsen-Anhalt beträgt  $11,2\text{ }^{\circ}\text{C}$ , mit einer räumlichen Varianz von  $1,08\text{ K}$ . Die zeitliche Varianz, die zwischen den einzelnen Messungen auftritt, fällt dahingegen mit  $0,87\text{ K}$  etwas geringer aus. Die mittlere vertikale Varianz der GWT innerhalb der Grundwassermessstellen beträgt  $0,03\text{ K}$ . Sie wurde aus allen Temperaturprofilen zwischen  $10$  und  $50\text{ m}$  Tiefe ( $n = 100$ ) erstellt, wobei beachtet werden muss, dass die Profile unterschiedliche Tiefenbereiche abdecken. An  $81\%$  der beprobten Messstellen beträgt die GWT unter  $12\text{ }^{\circ}\text{C}$  und kann damit unter den herrschenden klimatischen Bedingungen als natürlich betrachtet werden. Ergebnisse anderer Studien, die die Verteilung der GWT in einer Region oder einem Land ausgewertet haben, zeigen ähnliche Werte. Die

Vergleichbarkeit ist allerdings durch abweichende klimatische Bedingungen und Unterschiede in der Datenerhebung eingeschränkt. So beschreibt Riedel (2019) für Baden-Württemberg zwischen 2000 und 2015 eine mittlere GWT von 10,6 °C, während Benz et al. (2018b) für das Jahr 2013 in Österreich eine mittlere GWT von 11,4 °C angeben.

Auch wenn in dieser Studie versucht wurde, durch eigene Messkampagnen in urbanen Räumen alle Regionen des Landes abzudecken, werden Agrarflächen und Wald- bzw. Naturgebiete (zusammen 79% der Messstellen) aufgrund des an der Wasserrahmenrichtlinie orientierten Messnetzes des LHW stärker als urbane Räume repräsentiert. Ebenfalls werden die hohen Lagen des Harzes in dieser Studie nicht abgebildet. Darüber hinaus kann die unterschiedliche Anzahl der Beprobungen je Messstelle ebenso wie die ungleichmäßige Verteilung der Messzeitpunkte einen Einfluss auf die Ergebnisse haben (Figure C1). Eine Abhängigkeit der GWT von der Messtiefe ist innerhalb von 10 bis 50m Tiefe nicht ersichtlich (Figure B4). Der Fehler durch jahreszeitliche Temperaturschwankungen im oberflächennahen Bereich liegt unterhalb von 10m in der Regel bei <1 K (Anderson, 2005; Böttcher & Zosseder, 2022; Kurylyk et al., 2019) und wird in dieser Studie zusätzlich durch die Messwiederholungen verringert. Die unterschiedlichen Messmethoden und Messgeräte stellen ebenfalls eine mögliche Fehlerquelle dar. Temperaturwerte bei Grundwasser-Qualitätsmessungen könnten im Vergleich zu In-situ-Messungen aufgrund des Pumpvorgangs leicht erhöht sein. Dies wurde bisher jedoch nicht systematisch untersucht. Da in Sachsen-Anhalt keine begleitenden In-situ-Messungen durchgeführt wurden, können wir diesen Fehler hier ebenfalls nicht bestimmen. Daten aus einer Studie von Hemmerle et al. (2022) zeigen jedoch, dass die Temperatur bei Grundwasser-Qualitätsmessungen in Köln im Mittel um 0,29 K überschätzt wurde. Es ist ebenfalls möglich, dass ein Einhängen der Pumpe auf mittlerer Höhe der Filterstrecke nicht gewährleistet, dass das gepumpte Grundwasser aus dieser Tiefe stammt. Durch Heterogenität der hydraulischen Durchlässigkeit der Sedimente im Bereich der Filterstrecke kann die wahre Entnahmetiefe von der mittleren Filterstrecke abweichen.

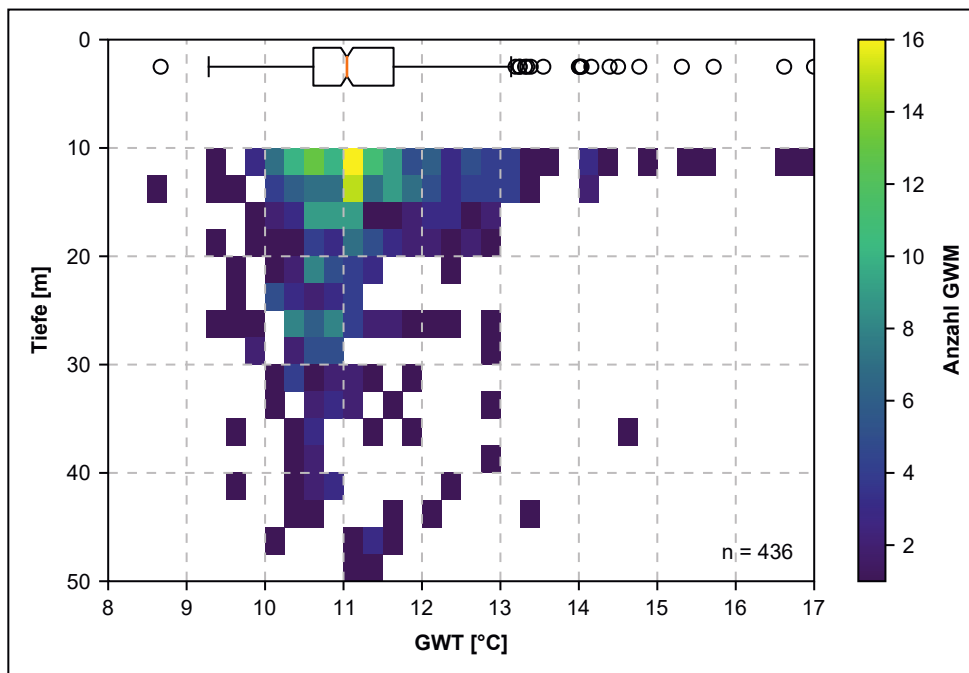


Figure B4. Durchschnittliche Messtiefe und Grundwassertemperatur (GWT) aller Messstellen, dargestellt als Streudiagramm mit Boxplot der GWT-Verteilung am oberen Rand. Die Farbe der Pixel zeigt die Anzahl der Grundwassermessstellen (GWM).

#### Vergleich zwischen gemessener und vorhergesagter Grundwassertemperatur

Die vorhergesagten Grundwassertemperaturen sind in Figure B3 als Raster dargestellt. Die Verteilung bildet die erwarteten Muster der Landoberflächentemperatur ab, die eine Zunahme der eGWT in urbanen Räumen sowie die kältesten eGWT von unter 8 °C im Harz zeigt. Um die Qualität der aus den Satellitenbildern berechneten eGWT zu beurteilen, werden die Ergebnisse mit den gemessenen GWT verglichen. Figure B5 zeigt Streudiagramme, die die Korrelationen von eGWT/GWT sowie Landoberflächentemperatur/GWT abbilden. Eine Vorhersage, die allein auf der Landoberflächentemperatur basiert, würde einen RMSE, also die Abweichung des gemessenen vom vorhergesagten Wert, von 1,22 K haben und die wahre GWT um durchschnittlich 0,94 K unterschätzen. Eine bessere Schätzung würde allein der Mittelwert der gemessenen GWT von 11,2 °C liefern (RMSE 0,84 K). Die Vorhersage mithilfe jeweils eines einzigen zusätzlichen Fernerkundungsparameters verringert den RMSE bereits erheblich auf 0,77 K (Evapotranspiration; Anteil der Schneetage), bzw. auf 0,75 K (Gebäudedichte).

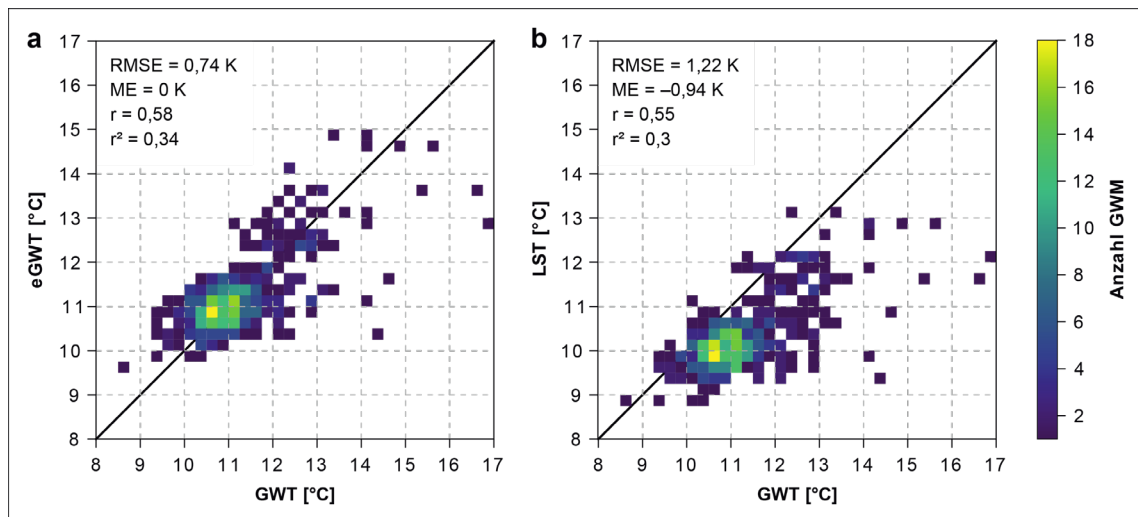


Figure B5. Streudiagramme zur Korrelation von a vorhergesagter (eGWT) und gemessener Grundwassertemperatur (GWT); b Land Surface Temperature (LST) und GWT. Die Farbe der Pixel zeigt die Anzahl der Grundwassermessstellen (GWM). Die Fehler werden durch den Root Mean Square Error (RMSE) und den Mean Error (ME) angegeben. Der Spearman-Korrelationskoeffizient wird mit  $r$  und das Bestimmtheitsmaß mit  $r^2$  angezeigt.

Die Genauigkeit der Vorhersage mit allen Regressoren wurde durch einen erzielten RMSE von 0,74 K im Vergleich zu vorangegangenen Arbeiten verbessert. Vorherige Studien für einen globalen Datensatz, für Köln und für Paris (Benz et al., 2017a; Hemmerle et al., 2020; Hemmerle et al., 2019) zeigen höhere RMSE von 0,86–1,4 K. Das leicht verbesserte Ergebnis kann u. a. auf die hohe Anzahl und flächige Verteilung der Messstellen zurückgeführt werden. Des Weiteren sind in ländlichen Gebieten weniger Ausreißer mit hoher GWT, die durch lokale Wärmequellen hervorgerufen werden, zu beobachten. Dadurch ist für Studien in urbanen Räumen, wie z. B. Paris und Köln, wo das Grundwasser häufiger durch Bebauung beeinflusst wird, ein höherer Fehler zu erwarten.

Die drei höchsten positiven und negativen Ausreißer sind in Table C3 zusammengestellt. Starke Unterschätzungen der GWT sind in Magdeburg (–4,2 K) und Dessau-Roßlau (–3,1 K) auf lokale Temperaturanomalien durch Bebauung zurückzuführen. In Klöden hängt die niedrigere Vorhersage (–3,9 K) vermutlich mit der Nähe zur Elbe und der damit verbundenen Infiltration wärmerer Oberflächenwässer zusammen. Eine Überschätzung der GWT durch das Modell kann insbesondere für Grünflächen (Agrarflächen oder Stadtparks) innerhalb oder in der Nähe von Stadtgefüge beobachtet werden. In dieser Studie ist die gemessene GWT in verschiedenen Fällen in Halle (Saale) niedriger als die Vorhersage (1,5–1,8 K). Grünflächen in Städten zeigen in der Regel niedrigere GWT als umliegende bebauten Flächen. Die Satellitendaten hingegen sind mit einer Auflösung von 500 m in manchen Fällen zu grob, um kleinere Grünflächen in Städten zu erfassen. Dies zeigt das generelle Problem von GWT-Vorhersagen mit niedrig aufgelösten Satellitendaten, dass zwar regionale Effekte wie urbane Wärmeinseln im Untergrund gut wiedergegeben werden können, lokale Anomalien hingegen nur unzureichend

abgebildet werden. Aus diesem Effekt resultiert auch das relativ geringe Bestimmtheitsmaß von 34% in der Prognose. Hinzu kommen Einflüsse durch die Mittelung der Eingangsdaten über mehrere Jahre, die Mittelung über die Tiefe und die Messfehler bei der Bestimmung der Grundwassertemperatur, die die Genauigkeit der Modellergebnisse negativ beeinflussen. Beispielsweise kann von einem Fehler durch die Erwärmung des Wassers während des Pumpvorgangs bei den Grundwasserqualitäts-Messungen ausgegangen werden, der mit den anderen Unsicherheiten in den hohen Restfehler der Prognose mit einfließt und diesen teilweise begründet.

#### Einfluss der Landnutzung auf die Grundwassertemperatur

Um den Einfluss der Landnutzung auf die GWT und eGWT, der bereits bei den Ausreißern der Vorhersage ersichtlich wurde, besser bewerten zu können, sollen die CLC-Klassifizierungen der Messstellen ausgewertet werden. Die Durchschnittswerte für die GWT und eGWT der jeweiligen CLC-Gruppen sowie der resultierende RMSE (Table C4) geben dabei Auskunft über die Tauglichkeit der Methodik für die verschiedenen Landnutzungsklassen (Figure B6).

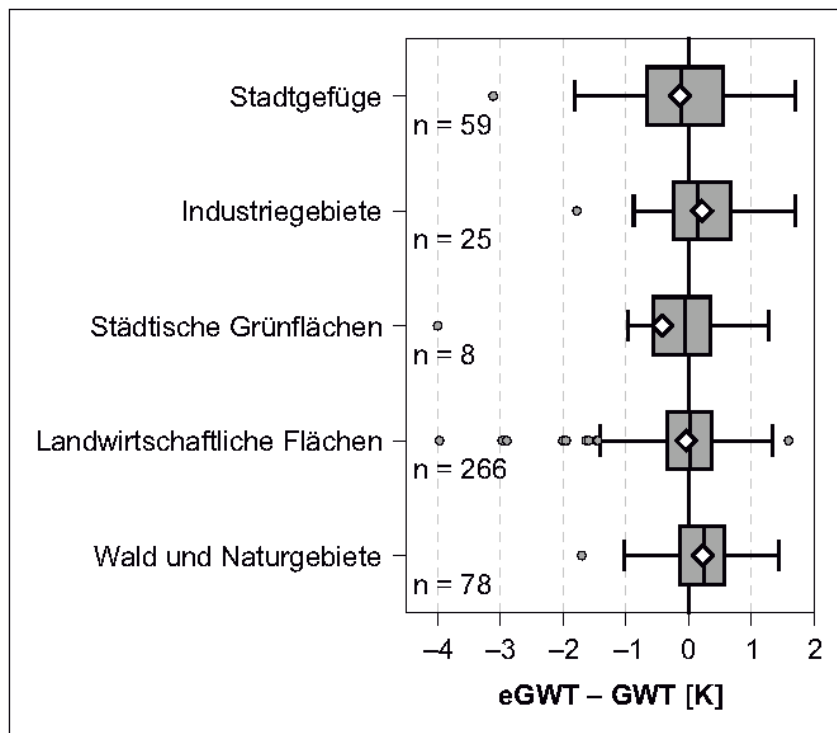


Figure B6. Differenz zwischen vorhergesagter (eGWT) und gemessener Grundwassertemperatur (GWT) als Boxplot pro Landnutzungs-Gruppe. Die Anzahl der Messstellen in der jeweiligen Landnutzungs-Gruppe wird mit n angegeben. Die Mittelwerte sind mit Rauten markiert.

Wie erwartet sind im ländlichen Raum niedrigere GWT als auf urbanen Flächen messbar. Wald- und Naturgebiete haben in Sachsen-Anhalt mit 10,7 °C und einer Varianz von 0,48 K die niedrigsten durchschnittlichen GWT, gefolgt von landwirtschaftlichen Flächen (11,0 °C ± 0,44 K). In urbanen Räumen sind städtische Grünflächen mit 11,7 °C ± 4,01 K am kältesten, während in Stadtgefüge und



Industriegebieten die GWT auf  $12,3\text{ °C} \pm 1,21\text{ K}$ , bzw.  $12,6\text{ °C} \pm 0,85\text{ K}$  ansteigt. Die Differenz zwischen der kältesten und wärmsten CLC-Gruppe liegt daher bei 1,9 K.

Die besten Ergebnisse werden für die Messstellen in Wald- und Naturgebieten (RMSE = 0,55 K,  $n = 78$ ) und auf städtischen Grünflächen (RMSE = 0,62 K,  $n = 8$ ) erzielt. Dies ist für die Wald- und Naturgebiete mit der geringeren Beeinflussung durch lokale Wärmequellen zu begründen. Als städtische Grünflächen wurden nur acht Messstellen klassifiziert. Aufgrund der geringen Anzahl an Datenpunkten und damit geringen Repräsentativität muss das Ergebnis für die städtischen Grünflächen kritisch betrachtet werden. Gleichzeitig fallen dadurch Messstellen, die eigentlich auf Grünflächen oder -streifen liegen, in die Klasse des Stadtgefüges. Dadurch liegt der wahre Wert der durchschnittlichen GWT vermutlich höher als die berechneten  $12,3\text{ °C}$ .

Für landwirtschaftliche Flächen, auf denen sich 61% ( $n = 266$ ) der Messstellen befinden, beträgt der RMSE 0,71 K. Auch hier ist von einer geringen anthropogenen Beeinflussung und dadurch homogeneren Temperaturverteilung im Vergleich zu urbanen Räumen auszugehen. Die Heterogenität des Temperaturfeldes in Städten spiegelt sich in den Fehlern für die CLC-Gruppen „Stadtgefüge“ und „Industriegebiete“ wider, die mit 0,95 und 1,00 K höher als der Durchschnitt ausfallen. Urbane GWT hängen zusätzlich von unterirdischen Wärmequellen ab, die mit dieser Methodik nicht abgebildet werden können, und sind weniger stark an die Landoberflächentemperatur gekoppelt. Darüber hinaus können die lokal stark variierenden GWT in Städten bei einer Auflösung der Vorhersage von 500 m schlecht wiedergegeben werden.

Der Prognosefehler kann in Zukunft insbesondere durch eine höher auflösende räumliche und zeitliche Diskretisierung der Eingangsdaten verringert werden. Auch die Berücksichtigung von anthropogenen Wärmequellen wie Abwasser- und Fernwärmenetzen oder Tunneln würde genauere Abschätzungen als mit der Bebauungsdichte allein ermöglichen, benötigt aber detaillierte Datensätze. Ähnliche Ansätze wie von Menberg et al. (2013b) oder Benz et al. (2015b), um Wärmeflüsse in urbane Aquifere zu ermitteln, könnten genutzt werden, indem verschiedene Wärmequellen für Modellgebiete detailliert aufgelöst werden. Wenn die GWT für kleinere Räume hochauflösend abgeschätzt werden sollen, eignen sich hingegen numerische Modelle, die neben anthropogenen Einflussfaktoren auch Aquifereigenschaften berücksichtigen können, dafür aber entsprechend aufwendiger in der Parametrisierung und Berechnung sind (Epting et al., 2013; Makasis et al., 2021). Satellitengestützte Berechnungen, wie in dieser Studie vorgestellt, eignen sich, um zuverlässig regionalskalige Abschätzungen der GWT mit öffentlich zugänglichen Daten vorzunehmen. Das Vorgehen stellt eine zuverlässige Alternative zu den üblicherweise genutzten Interpolationsmethoden dar, insbesondere in Gebieten mit geringerer Datendichte oder ungleichmäßiger Verteilung der Messstellen. Die Ergebnisse der eGWT-Verteilung können beispielsweise zur Kartierung des geothermischen Potenzials verwendet werden (Hemmerle et al., 2022).

### *Appendix B-5: Fazit*

Die Verteilung der oberflächennahen GWT in Sachsen-Anhalt wird in dieser Studie erstmals charakterisiert. Die GWT beträgt im arithmetischen Mittel  $11,2\text{ °C}$ , mit einer räumlichen Varianz von  $1,08\text{ °C}$  und basierend auf wiederholten Messungen an 436 Messstellen. Der Wertebereich der GWT von  $8,7$  bis  $17,0\text{ °C}$  zeigt die Variabilität in der räumlichen Verteilung zwischen Naturräumen und Städten.

Die vorgestellte Berechnung der eGWT erfolgte mithilfe Multipler Linearer Regression und anhand von Satellitendaten sowie den gemessenen GWT-Daten. Das Ergebnis zeigt einen geringen Fehler ( $\text{RMSE} = 0,74\text{ K}$ ) und stellt eine Verbesserung im Vergleich zu vorherigen Studien dar. Nach Auswertung der Landnutzung können die wärmsten GWT in Stadtgefüge ( $12,3\text{ °C} \pm 1,21\text{ K}$ ) und Industriegebieten ( $12,6\text{ °C} \pm 0,85\text{ K}$ ) festgestellt werden, ebenso wie die größten Fehler bei der Berechnung der eGWT ( $\text{RMSE} = 0,95$  und  $1,00\text{ K}$ ). In Wald- und Naturgebieten sowie landwirtschaftlichen Flächen wurden die kältesten GWT gemessen ( $10,7\text{ °C} \pm 0,48\text{ K}$ ;  $11,0\text{ °C} \pm 0,44\text{ K}$ ), was der zu erwartenden Temperaturverteilung im Untergrund entspricht. Am zuverlässigsten ist die verwendete Methodik für Wald und Naturgebiete mit einem  $\text{RMSE}$  von  $0,55\text{ K}$ . Regionale Trends wie urbane Wärmeinseln im Untergrund werden zuverlässig abgebildet, während lokale Wärmeanomalien aufgrund der Pixelgröße in der Regel schlecht detektiert werden. Die aus den Fehlern ableitbare schlechtere Anwendbarkeit in urbanen Räumen liegt an der größeren Heterogenität der GWT aufgrund kleinräumiger Änderungen der Landnutzung und der Vielzahl anthropogener Wärmequellen. Eine geringere Pixelgröße der Satellitendaten sowie eine Einbeziehung weiterer Faktoren wie unterirdischer anthropogener Wärmequellen würde Verbesserungspotenzial für die Anwendung in urbanen Räumen bieten.

Die genutzte Methodik kann einfach und kostengünstig auf andere Regionen übertragen werden und bietet sich als Alternative zur einfachen Interpolation von Punktdaten an, die eine hohe Anzahl und homogene Verteilung der Messpunkte benötigt. Eine höhere Auflösung der Vorhersage kann mit numerischen Grundwassermodellen erreicht werden, die sich daher insbesondere für kleinskalige Fragestellungen eignen. Allerdings sind numerische Ansätze vergleichsweise aufwendig bei der Parametrisierung und Berechnung. Die Ergebnisse dieser Studie können beispielsweise genutzt werden, um das Potenzial für oberflächennahe Geothermie zu kartieren.

## Appendix C

### Appendix C-1: Comparison of regression methods

Different regression methods were tested against the established multiple linear regression (Table 1). These include support vector machines, simple neural networks, and nearest neighbor regression with different configurations (activation function, SVM kernel). For all methods, a Bayesian hyperparameter optimization with 100 initial randomized runs and 900 optimization cycles was performed. The data was split into 25% test data and 75% training data. Furthermore, in addition to the forecast of the difference between GWT and land surface temperature (GWT - land surface temperature), a forecast for the GWT was created directly with the land surface temperature as a variable.

Table C1. Metrics of the tested methods for calculating estimated groundwater temperatures.

5f-RMSE	Test R2	Test RMSE	Test ME	model
<i>Estimation parameter: GWT; Variables: LST, SDP, EVT, BD</i>				
0.71	0.45	0.80	0.01	MLP – logistic
1.27	0.45	0.80	-0.01	MLP – tanh
0.68	0.44	0.81	-0.01	MLR – with intercept
0.69	0.45	0.81	-0.03	NNR
0.70	0.4	0.84	-0.04	SVM – polynomial
0.74	0.03	0.84	0.02	SVM – linear
0.73	0.01	0.85	-0.02	SVM – radial basis
0.72	0.37	0.86	0.01	MLR – no intercept
0.71	0.44	0.87	-0.01	MLP – relu
<i>Estimation parameter: GWT-LST; Variables: SDP, EVT, BD</i>				
0.74	0.03	0.84	0.02	SVM – linear
0.73	0.01	0.85	-0.02	SVM – radial basis
0.75	0.03	0.85	0.00	SVM – polynomial
0.72	0.02	0.85	0.13	MLP – logistic
<b>0.72</b>	<b>0.01</b>	<b>0.85</b>	<b>0.02</b>	<b>MLR – with intercept</b>
0.72	0.02	0.85	-0.11	MLP – tanh
0.72	0.00	0.87	-0.01	MLR – no intercept
0.73	0.00	0.91	0.01	NNR
0.71	0.00	0.91	-0.05	MLP – relu

*RMSE* = Root Mean Square Error; *MAE* = Mean Absolute Error; *ME* = Mean Error; *5f* = 5-fold Cross-Validation; *MLR* = Multiple Linear Regression; *SVM* = Support Vector Machine; *MLP* = Multilayer Perceptron; *NNR* = Nearest Neighbor Regression

## Appendix C-2: Assignment of CLC classes

Table C2. Land use groups and associated classes according to CORINE Land Cover (CLC).

CLC-Group	Included CLC-Classes
Urban fabric	1, 2
Industrial areas	3 – 9
Urban green spaces	10, 11
Agricultural areas	12 – 22
Forest and natural areas	23 – 34

## Appendix C-3: Estimation outliers

Table C3. Estimation outliers as temperature difference ( $\Delta T$ ) between groundwater temperature (GWT) and estimated groundwater temperature (eGWT) as well as assigned CORINE Land Cover (CLC) groups.

Site	$\Delta T$ (K)	GWT (°C)	eGWT (°C)	CLC-Group	Possible reason
Magdeburg	-4.2	17	12.8	Urban green spaces	Proximity to medical facility (12 m)
Klöden	-3.9	14.4	10.5	Agricultural areas	Proximity to Elbe River (130 m)
Dessau-Roßlau	-3.1	16.6	13.5	Urban fabric	City center, proximity to residential building (1 m)
Halle (Saale)	1.5	11.2	12.7	Agricultural areas	High LST due to urban location
Halle (Saale)	1.5	12.4	13.9	Urban fabric	Location in green space
Halle (Saale)	1.8	12.3	14.1	Urban fabric	Location in green space

## Appendix C-4: Results and errors per CLC group

Table C4. Average groundwater temperature (GWT) and estimated groundwater temperature (eGWT) as well as Mean Error (ME) and Root Mean Square Error (RMSE) per CORINE Land Cover (CLC) group.

CLC-Group	No. of GWM	$\bar{\text{GWT}}$ (°C)	$\bar{\text{eGWT}}$ (°C)	ME (K)	RMSE (K)
Urban fabric	59	12.3	12.2	-0.09	0.95
Industrial areas	25	12.6	12.3	-0.25	1.00
Urban green spaces	8	11.7	12.1	0.39	0.62
Agricultural areas	266	11.0	11.0	-0.02	0.71
Forest and natural areas	78	10.7	10.8	0.13	0.55
<b>Total</b>	<b>436</b>	<b>11.2</b>	<b>11.2</b>	<b>-0.01</b>	<b>0.74</b>

### Appendix C-5: Measurement frequency and repetitions

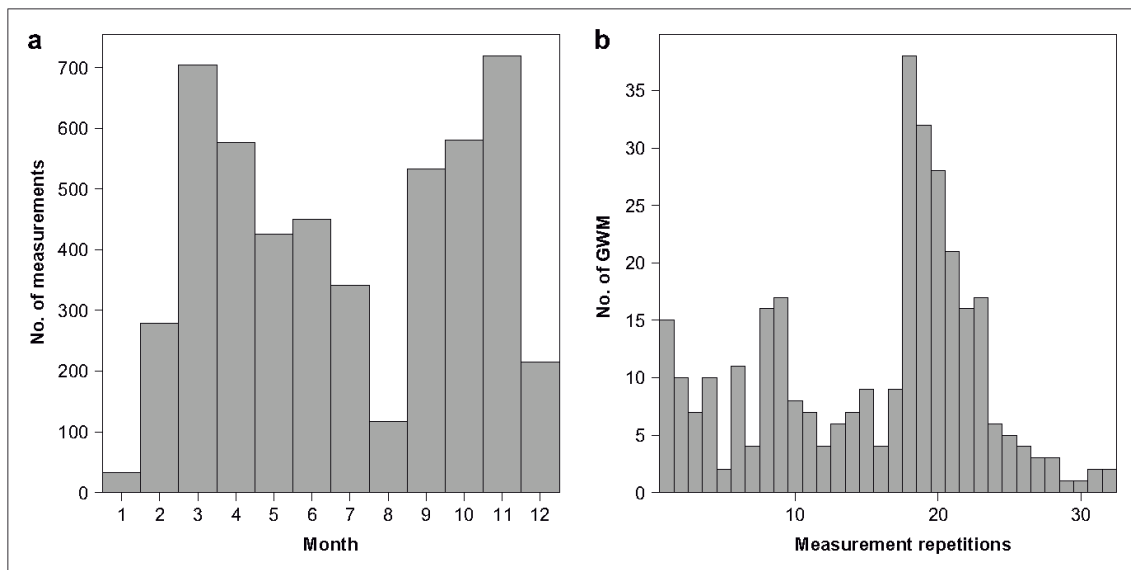


Figure C1. Histograms visualizing (a) the distribution of the LHW measurement data over the months; (b) the frequency of the number of measurement repetitions per LHW well (GWM).

# Appendix D

## Appendix D-1: Complete sets of temperature depth profiles

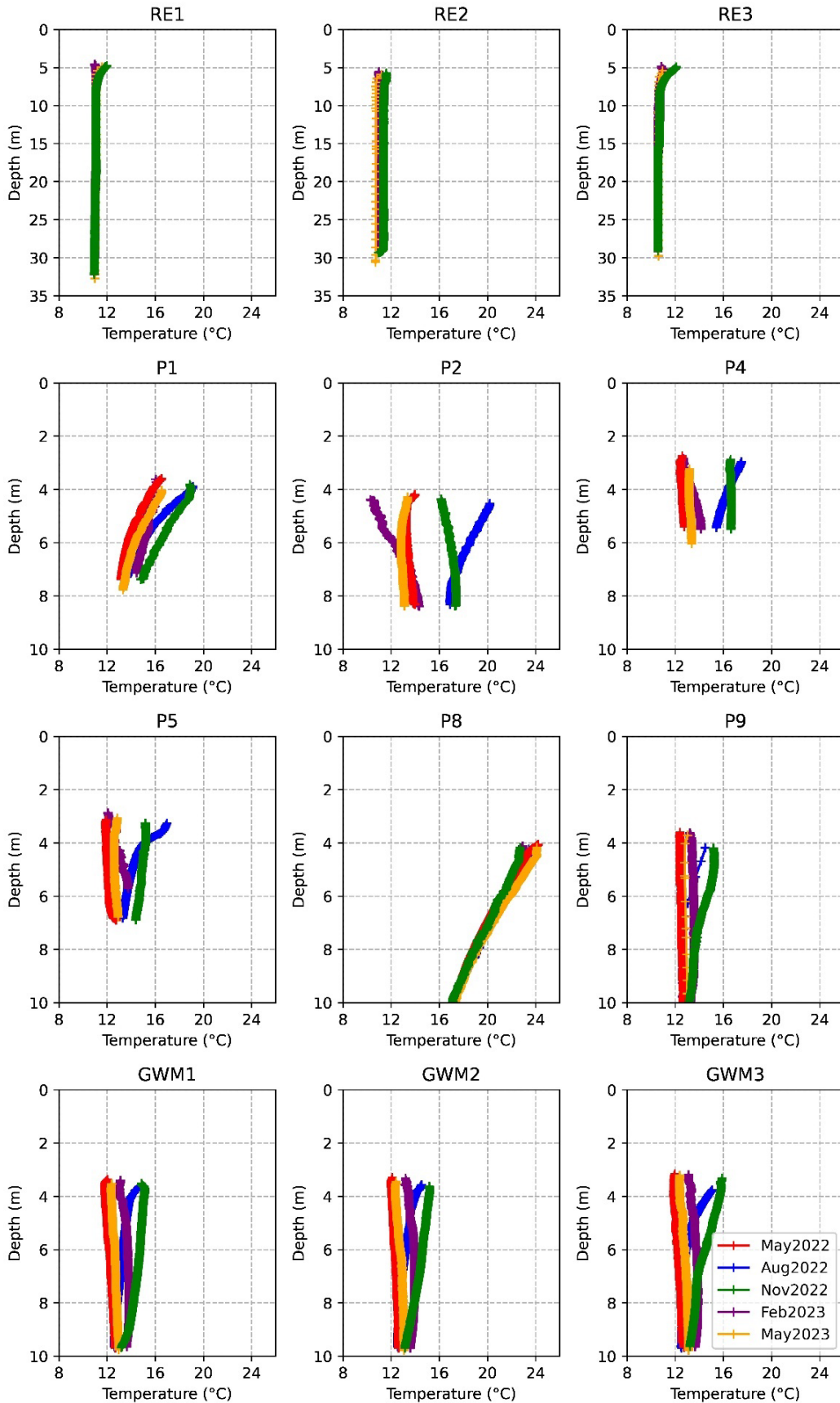


Figure D1. Temperature depth profiles of all wells during different seasons.

## Appendix D-2: Results of measured parameters per location

Table D1. Mean values of measured physical, chemical, microbiological, and faunistic parameters, calculated consecutively for each well and for the classes. Temperature depth profiles were used to calculate the groundwater temperature (GWT) at 5 m depth below surface level. Thermally unaffected wells include GWM1–3 and P9. Thermally affected wells include P1, P5, and P8 as well as P2 and P4 (only GWT). Reference wells are RE1–3. The number of samples (n) is indexed in the footnotes, the Groundwater-Fauna-Index (GFI) was calculated according to Eq. 1. EC = electrical conductivity; DOC = dissolved organic carbon; ATP = adenosine triphosphate; BA = bacterial abundance, FA = faunal abundance; SD = standard deviation.

Parameter (unit)	Thermally unaffected wells (SD)	Thermally affected wells (SD)	Reference wells (SD)	Limit according to German drinking water regulations
<b>GWT</b> (°C)	13.2 <sup>a</sup> (0.07)	16.2 <sup>b</sup> (3.69)	11.3 <sup>c</sup> (0.05)	-
<b>EC</b> (mS/cm)	1.5 <sup>d</sup> (0.19)	1.5 <sup>e</sup> (0.06)	0.7 <sup>c</sup> (0.12)	2.79
<b>pH</b> (-)	6.8 <sup>d</sup> (0.06)	6.8 <sup>e</sup> (0.03)	7.3 <sup>c</sup> (0.10)	6.5–9.5
<b>O<sub>2</sub></b> (mg/l)	0.7 <sup>d</sup> (0.06)	0.5 <sup>e</sup> (0.04)	1.0 <sup>c</sup> (1.52)	-
<b>NO<sub>3</sub><sup>-</sup></b> (mg/l)	85% < detection limit (0.125) <sup>f</sup>	87% < detection limit (0.125) <sup>g</sup>	89% < detection limit (0.125) <sup>c</sup>	50
<b>NH<sub>4</sub><sup>+</sup></b> (mg/l)	68% < detection limit (0.025) <sup>f</sup>	53% < detection limit (0.025) <sup>g</sup>	100% < detection limit (0.025) <sup>c</sup>	50
<b>SO<sub>4</sub><sup>2-</sup></b> (mg/l)	355.0 <sup>f</sup> (14.63)	412.1 <sup>g</sup> (53.83)	132.9 <sup>c</sup> (73.16)	250
<b>Cl<sup>-</sup></b> (mg/l)	98.7 <sup>f</sup> (33.82)	97.3 <sup>g</sup> (20.51)	24.4 <sup>c</sup> (15.29)	250
<b>K<sup>+</sup></b> (mg/l)	3.0 <sup>f</sup> (0.28)	6.2 <sup>g</sup> (4.98)	1.4 <sup>c</sup> (0.87)	-
<b>DOC</b> (mg/l)	12.5 <sup>f</sup> (6.2)	9.6 <sup>g</sup> (1.6)	8.1 <sup>c</sup> (3.9)	-
<b>ATP</b> (pM)	134 <sup>f</sup> (77)	108 <sup>g</sup> (38)	50 <sup>c</sup> (34)	-
<b>BA</b> (cells/ml)	1.3 · 10 <sup>5 f</sup> (1.2 · 10 <sup>4</sup> )	1.1 · 10 <sup>5 g</sup> (1.3 · 10 <sup>4</sup> )	4.3 · 10 <sup>4 c</sup> (4.1 · 10 <sup>4</sup> )	-
<b>FA</b> (individuals/ sample)	3.3 <sup>a</sup> (5.7)	0.3 <sup>g</sup> (0.4)	1.8 <sup>c</sup> (2.5)	-
<b>GFI</b> (-)	0.25 (0.14)	0.58 (0.18)	0.23 (0.26)	-

<sup>a</sup> n = 20; <sup>b</sup> n = 25; <sup>c</sup> n = 9; <sup>d</sup> n = 15; <sup>e</sup> n = 12; <sup>f</sup> n = 19; <sup>g</sup> n = 15.





## References

- Gebäudeenergiegesetz, (2020).
- Garagenverordnung, (2022).
- Adam, D., & Markiewicz, R. (2009). Energy from earth-coupled structures, foundations, tunnels and sewers. *Géotechnique*, 59(3), 229-236.
- Adjali, M., Davies, M., Riain, C. N., & Littler, J. (2000). In situ measurements and numerical simulation of heat transfer beneath a heated ground floor slab. *Energy and Buildings*, 33(1), 75-83.
- Agudelo-Vera, C., Avvedimento, S., Boxall, J., Creaco, E., de Kater, H., Di Nardo, A., Djukic, A., Douterelo, I., Fish, K. E., & Iglesias Rey, P. L. (2020). Drinking water temperature around the globe: understanding, policies, challenges and opportunities. *Water*, 12(4), 1049.
- Agudelo-Vera, C. M., Blokker, M., de Kater, H., & Lafort, R. (2017). Identifying (subsurface) anthropogenic heat sources that influence temperature in the drinking water distribution system. *Drinking water engineering and science*, 10(2), 83-91.
- Allen, P. A. (2009). *Earth surface processes*. John Wiley & Sons.
- Ampofo, F., Maidment, G., & Missenden, J. (2006). Review of groundwater cooling systems in London. *Applied Thermal Engineering*, 26(17-18), 2055-2062.
- Anderson, M. P. (2005). Heat as a ground water tracer. *Groundwater*, 43(6), 951-968.
- Arias, P., Bellouin, N., Coppola, E., Jones, R., Krinner, G., Marotzke, J., Naik, V., Palmer, M., Plattner, G.-K., & Rogelj, J. (2021). Climate Change 2021: The Physical Science Basis. Contribution of Working Group I to the Sixth Assessment Report of the Intergovernmental Panel on Climate Change; Technical Summary.
- Arola, T., & Korkka-Niemi, K. (2014). The effect of urban heat islands on geothermal potential: examples from Quaternary aquifers in Finland. *Hydrogeology Journal*, 22(8), 1953-1967.
- Attard, G., Bayer, P., Rossier, Y., Blum, P., & Eisenlohr, L. (2020). A novel concept for managing thermal interference between geothermal systems in cities. *Renewable energy*, 145, 914-924.
- Attard, G., Rossier, Y., Winiarski, T., & Eisenlohr, L. (2016a). Deterministic modeling of the impact of underground structures on urban groundwater temperature. *Science of the Total Environment*, 572, 986-994.
- Attard, G., Winiarski, T., Rossier, Y., & Eisenlohr, L. (2016b). Impact of underground structures on the flow of urban groundwater. *Hydrogeology Journal*, 24(1), 5-19.
- Bai, Y., Wang, Z., Fan, J., Yang, M., Li, X., Chen, L., Yuan, G., & Yang, J. (2020). Numerical and experimental study of an underground water pit for seasonal heat storage. *Renewable energy*, 150, 487-508.
- Barla, M., & Di Donna, A. (2018). Energy tunnels: concept and design aspects. *Underground Space*, 3(4), 268-276.
- Bartram, J., Chartier, Y., Lee, J. V., Pond, K., & Surman-Lee, S. (2007). *Legionella and the prevention of legionellosis*. World Health Organization.

- Bates, B., Kundzewicz, Z., & Wu, S. (2008). *Climate change and water*. Intergovernmental Panel on Climate Change Secretariat.
- Bauer, D., Heidemann, W., & Müller-Steinhagen, H. (2008). Solar unterstützte Nahwärmeversorgung: Langzeiterfahrungen der Anlage in Friedrichshafen. Tagungsband 18. Symposium Thermische Solarenergie,
- Bauer, M., Eppinger, A., Franßen, W., Heinz, M., Keim, B., Mahler, D., Milkowski, N., Pasler, U., Rolland, K., Schölch-Ighodaro, R., Stein, U., Vöröshazi, M., & Wingerling, M. (2009). Leitfaden zur Nutzung von Erdwärme mit Grundwasserwärmepumpen. *Stuttgart: Umweltministerium Baden-Württemberg*.
- Bayer, P., Attard, G., Blum, P., & Menberg, K. (2019). The geothermal potential of cities. *Renewable and Sustainable Energy Reviews, 106*, 17-30.
- Becher, J., Englisch, C., Griebler, C., & Bayer, P. (2022). Groundwater fauna downtown—Drivers, impacts and implications for subsurface ecosystems in urban areas. *Journal of Contaminant Hydrology, 248*, 104021.
- Becker, D., & Epting, J. (2021). Thermischer Einfluss urbaner Untergrundstrukturen auf die Grundwassertemperaturen im Kanton Basel-Stadt. *Grundwasser, 1*-20.
- Bense, V., Kurylyk, B., de Bruin, J., & Visser, P. (2020). Repeated subsurface thermal profiling to reveal temporal variability in deep groundwater flow conditions. *Water Resources Research, 56*(6), e2019WR026913.
- Benz, S. A., Bayer, P., & Blum, P. (2017a). Global patterns of shallow groundwater temperatures. *Environmental Research Letters, 12*(3), 034005.
- Benz, S. A., Bayer, P., & Blum, P. (2017b). Identifying anthropogenic anomalies in air, surface and groundwater temperatures in Germany. *Science of the Total Environment, 584*, 145-153.
- Benz, S. A., Bayer, P., Blum, P., Hamamoto, H., Arimoto, H., & Taniguchi, M. (2018a). Comparing anthropogenic heat input and heat accumulation in the subsurface of Osaka, Japan. *Science of the Total Environment, 643*, 1127-1136.
- Benz, S. A., Bayer, P., Goettsche, F. M., Olesen, F. S., & Blum, P. (2015a). Linking surface urban heat islands with groundwater temperatures. *Environmental science & technology, 50*(1), 70-78.
- Benz, S. A., Bayer, P., Menberg, K., Jung, S., & Blum, P. (2015b). Spatial resolution of anthropogenic heat fluxes into urban aquifers. *Science of the Total Environment, 524*, 427-439.
- Benz, S. A., Bayer, P., Winkler, G., & Blum, P. (2018b). Recent trends of groundwater temperatures in Austria. *Hydrology and Earth System Sciences, 22*(6), 3143-3154.
- Benz, S. A., Irvine, D. J., Rau, G. C., Bayer, P., Menberg, K., Blum, P., Jamieson, R. C., Griebler, C., & Kurylyk, B. L. (2024). Global groundwater warming due to climate change. *Nature Geoscience, 1*-7.
- Benz, S. A., Menberg, K., Bayer, P., & Kurylyk, B. L. (2022). Shallow subsurface heat recycling is a sustainable global space heating alternative. *Nature Communications, 13*(1), 3962.
- Beyer, C., Popp, S., & Bauer, S. (2016). Simulation of temperature effects on groundwater flow, contaminant dissolution, transport and biodegradation due to shallow geothermal use. *Environmental earth sciences, 75*(18), 1-20.

- Bidarmaghz, A., Choudhary, R., Soga, K., Kessler, H., Terrington, R. L., & Thorpe, S. (2019). Influence of geology and hydrogeology on heat rejection from residential basements in urban areas. *Tunnelling and Underground Space Technology*, *92*, 103068.
- Bidarmaghz, A., Choudhary, R., Soga, K., Terrington, R. L., Kessler, H., & Thorpe, S. (2020). Large-scale urban underground hydro-thermal modelling – A case study of the Royal Borough of Kensington and Chelsea, London. *Science of the Total Environment*, *700*, 134955.
- Bloomfield, J. P., Jackson, C. R., & Stuart, M. E. (2013). Changes in groundwater levels, temperature and quality in the UK over the 20th century: an assessment of evidence of impacts from climate change. *Groundwater in the 20th century*.
- Blum, P., Fleuchaus, P., Koenigsdorff, R., Ryba, M., Zorn, R., Schüppler, S., Braun, J., Giannelli, G., Moormann, C., & Buhmann, P. (2021a). Geothermische Speicherung in Baden-Württemberg: Abschlussbericht GeoSpeicher. bw.
- Blum, P., Menberg, K., Koch, F., Benz, S. A., Tissen, C., Hemmerle, H., & Bayer, P. (2021b). Is thermal use of groundwater a pollution? *Journal of Contaminant Hydrology*, *239*, 103791.
- Bodmann, M., & Fisch, M. (2004). Solar unterstützte Nahwärmeversorgung-Pilotprojekte Hamburg, Hannover und Steinfurt. FKS-Symposium: FKS-Forschungskreis Solarenergie TU Braunschweig, Braunschweig.
- Bonte, M., Stuyfzand, P., Van den Berg, G., & Hijnen, W. (2011). Effects of aquifer thermal energy storage on groundwater quality and the consequences for drinking water production: a case study from the Netherlands. *Water Science and Technology*, *63*(9), 1922-1931.
- Bonte, M., van Breukelen, B. M., & Stuyfzand, P. J. (2013). Temperature-induced impacts on groundwater quality and arsenic mobility in anoxic aquifer sediments used for both drinking water and shallow geothermal energy production. *Water Research*, *47*(14), 5088-5100.
- Bott, C., Dahash, A., Noethen, M., & Bayer, P. (2024). Influence of thermal energy storage basins on the subsurface and shallow groundwater. *Journal of Energy Storage*, *92*, 112222.
- Bott, C., Dressel, I., & Bayer, P. (2019). State-of-technology review of water-based closed seasonal thermal energy storage systems. *Renewable and Sustainable Energy Reviews*, *113*, 109241.
- Böttcher, F., & Zosseder, K. (2022). Thermal influences on groundwater in urban environments—A multivariate statistical analysis of the subsurface heat island effect in Munich. *Science of the Total Environment*, *810*.
- Boulton, A. J., Fenwick, G. D., Hancock, P. J., & Harvey, M. S. (2008). Biodiversity, functional roles and ecosystem services of groundwater invertebrates. *Invertebrate Systematics*, *22*(2), 103-116.
- Brandl, H. (2006). Energy foundations and other thermo-active ground structures. *Géotechnique*, *56*(2), 81-122.
- Brielmann, H., Griebler, C., Schmidt, S. I., Michel, R., & Lueders, T. (2009). Effects of thermal energy discharge on shallow groundwater ecosystems. *68*(3), 273-286.
- Brielmann, H., Lueders, T., Schreglmann, K., Ferraro, F., Avramov, M., Hammerl, V., Blum, P., Bayer, P., & Griebler, C. (2011). Oberflächennahe Geothermie und ihre

- potenziellen Auswirkungen auf Grundwasserökosysteme. *Grundwasser*, 16(2), 77-91.
- Brinks, P., Kornadt, O., & Oly, R. (2014). Thermal Losses via Large Slabs on Grade. The 2nd Asia Conference of International Building Performance Simulation Association, Nagoya, Japan,
- Bucci, A., Barbero, D., Lasagna, M., Forno, M. G., & De Luca, D. A. (2017). Shallow groundwater temperature in the Turin area (NW Italy): vertical distribution and anthropogenic effects. *Environmental earth sciences*, 76(5), 221.
- Burns, E. R., Zhu, Y., Zhan, H., Manga, M., Williams, C. F., Ingebritsen, S. E., & Dunham, J. B. (2017). Thermal effect of climate change on groundwater-fed ecosystems. *Water Resources Research*, 53(4), 3341-3351.
- Čermák, V., Bodri, L., Kresl, M., Dedecek, P., & Safanda, J. (2017). Eleven years of ground-air temperature tracking over different land cover types. *International Journal of Climatology*, 37(2), 1084-1099.
- Čermák, V., Bodri, L., Šafanda, J., Krešl, M., & Dědeček, P. (2014). Ground-air temperature tracking and multi-year cycles in the subsurface temperature time series at geothermal climate-change observatory. *Studia Geophysica et Geodaetica*, 58(3), 403-424.
- Chapuis, R. P. (2010). Using a leaky swimming pool for a huge falling-head permeability test. *Engineering Geology*, 114(1-2), 65-70.
- Cheon, J.-Y., Ham, B.-S., Lee, J.-Y., Park, Y., & Lee, K.-K. (2014). Soil temperatures in four metropolitan cities of Korea from 1960 to 2010: implications for climate change and urban heat. *Environmental earth sciences*, 71(12), 5215-5230.
- Cipolla, S. S., & Maglionico, M. (2014). Heat recovery from urban wastewater: Analysis of the variability of flow rate and temperature. *Energy and Buildings*, 69, 122-130.
- Coccia, C. J., Gupta, R., Morris, J., & McCartney, J. S. (2013). Municipal solid waste landfills as geothermal heat sources. *Renewable and Sustainable Energy Reviews*, 19, 463-474.
- Dernbach, H. (1982). Versuche zur Abschätzung des Gaspotentials einer Deponie anhand von Müllproben. *Veröffentlichung des Instituts für Stadtbauwesen, Gas-und Wasserhaushalt von Mülldeponien*(33 S 447).
- Destatis. (2023). *Statistisches Bundesamt*, URL, <https://www.destatis.de/DE/Themen/Gesellschaft-Umwelt/Umwelt/UGR/private-haushalte/Tabellen/raumwaerme-haushalte.html>.
- Di Donna, A., Loveridge, F., Piemontese, M., & Barla, M. (2021). The role of ground conditions on the heat exchange potential of energy walls. *Geomechanics for Energy and the Environment*, 25, 100199.
- Dillon, P., Stuyfzand, P., Grischek, T., Lluria, M., Pyne, R., Jain, R., Bear, J., Schwarz, J., Wang, W., & Fernandez, E. (2019). Sixty years of global progress in managed aquifer recharge. *Hydrogeology Journal*, 27(1), 1-30.
- DIN EN ISO 6946. (2018). Bauteile - Wärmedurchlasswiderstand und Wärmedurchgangskoeffizient - Berechnungsverfahren.
- Dolna, O., & Mikielewicz, J. (2020). The ground impact on the ultra-low and low-temperature district heating operation. *Renewable energy*, 146, 1232-1241.

- Dugord, P.-A., Lauf, S., Schuster, C., & Kleinschmit, B. (2014). Land use patterns, temperature distribution, and potential heat stress risk—the case study Berlin, Germany. *Computers, Environment and Urban Systems*, *48*, 86-98.
- DWD. (2023). *Climate Data Center* <https://cdc.dwd.de/portal/>
- Eggleston, J., & McCoy, K. J. (2015). Assessing the magnitude and timing of anthropogenic warming of a shallow aquifer: example from Virginia Beach, USA. *Hydrogeology Journal*, *23*(1), 105-120.
- Emery, A., Heerwagen, D., Kippenhan, C., & Steele, D. (2007). Measured and predicted thermal performance of a residential basement. *HVAC&R Research*, *13*(1), 39-57.
- Epting, J. (2017). Thermal management of urban subsurface resources - Delineation of boundary conditions. *Procedia engineering*, *209*, 83-91.
- Epting, J., Baralis, M., Künze, R., Mueller, M. H., Insana, A., Barla, M., & Huggenberger, P. (2020a). Geothermal potential of tunnel infrastructures – development of tools at the city-scale of Basel, Switzerland. *Geothermics*, *83*, 101734.
- Epting, J., Böttcher, F., Mueller, M. H., García-Gil, A., Zosseder, K., & Huggenberger, P. (2020b). City-scale solutions for the energy use of shallow urban subsurface resources – Bridging the gap between theoretical and technical potentials. *Renewable energy*, *147*, 751-763.
- Epting, J., García-Gil, A., Huggenberger, P., Vázquez-Suñe, E., & Mueller, M. H. (2017a). Development of concepts for the management of thermal resources in urban areas – Assessment of transferability from the Basel (Switzerland) and Zaragoza (Spain) case studies. *Journal of Hydrology*, *548*, 697-715.
- Epting, J., Händel, F., & Huggenberger, P. (2013). Thermal management of an unconsolidated shallow urban groundwater body. *Hydrology and Earth System Sciences*, *17*(5), 1851-1869.
- Epting, J., & Huggenberger, P. (2013). Unraveling the heat island effect observed in urban groundwater bodies – Definition of a potential natural state. *Journal of Hydrology*, *501*, 193-204.
- Epting, J., Scheidler, S., Affolter, A., Borer, P., Mueller, M. H., Egli, L., García-Gil, A., & Huggenberger, P. (2017b). The thermal impact of subsurface building structures on urban groundwater resources – a paradigmatic example. *Science of the Total Environment*, *596*, 87-96.
- European Environment Agency. (2023). *Copernicus Land Monitoring Service* <https://land.copernicus.eu/en/products/corine-land-cover>
- Felix, M., Sohr, A., Riedel, P., & Assmann, L. (2009). *Kurzbericht zu den Forschungsberichten 2005 bis 2007 zur Thematik Gefährdungspotenzial Steinkohlenhalden Zwickau/Oelsnitz*.
- Ferguson, G., & Woodbury, A. D. (2004). Subsurface heat flow in an urban environment. *Journal of Geophysical Research: Solid Earth*, *109*(B2).
- Ferguson, G., & Woodbury, A. D. (2007). Urban heat island in the subsurface. *Geophysical Research Letters*, *34*(23).
- Figura, S., Livingstone, D. M., Hoehn, E., & Kipfer, R. (2011). Regime shift in groundwater temperature triggered by the Arctic Oscillation. *Geophysical Research Letters*, *38*(23).

- Figura, S., Livingstone, D. M., & Kipfer, R. (2013). Competing controls on groundwater oxygen concentrations revealed in multidecadal time series from riverbank filtration sites. *Water Resources Research*, *49*(11), 7411-7426.
- Figura, S., Livingstone, D. M., & Kipfer, R. (2015). Forecasting groundwater temperature with linear regression models using historical data. *Groundwater*, *53*(6), 943-954.
- Fillinger, L., Hug, K., Trimbach, A. M., Wang, H., Kellermann, C., Meyer, A., Bendinger, B., & Griebler, C. (2019). The DA-(C) index: A practical approach towards the microbiological-ecological monitoring of groundwater ecosystems. *Water Research*, *163*, 114902.
- Fischer, D., Charles, E. G., & Baehr, A. L. (2003). Effects of stormwater infiltration on quality of groundwater beneath retention and detention basins. *Journal of Environmental Engineering*, *129*(5), 464-471.
- Fleuchaus, P., Godschalk, B., Stober, I., & Blum, P. (2018). Worldwide application of aquifer thermal energy storage – A review. *Renewable and Sustainable Energy Reviews*, *94*, 861-876.
- Ford, M., & Tellam, J. (1994). Source, type and extent of inorganic contamination within the Birmingham urban aquifer system, UK. *Journal of Hydrology*, *156*(1-4), 101-135.
- Forster, P., Storelvmo, T., Armour, K., Collins, W., Dufresne, J.-L., Frame, D., Lunt, D., Mauritsen, T., Palmer, M., & Watanabe, M. (2021). The Earth's energy budget, climate feedbacks, and climate sensitivity.
- Foulquier, A., Malard, F., Barraud, S., & Gibert, J. (2009). Thermal influence of urban groundwater recharge from stormwater infiltration basins. *Hydrological Processes: An International Journal*, *23*(12), 1701-1713.
- Founda, D., & Santamouris, M. (2017). Synergies between Urban Heat Island and Heat Waves in Athens (Greece), during an extremely hot summer (2012). *Scientific reports*, *7*(1), 10973.
- Fourier, J. B. J. (1888). *Théorie analytique de la chaleur*. Gauthier-Villars et fils.
- Fuchs, A. (2008). Erhebung und Beschreibung der Grundwasserfauna in Baden-Württemberg.
- García-Gil, A., Gasco-Cavero, S., Garrido, E., Mejías, M., Epting, J., Navarro-Elipe, M., Alexandre, C., & Sevilla-Alcaine, E. (2018a). Decreased waterborne pathogenic bacteria in an urban aquifer related to intense shallow geothermal exploitation. *Science of the Total Environment*, *633*, 765-775.
- García-Gil, A., Goetzl, G., Kłonowski, M. R., Borovic, S., Boon, D. P., Abesser, C., Janza, M., Herms, I., Petitclerc, E., & Erlström, M. (2020a). Governance of shallow geothermal energy resources. *Energy Policy*, *138*, 111283.
- García-Gil, A., Mejías Moreno, M., Garrido Schneider, E., Marazuela, M. Á., Abesser, C., Mateo Lázaro, J., & Sánchez Navarro, J. Á. (2020b). Nested shallow geothermal systems. *Sustainability*, *12*(12), 5152.
- García-Gil, A., Schneider, E. G., Mejías, M., Barceló, D., Vázquez-Suñé, E., & Díaz-Cruz, S. (2018b). Occurrence of pharmaceuticals and personal care products in the urban aquifer of Zaragoza (Spain) and its relationship with intensive shallow geothermal energy exploitation. *Journal of Hydrology*, *566*, 629-642.
- Geoportal Berlin. (2023). *Senatsverwaltung für Stadtentwicklung, Bauen und Wohnen*, URL, <https://fbinter.stadt-berlin.de/fb/index.jsp>.

- Griebler, C. (2015). *Auswirkungen thermischer Veränderungen infolge der Nutzung oberflächennaher Geothermie auf die Beschaffenheit des Grundwassers und seiner Lebensgemeinschaften: Empfehlungen für eine umweltverträgliche Nutzung*. Umweltbundesamt.
- Griebler, C., & Avramov, M. (2015). Groundwater ecosystem services: a review. *Freshwater Science*, 34(1), 355-367.
- Griebler, C., Brielmann, H., Haberer, C. M., Kaschuba, S., Kellermann, C., Stumpp, C., Hegler, F., Kuntz, D., Walker-Hertkorn, S., & Lueders, T. (2016). Potential impacts of geothermal energy use and storage of heat on groundwater quality, biodiversity, and ecosystem processes. *Environmental earth sciences*, 75(20), 1-18.
- Griebler, C., Stein, H., Hahn, H., Steube, C., Kelleman, C., Fuchs, A., Berkhoff, S., & Brielmann, H. (2014). Entwicklung biologischer Bewertungsmethoden und -kriterien für Grundwasserökosysteme. *Umweltbundesamt, Dessau*.
- Griffioen, J., & Appelo, C. A. J. (1993). Nature and extent of carbonate precipitation during aquifer thermal energy storage. *Applied Geochemistry*, 8(2), 161-176.
- Grillo, R. J. (2014). Energy recycling – landfill waste heat generation and recovery. *Current Sustainable/Renewable Energy Reports*, 1(4), 150-156.
- Gunawardhana, L. N., & Kazama, S. (2011). Climate change impacts on groundwater temperature change in the Sendai plain, Japan. *Hydrological Processes*, 25(17), 2665-2678.
- Gunawardhana, L. N., & Kazama, S. (2012). Statistical and numerical analyses of the influence of climate variability on aquifer water levels and groundwater temperatures: The impacts of climate change on aquifer thermal regimes. *Global and Planetary Change*, 86, 66-78.
- Gunkel, G., Michels, U., & Scheideler, M. (2022). Climate Change: Water Temperature and Invertebrate Propagation in Drinking-Water Distribution Systems, Effects, and Risk Assessment. *Water*, 14(8), 1246.
- Guo, L., Guo, L., Zhong, L., & Zhu, Y. (2011). Thermal conductivity and heat transfer coefficient of concrete. *Journal of Wuhan University of Technology-Mater. Sci. Ed.*, 26(4), 791-796.
- Hahn, H. J. (2006). The GW-Fauna-Index: A first approach to a quantitative ecological assessment of groundwater habitats. *Limnologica*, 36(2), 119-137.
- Hahn, H. J., & Fuchs, A. (2009). Distribution patterns of groundwater communities across aquifer types in south-western Germany. *Freshwater Biology*, 54(4), 848-860.
- Hahn, H. J., Schweer, C., & Griebler, C. (2018). Grundwasserökosysteme im Recht? Eine kritische Betrachtung zur rechtlichen Stellung von Grundwasserökosystemen. *Grundwasser*, 23(3), 209-218.
- Hähnlein, S., Bayer, P., & Blum, P. (2010). International legal status of the use of shallow geothermal energy. *Renewable and Sustainable Energy Reviews*, 14(9), 2611-2625.
- Hähnlein, S., Blum, P., & Bayer, P. (2011). Oberflächennahe Geothermie–aktuelle rechtliche Situation in Deutschland. *Grundwasser*, 16(2), 69-75.
- Hall, D., Riggs, G., & Salomonson, V. (2006). *MODIS/Terra Snow Cover 5-Min L2 Swath 500m, Version 5, NASA National Snow and Ice Data Center Distributed Active Archive Center, Boulder, Colorado, USA*

- Hammes, F., & Egli, T. (2010). Cytometric methods for measuring bacteria in water: advantages, pitfalls and applications. *Analytical and bioanalytical chemistry*, 397, 1083-1095.
- Hancock, P. J., Boulton, A. J., & Humphreys, W. F. (2005). Aquifers and hyporheic zones: towards an ecological understanding of groundwater. *Hydrogeology Journal*, 13, 98-111.
- Hannappel, S., & Limberg, A. (2007). Ermittlung des Flurabstandes des oberflächennahen Grundwassers in Berlin (Determination of the floor distance of shallow groundwater in Berlin). *Brandenburg Geowiss Beitr*, 14, 65-74.
- Harris, R. N., & Chapman, D. S. (1997). Borehole temperatures and a baseline for 20th-century global warming estimates. *Science*, 275(5306), 1618-1621.
- Hartog, N., Drijver, B., Dinkla, I., & Bonte, M. (2013). Field assessment of the impacts of Aquifer Thermal Energy Storage (ATES) systems on chemical and microbial groundwater composition. Proceedings of the European Geothermal Conference, Pisa, Italy,
- He, X., Yang, X., Luo, Z., & Guan, T. (2020). Application of unmanned aerial vehicle (UAV) thermal infrared remote sensing to identify coal fires in the Huojitu coal mine in Shenmu city, China. *Scientific Reports*, 10(1), 1-13.
- Helbig, U., & Weidlich, I. (2018). Wärme-und Kälteschutz bei Rohrleitungen. In *Rohrleitungen 2* (pp. 885-931). Springer.
- Hemmerle, H., & Bayer, P. (2020). Climate change yields groundwater warming in Bavaria, Germany. *Frontiers in Earth Science*, 8, 523.
- Hemmerle, H., Dressel, I., Blum, P., Menberg, K., Benz, S. A., & Bayer, P. (2020). Benefits from Subsurface Urban Heat Islands to Shallow Geothermal Applications – an Example from the City of Cologne, Germany. *Proceedings World Geothermal Congress*.
- Hemmerle, H., Ferguson, G., Blum, P., & Bayer, P. (2022). The evolution of the geothermal potential of a subsurface urban heat island. *Environmental Research Letters*, 17(8), 084018.
- Hemmerle, H., Hale, S., Dressel, I., Benz, S. A., Attard, G., Blum, P., & Bayer, P. (2019). Estimation of Groundwater Temperatures in Paris, France. *Geofluids*, 2019.
- Henning, A. (2016). *Untersuchung und Bewertung der Veränderung des Temperaturfeldes in Berlin im Umfeld des Fehrbelliner Platzes im Stadtteil Wilmersdorf*.
- Henning, A., & Limberg, A. (2012). Veränderung des oberflächennahen Temperaturfeldes von Berlin durch Klimawandel und Urbanisierung. *Brandenburgische Geowiss. Beitr*, 19(1), 81-92.
- Hepbasli, A. (2012). Low exergy (LowEx) heating and cooling systems for sustainable buildings and societies. *Renewable and Sustainable Energy Reviews*, 16(1), 73-104.
- HGK. (2001). *Hydrogeologische Kartierung und Grundwasserbewirtschaftung Rhein-Neckar-Raum*.
- Janssen, H., Carmeliet, J., & Hens, H. (2004). The influence of soil moisture transfer on building heat loss via the ground. *Building and Environment*, 39(7), 825-836.
- Kabuth, A., Dahmke, A., Beyer, C., Bilke, L., Dethlefsen, F., Dietrich, P., Duttmann, R., Ebert, M., Feeser, V., & Görke, U.-J. (2017). Energy storage in the geological



- subsurface: dimensioning, risk analysis and spatial planning: the ANGUS+ project. *Environmental earth sciences*, 76, 1-17.
- Kammen, D. M., & Sunter, D. A. (2016). City-integrated renewable energy for urban sustainability. *Science*, 352(6288), 922-928.
- Kaown, D., Koh, D.-C., Mayer, B., & Lee, K.-K. (2009). Identification of nitrate and sulfate sources in groundwater using dual stable isotope approaches for an agricultural area with different land use (Chuncheon, mid-eastern Korea). *Agriculture, Ecosystems & Environment*, 132(3-4), 223-231.
- Kelly, W. R., Panno, S. V., & Hackley, K. C. (2012). Impacts of road salt runoff on water quality of the Chicago, Illinois, region. *Environmental & engineering geoscience*, 18(1), 65-81.
- Koch, F., Menberg, K., Schweikert, S., Spengler, C., Hahn, H. J., & Blum, P. (2021). Groundwater fauna in an urban area: natural or affected? *Hydrology and earth system sciences discussions*, 25(6), 3053-3070.
- Korneva, I., & Lokoshchenko, M. (2015). Soil temperature in Moscow and its contemporary variations. *Russian Meteorology and Hydrology*, 40(1), 25-33.
- Kottmeier, C., Biegert, C., & Corsmeier, U. (2007). Effects of urban land use on surface temperature in Berlin: Case study. *Journal of urban planning and development*, 133(2), 128-137.
- Krcmar, D., Flakova, R., Ondrejko, I., Hodasova, K., Rusnakova, D., Zenisova, Z., & Zatlakovic, M. (2020). Assessing the impact of a heated basement on groundwater temperatures in Bratislava, Slovakia. *Groundwater*, 58(3), 406-412.
- Kretschmer, F., Simperler, L., & Ertl, T. (2016). Analysing wastewater temperature development in a sewer system as a basis for the evaluation of wastewater heat recovery potentials. *Energy and Buildings*, 128, 639-648.
- Kroener, E., Vallati, A., & Bittelli, M. (2014). Numerical simulation of coupled heat, liquid water and water vapor in soils for heat dissipation of underground electrical power cables. *Applied Thermal Engineering*, 70(1), 510-523.
- Kurylyk, B. L., Irvine, D. J., & Bense, V. F. (2019). Theory, tools, and multidisciplinary applications for tracing groundwater fluxes from temperature profiles. *Wiley Interdisciplinary Reviews: Water*, 6(1), e1329.
- Kurylyk, B. L., MacQuarrie, K. T., & McKenzie, J. M. (2014). Climate change impacts on groundwater and soil temperatures in cold and temperate regions: Implications, mathematical theory, and emerging simulation tools. *Earth-Science Reviews*, 138, 313-334.
- Lachenbruch, A. H., & Marshall, B. V. (1986). Changing climate: geothermal evidence from permafrost in the Alaskan Arctic. *Science*, 234(4777), 689-696.
- LeBleu, C., Dougherty, M., Rahn, K., Wright, A., Bowen, R., Wang, R., Orjuela, J. A., & Britton, K. (2019). Quantifying thermal characteristics of stormwater through low impact development systems. *Hydrology*, 6(1), 16.
- Lee, S., Park, S., Han, T. H., Won, J., & Choi, H. (2023). Applicability Evaluation of Energy Slabs Installed in an Underground Parking Lot. *Sustainability*, 15(4), 2973.
- Lee, S., Park, S., Won, J., & Choi, H. (2021). Influential factors on thermal performance of energy slabs equipped with an insulation layer. *Renewable energy*, 174, 823-834.

- LHW. (2023). *Landesbetrieb für Hochwasserschutz und Wasserwirtschaft Sachsen-Anhalt* <https://gld.lhw-sachsen-anhalt.de/>
- Li, D., & Bou-Zeid, E. (2013). Synergistic interactions between urban heat islands and heat waves: The impact in cities is larger than the sum of its parts. *Journal of applied Meteorology and Climatology*, 52(9), 2051-2064.
- Li, Y., Nord, N., Huang, G., & Li, X. (2020). Swimming pool heating technology: A state-of-the-art review. *Building Simulation*,
- Lienen, T., Lüders, K., Halm, H., Westphal, A., Köber, R., & Würdemann, H. (2017). Effects of thermal energy storage on shallow aerobic aquifer systems: temporary increase in abundance and activity of sulfate-reducing and sulfur-oxidizing bacteria. *Environmental earth sciences*, 76(6), 261.
- Limberg, A., & Thierbach, J. (1997). Gliederung der Grundwasserleiter in Berlin. *Brandenburgische Geowiss. Beitr*, 4(2), 21-26.
- Limberger, J., Boxem, T., Pluymaekers, M., Bruhn, D., Manzella, A., Calcagno, P., Beekman, F., Cloetingh, S., & van Wees, J.-D. (2018). Geothermal energy in deep aquifers: A global assessment of the resource base for direct heat utilization. *Renewable and Sustainable Energy Reviews*, 82, 961-975.
- Loeb, N. G., Johnson, G. C., Thorsen, T. J., Lyman, J. M., Rose, F. G., & Kato, S. (2021). Satellite and ocean data reveal marked increase in Earth's heating rate. *Geophysical Research Letters*, 48(13), e2021GL093047.
- Lofi, W., Mehlhorn, H., & Kobus, H. (1977). Betrachtungen zum Wärmehaushalt des Untergrundes im Raum Karlsruhe. *Institut für Hydromechanik, Universität Karlsruhe*, 544.
- Loveridge, F., McCartney, J. S., Narsilio, G. A., & Sanchez, M. (2020). Energy geostructures: a review of analysis approaches, in situ testing and model scale experiments. *Geomechanics for Energy and the Environment*, 22, 100173.
- Lucazeau, F. (2019). Analysis and mapping of an updated terrestrial heat flow data set. *Geochemistry, Geophysics, Geosystems*, 20(8), 4001-4024.
- Luo, Z., & Asproudi, C. (2015). Subsurface urban heat island and its effects on horizontal ground-source heat pump potential under climate change. *Applied Thermal Engineering*, 90, 530-537.
- Mahmood, K., Batool, S. A., & Chaudhry, M. N. (2016). Studying bio-thermal effects at and around MSW dumps using Satellite Remote Sensing and GIS. *Waste Management*, 55, 118-128.
- Makasis, N., Kreitmair, M., Bidarmaghz, A., Farr, G., Scheidegger, J., & Choudhary, R. (2021). Impact of simplifications on numerical modelling of the shallow subsurface at city-scale and implications for shallow geothermal potential. *Science of the Total Environment*, 791, 148236.
- MDR. (2023). Uni Halle: Tiefgaragen erwärmen das Grundwasser. *mdr Wissen*. <https://www.mdr.de/wissen/news-Uni-Halle-Tiefgaragen-erwaermen-Grundwasser-100.html>
- Medved, S., & Černe, B. (2002). A simplified method for calculating heat losses to the ground according to the EN ISO 13370 standard. *Energy and buildings*, 34(5), 523-528.
- Menberg, K., Bayer, P., Zosseder, K., Rumohr, S., & Blum, P. (2013a). Subsurface urban heat islands in German cities. *Science of the Total Environment*, 442, 123-133.

- Menberg, K., Blum, P., Kurylyk, B. L., & Bayer, P. (2014). Observed groundwater temperature response to recent climate change. *Hydrology and Earth System Sciences*, *18*(11), 4453-4466.
- Menberg, K., Blum, P., Rivera, J., Benz, S., & Bayer, P. (2015). Exploring the geothermal potential of waste heat beneath cities. Proceedings World Geothermal Congress,
- Menberg, K., Blum, P., Schaffitel, A., & Bayer, P. (2013b). Long-term evolution of anthropogenic heat fluxes into a subsurface urban heat island. *Environmental science & technology*, *47*(17), 9747-9755.
- Mielke, P., Bauer, D., Homuth, S., Götz, A. E., & Sass, I. (2014). Thermal effect of a borehole thermal energy store on the subsurface. *Geothermal Energy*, *2*(1), 1-15.
- Molnar, P. (2022). Differences between soil and air temperatures: Implications for geological reconstructions of past climate. *Geosphere*, *18*(2), 800-824.
- Mortada, A. (2019). *Energy Efficient Passenger Comfort in Underground Subway Environments*. University of Cambridge.
- Mortada, A., Choudhary, R., & Soga, K. (2015). Thermal modeling and parametric analysis of underground rail systems. *Energy Procedia*, *78*, 2262-2267.
- Mu, Q., Zhao, M., & Running, S. W. (2014). *MODIS Global Terrestrial Evapotranspiration (ET) Product MOD16A2 Collection 5*
- Mueller, M. H., Huggenberger, P., & Epting, J. (2018). Combining monitoring and modelling tools as a basis for city-scale concepts for a sustainable thermal management of urban groundwater resources. *Science of the Total Environment*, *627*, 1121-1136.
- Müller, N., Kuttler, W., & Barlag, A.-B. (2014). Analysis of the subsurface urban heat island in Oberhausen, Germany. *Climate research*, *58*(3), 247-256.
- Murata, T., & Kawai, N. (2018). Degradation of the urban ecosystem function due to soil sealing: involvement in the heat island phenomenon and hydrologic cycle in the Tokyo metropolitan area. *Soil Science and Plant Nutrition*, *64*(2), 145-155.
- Noethen, M., Hemmerle, H., & Bayer, P. (2022). Sources, intensities, and implications of subsurface warming in times of climate change. *Critical Reviews in Environmental Science and Technology*, 1-23.
- Noethen, M., Hemmerle, H., Menberg, K., Epting, J., Benz, S. A., Blum, P., & Bayer, P. (2023). Thermal impact of underground car parks on urban groundwater. *Science of the Total Environment*, *903*, 166572.
- O'Malley, C., Piroozfar, P., Farr, E. R., & Pomponi, F. (2015). Urban Heat Island (UHI) mitigating strategies: A case-based comparative analysis. *Sustainable Cities and Society*, *19*, 222-235.
- Octoń, P., Cisek, P., Pilarczyk, M., & Taler, D. (2015). Numerical simulation of heat dissipation processes in underground power cable system situated in thermal backfill and buried in a multilayered soil. *Energy Conversion and Management*, *95*, 352-370.
- Oke, T. R. (1973). City size and the urban heat island. *Atmospheric Environment (1967)*, *7*(8), 769-779.
- Page, D., Peeters, L., Vanderzalm, J., Barry, K., & Gonzalez, D. (2017). Effect of aquifer storage and recovery (ASR) on recovered stormwater quality variability. *Water Research*, *117*, 1-8.

- Park, Y.-C., Jo, Y.-J., & Lee, J.-Y. (2011). Trends of groundwater data from the Korean National Groundwater Monitoring Stations: indication of any change? *Geosciences Journal*, *15*(1), 105-114.
- Peche, A. (2019). *Numerical modeling of pipe leakage in variably saturated soil*. Gottfried Wilhelm Leibniz Universität Hannover.
- Perera, N., Gharabaghi, B., & Howard, K. (2013). Groundwater chloride response in the Highland Creek watershed due to road salt application: A re-assessment after 20 years. *Journal of Hydrology*, *479*, 159-168.
- Pollack, H. N., Huang, S., & Shen, P.-Y. (1998). Climate change record in subsurface temperatures: a global perspective. *Science*, *282*(5387), 279-281.
- Pollack, H. N., Hurter, S. J., & Johnson, J. R. (1993). Heat flow from the Earth's interior: analysis of the global data set. *Reviews of Geophysics*, *31*(3), 267-280.
- Popiel, C., & Wojtkowiak, J. (2013). Temperature distributions of ground in the urban region of Poznan City. *Experimental Thermal and Fluid Science*, *51*, 135-148.
- Previati, A., & Crosta, G. B. (2021a). Characterization of the subsurface urban heat island and its sources in the Milan city area, Italy. *Hydrogeology Journal*, *29*(7), 2487-2500.
- Previati, A., & Crosta, G. B. (2021b). Regional-scale assessment of the thermal potential in a shallow alluvial aquifer system in the Po plain (northern Italy). *Geothermics*, *90*, 101999.
- Qian, B., Gregorich, E. G., Gameda, S., Hopkins, D. W., & Wang, X. L. (2011). Observed soil temperature trends associated with climate change in Canada. *Journal of Geophysical Research: Atmospheres*, *116*(D2).
- Rammal, D., Mroueh, H., & Burlon, S. (2020). Thermal behaviour of geothermal diaphragm walls: Evaluation of exchanged thermal power. *Renewable energy*, *147*, 2643-2653.
- Rees, S., Adjali, M., Zhou, Z., Davies, M., & Thomas, H. (2000). Ground heat transfer effects on the thermal performance of earth-contact structures. *Renewable and Sustainable Energy Reviews*, *4*(3), 213-265.
- Retter, A., Griebler, C., Haas, J., Birk, S., Stumpp, C., Brielmann, H., & Fillinger, L. (2021). Anwendung des DA-(C)-Index als einfache Methode zur mikrobiologisch-ökologischen Charakterisierung und Überwachung von Grundwasserökosystemen—eine Fallstudie anhand des österreichischen Murtals. *Österreichische Wasser-und Abfallwirtschaft*, *73*, 455-467.
- Retter, A., Karwautz, C., & Griebler, C. (2020). Groundwater microbial communities in times of climate change. *Current Issues in Molecular Biology*, *41*(1), 509-538.
- Riedel, T. (2019). Temperature-associated changes in groundwater quality. *Journal of Hydrology*, *572*, 206-212.
- Rivera, J. A., Blum, P., & Bayer, P. (2015). Analytical simulation of groundwater flow and land surface effects on thermal plumes of borehole heat exchangers. *Applied energy*, *146*, 421-433.
- Rivera, J. A., Blum, P., & Bayer, P. (2017). Increased ground temperatures in urban areas: Estimation of the technical geothermal potential. *Renewable energy*, *103*, 388-400.
- Rotta Loria, A. F., Thota, A., Thomas, A. M., Friedle, N., Lautenberg, J. M., & Song, E. C. (2022). Subsurface heat island across the Chicago Loop district: Analysis of localized drivers. *Urban Climate*, *44*, 101211.

- Sani, A. K., Singh, R. M., Amis, T., & Cavarretta, I. (2019). A review on the performance of geothermal energy pile foundation, its design process and applications. *Renewable and Sustainable Energy Reviews*, *106*, 54-78.
- Sartirana, D., Rotiroti, M., Zanotti, C., Bonomi, T., Fumagalli, L., & De Amicis, M. (2020). A 3D Geodatabase for Urban Underground Infrastructures: Implementation and Application to Groundwater Management in Milan Metropolitan Area. *ISPRS International Journal of Geo-Information*, *9*(10), 609.
- Scalenghe, R., & Marsan, F. A. (2009). The anthropogenic sealing of soils in urban areas. *Landscape and urban planning*, *90*(1-2), 1-10.
- Schmid, F. (2008). Sewage water: interesting heat source for heat pumps and chillers. Proceedings of the 9th International IEA Heat Pump Conference, Zürich, Switzerland,
- Schmidt, D., Kallert, A., Blesl, M., Svendsen, S., Li, H., Nord, N., & Sipilä, K. (2017). Low temperature district heating for future energy systems. *Energy Procedia*, *116*, 26-38.
- Shukla, J., & Mintz, Y. (1982). Influence of land-surface evapotranspiration on the earth's climate. *Science*, *215*(4539), 1498-1501.
- Spengler, C. (2017). *Die Auswirkungen von anthropogenen Temperaturerhöhungen auf die Crustaceagemeinschaften im Grundwasser - Versuch einer Prognose zur Klimaerwärmung und lokalen Wärmeeinträgen*. Universität Koblenz-Landau.
- Spengler, C., & Hahn, H. (2018). Thermostress: Ökologisch gegründete, thermische Schwellenwerte und Bewertungsansätze für das Grundwasser (Ecological based temperature thresholds and ecosystem assessment schemes for groundwater). *Korrespondenz Wasserwirtschaft*, *9*, 521-525.
- Spoelstra, J., Leal, K. A., Senger, N. D., Schiff, S. L., & Post, R. (2021). Isotopic characterization of sulfate in a shallow aquifer impacted by agricultural fertilizer. *Groundwater*, *59*(5), 658-670.
- Stadt Zürich. (2023). *Open Data Zürich*, URL, <https://www.stadt-zuerich.ch/portal/de/index/ogd.html>.
- Stadwerke Hockenheim. (2023). *Analyse des Hockenheimer Trinkwassers*.
- Stauffer, F., Bayer, P., Blum, P., Giraldo, N. M., & Kinzelbach, W. (2013). *Thermal use of shallow groundwater*. CRC Press.
- Stegner, J. (2016). *Bestimmung thermischer Materialkennwerte von Erdkabelbettungen*. TU Darmstadt.
- Stegner, J., Drefke, C., Hailemariam, H., Anbergen, H., Wuttke, F., & Sass, I. (2017). Messtechnik für den Erdkabeltrassenbau – Ermittlung der Wärmeleitfähigkeit von Bettungsmaterialien. *Bauphysik*, *39*(1), 41-48.
- Stober, I., & Bucher, K. (2012). *Geothermie*. Springer.
- Sun, Z., Wang, Q., Batkhishig, O., & Ouyang, Z. (2016). Relationship between evapotranspiration and land surface temperature under energy- and water-limited conditions in dry and cold climates. *Advances in Meteorology*, *2016*(1).
- Taniguchi, M., & Uemura, T. (2005). Effects of urbanization and groundwater flow on the subsurface temperature in Osaka, Japan. *Physics of the Earth and Planetary Interiors*, *152*(4), 305-313.
- Taylor, C. A., & Stefan, H. G. (2009). Shallow groundwater temperature response to climate change and urbanization. *Journal of Hydrology*, *375*(3-4), 601-612.

- Thomas, H., & Rees, S. (1998). The thermal performance of ground floor slabs - a full scale in-situ experiment. *Building and Environment*, *34*(2), 139-164.
- Thomas, H., & Rees, S. (1999). The thermal performance of ground floor slabs - a full scale in-situ experiment. *Building and Environment*, *34*(2), 139-164.
- Tidden, F., & Scharrer, K. (2017). Depohermie – Ein neuer Ansatz zur Wärmegewinnung aus Deponien und Altablagerungen. *Altlasten Spektrum*, *2*, 45-54.
- Tissen, C., Benz, S. A., Menberg, K., Bayer, P., & Blum, P. (2019). Groundwater temperature anomalies in central Europe. *Environmental Research Letters*, *14*(10), 104012.
- Tissen, C., Menberg, K., Benz, S. A., Bayer, P., Steiner, C., Götzl, G., & Blum, P. (2021). Identifying key locations for shallow geothermal use in Vienna. *Renewable energy*, *167*, 1-19.
- Tuxen, N., Albrechtsen, H.-J., & Bjerg, P. L. (2006). Identification of a reactive degradation zone at a landfill leachate plume fringe using high resolution sampling and incubation techniques. *Journal of Contaminant Hydrology*, *85*(3-4), 179-194.
- Tzavali, A., Paravantis, J. P., Mihalakakou, G., Fotiadi, A., & Stigka, E. (2015). Urban heat island intensity: A literature review. *Fresenius Environmental Bulletin*, *24*(12b), 4537-4554.
- van den Bos, L. (2020). *Quantifying the effects of anthropogenic heat sources on the water temperature in the drinking water distribution system*. TU Delft.
- VDI 4640. (2010). Blatt 1: Thermal use of the underground. In (pp. 33). Düsseldorf: VDI-Gesellschaft Energie und Umwelt.
- Vienken, T., Händel, F., Epting, J., Dietrich, P., Liedl, R., & Huggenberger, P. (2016). Energiewende braucht Wärmewende-Chancen und Limitierungen der intensiven thermischen Nutzung des oberflächennahen Untergrundes in urbanen Gebieten vor dem Hintergrund der aktuellen Energiedebatte in Deutschland. *Grundwasser*, *21*(1), 69-73.
- Vienken, T., Kreck, M., & Dietrich, P. (2019). Monitoring the impact of intensive shallow geothermal energy use on groundwater temperatures in a residential neighborhood. *Geothermal Energy*, *7*(1), 1-14.
- Visser, P. W., Kooi, H., Bense, V., & Boerma, E. (2020). Impacts of progressive urban expansion on subsurface temperatures in the city of Amsterdam (The Netherlands). *Hydrogeology Journal*, *28*(5), 1755-1772.
- Vogel, J., & Afshari, A. (2020). Comparison of urban heat island intensity estimation methods using urbanized WRF in Berlin, Germany. *Atmosphere*, *11*(12), 1338.
- von Schuckmann, K., Cheng, L., Palmer, M. D., Hansen, J., Tassone, C., Aich, V., Adusumilli, S., Beltrami, H., Boyer, T., & Cuesta-Valero, F. J. (2020). Heat stored in the Earth system: where does the energy go? *Earth System Science Data*, *12*(3), 2013-2041.
- Wan, Z., Hook, S., & Hulley, G. (2021). *MODIS/Terra Land Surface Temperature/Emissivity Monthly L3 Global 0.05 Deg CMG V061*
- Ward, K., Lauf, S., Kleinschmit, B., & Endlicher, W. (2016). Heat waves and urban heat islands in Europe: A review of relevant drivers. *Science of the Total Environment*, *569*, 527-539.

- Warren, E., & Bekins, B. A. (2018). Relative contributions of microbial and infrastructure heat at a crude oil-contaminated site. *Journal of Contaminant Hydrology*, 211, 94-103.
- Westaway, R., Scotney, P. M., Younger, P. L., & Boyce, A. J. (2015). Subsurface absorption of anthropogenic warming of the land surface: the case of the world's largest brickworks (Stewartby, Bedfordshire, UK). *Science of the Total Environment*, 508, 585-603.
- Wiemer, K. (1982). Messungen des Wasserhaushaltes und der Dichte von ungestörten Müllproben. *Veröffentlichung des Instituts für Stadtbauwesen*(33), 289-300.
- Willscher, S., Hertwig, T., Frenzel, M., Felix, M., & Starke, S. (2010). Results of remediation of hard coal overburden and tailing dumps after a few decades: Insights and conclusions. *Hydrometallurgy*, 104(3-4), 506-517.
- Wöhrl, N. R., Reinhard. (2023). (No. Mi276) In *Methodisch inkorrekt!* <https://minkorrekt.de/2023/11/>
- Yasukawa, K., Uchida, Y., Tenma, N., Taguchi, Y., Muraoka, H., Ishii, T., Suwanlert, J., Buapeng, S., & Nguyen, T. H. (2009). Groundwater temperature survey for geothermal heat pump application in tropical Asia. *Bulletin of the Geological Survey of Japan*, 60(9-10), 459-467.
- Yeşiller, N., & Hanson, J. L. (2003). Analysis of temperatures at a municipal solid waste landfill. *Ninth International Waste Management and Landfill Symposium*, 1-10.
- Yeşiller, N., Hanson, J. L., & Liu, W.-L. (2005). Heat generation in municipal solid waste landfills. *Journal of Geotechnical and Geoenvironmental Engineering*, 131(11), 1330-1344.
- ZAMG. (2023). *GeoSphere Austria Data Hub*, URL, <https://data.hub.zamg.ac.at/>.
- Zhan, W., Ju, W., Hai, S., Ferguson, G., Quan, J., Tang, C., Guo, Z., & Kong, F. (2014). Satellite-derived subsurface urban heat island. *Environmental science & technology*, 48(20), 12134-12140.
- Zhang, T. (2005). Influence of the seasonal snow cover on the ground thermal regime: An overview. *Reviews of Geophysics*, 43(4).
- Zhou, S., O'Neill, Z., & O'Neill, C. (2018). A review of leakage detection methods for district heating networks. *Applied Thermal Engineering*, 137, 567-574.
- Zhu, K. (2013). *Urban heat island in the subsurface and geothermal potential in urban areas*. University of Tübingen.
- Zhu, K., Bayer, P., Grathwohl, P., & Blum, P. (2015). Groundwater temperature evolution in the subsurface urban heat island of Cologne, Germany. *Hydrological Processes*, 29(6), 965-978.
- Zhu, K., Blum, P., Ferguson, G., Balke, K.-D., & Bayer, P. (2010). The geothermal potential of urban heat islands. *Environmental Research Letters*, 5(4), 044002.
- Zito, M., Freitas, T. M. B., Bourne-Webb, P. J., & Sterpi, D. (2021). Effect of Domain Size in the Modelled Response of Thermally-Activated Piles. International Conference of the International Association for Computer Methods and Advances in Geomechanics,

# Curriculum vitae

## Personal Information

Name	Maximilian Noethen
Date of birth	██████████
Place of birth	██████████

## Professional Experience

January 2021 – Current: **Research Assistant**, Applied Geology, Institute of Geosciences and Geography, MLU Halle-Wittenberg, Halle (Saale), Germany

February 2020 – December 2020: **Student Employee**, Applied Geology, Institute of Geosciences and Geography, MLU Halle-Wittenberg, Halle (Saale), Germany

September 2013 – September 2014: **Volunteer in development policy**, VIA e.V., UMRA Orphanage Center, Daressalam, Tanzania

## Education

January 2021 – Current: **PhD Student**, Applied Geology, Institute of Geosciences and Geography, MLU Halle-Wittenberg, Halle (Saale), Germany

January 2021 – December 2023: **Scholarship holder**, German Federal Environmental Foundation (DBU)

October 2018 – November 2022: **M.Sc. Applied Geosciences**, Institute of Geosciences and Geography, MLU Halle-Wittenberg, Halle (Saale), Germany, Thesis: “Geothermisches Potential der urbanen Wärmeinsel im Untergrund von Halle (Saale)”

October 2014 – August 2018: **B.Sc. Geosciences**, Department of Geosciences, University of Kiel, Germany, Thesis: “Ermittlung hydraulischer und thermischer Kennwerte quartärer Sedimente im Rahmen der Vorerkundung eines Testfeldes bei Wittstock”



## List of publications

### Peer-reviewed publications

- Noethen, M.,** Hemmerle, H., Meyer, L., & Bayer, P. (2024). Prognose der oberflächennahen Grundwassertemperatur in Sachsen-Anhalt. *Grundwasser – Zeitschrift der Fachsektion Hydrogeologie*, DOI: <https://doi.org/10.1007/s00767-024-00570-z>.
- Bott, C., Dahash, A., **Noethen, M.,** & Bayer, P. (2024). Influence of thermal energy storage basins on the subsurface and shallow groundwater. *Journal of Energy Storage*, 92, 112222, DOI: <https://doi.org/10.1016/j.est.2024.112222>.
- Noethen, M.,** Hemmerle, H., Menberg, K., Epting, J., Benz, S. A., Blum, P., & Bayer, P. (2023). Thermal impact of underground car parks on urban groundwater. *Science of the Total Environment*, 903, 166572, DOI: <https://doi.org/10.1016/j.scitotenv.2023.166572>.
- Noethen, M.,** Hemmerle, H., & Bayer, P. (2022). Sources, intensities, and implications of subsurface warming in times of climate change. *Critical Reviews in Environmental Science and Technology*, 53(5), 700–722, DOI: <https://doi.org/10.1080/10643389.2022.2083899>.

### Conference contributions

- Noethen, M.,** Hemmerle, H., Benz, S., Menberg, K., Epting, J., Blum, P., & Bayer, P. (2024). Assessing the thermal impact of underground car parks on shallow urban aquifers, *IAH 2024 World Groundwater Congress*, Davos, Switzerland, 108992.
- Noethen, M.,** Becher, J., Menberg, K., Blum, P., Schüppler, S., Metzler, E., & Bayer, P. (2024). Does an anthropogenically induced subsurface temperature hotspot affect groundwater ecology?, *EGU General Assembly 2024*, Vienna, Austria, 14–19 Apr 2024, EGU24-1879.
- Noethen, M.,** Becher, J., Menberg, K., Blum, P., Schüppler, S., Metzler, E., & Bayer, P. (2023). Ecological impact of a groundwater temperature hotspot. Abstract H21R-1576 presented at *2023 Fall Meeting*, AGU, San Francisco, California, 11–15 December.
- Noethen, M.,** Hemmerle, H., Meyer, L., & Bayer, P. (2023). Estimation of shallow groundwater temperatures in Saxony-Anhalt, Germany. Poster presented at *GeoBerlin*.
- Noethen, M.,** Hemmerle, H., Benz, S., Menberg, K., Epting, J., Blum, P., & Bayer, P. (2023). Thermal impact of underground car parks on groundwater, *EGU General Assembly 2023*, Vienna, Austria, 24–28 Apr 2023, EGU23-2785.



## Declaration / Erklärung

Ich erkläre an Eides statt, dass ich die Arbeit selbstständig und ohne fremde Hilfe verfasst, keine anderen als die von mir angegebenen Quellen und Hilfsmittel benutzt und die den benutzten Werken wörtlich oder inhaltlich entnommenen Stellen als solche kenntlich gemacht habe.

*I declare under penalty of perjury that this thesis is my own work entirely and has been written without any help from other people. I used only the sources mentioned and included all the citations correctly both in word or content.*

---

Ort & Datum / Place & Date

Maximilian Noethen